NOVEL FUNCTIONS OF MITOCHONDRIAL PROTEINS IN HEALTH AND DISEASE

A Dissertation

Presented to the Faculty of the Weill Cornell Graduate School

of Medical Sciences

in Partial Fulfillment of the Requirements for the Degree of

Doctor of Philosophy

by

Suzanne R. Burstein

June 2017

NOVEL FUNCTIONS OF MITOCHONDRIAL PROTEINS IN HEALTH AND DISEASE

Suzanne R. Burstein, Ph.D.

Cornell University 2017

Mitochondria are organelles critical for many cellular functions including energy production, ion homeostasis, cellular protein trafficking, and apoptosis induction. While the mitochondrial protein machinery that performs these roles has been studied for many years, the functions of many of these proteins have not been fully elucidated.

This dissertation is focused on understanding the functions of two proteins in mitochondria, and their involvement in disease. We describe a novel function for estrogen receptor beta (ERβ) in brain mitochondria. We find that ERβ modulates cyclophilin D-dependent mitochondrial permeability transition (MPT) in brain. MPT is critical in cell death following brain injuries, such as stroke. Based on sex differences in ERβ modulation of MPT, we suggest that it may contribute to sex differences in cellular responses to ischemia.

We also explore the protein CHCHD10, a mitochondrial protein with yet unknown function. This protein is of particular interest, as its mutations have been recently associated with familial myopathy and neurodegenerative diseases, such as ALS. We find that CHCHD10 binds to its homolog CHCHD2, and both of these proteins bind to the mitochondrial protein P32.

Transient silencing of CHCHD10 expression in HEK293 cells triggers the induction of mitochondria-dependent apoptosis. We also generated and began to characterize the first CHCHD10 knockout mouse model. Data from the cellular and mouse models suggest different yet similar roles for CHCHD10 and CHCHD2 in mitochondria.

Uncovering these functions and understanding the pathways that these proteins participate in is critical to understanding of basic biology, but also of the pathophysiology of disease, as the brain relies heavily on mitochondria, and mitochondrial dysfunction occurs in many neurodegenerative diseases.

BIOGRAPHICAL SKETCH

Suzanne R. Burstein was raised in Livingston, NJ and attended Livingston High School. She received her undergraduate degree from Lehigh University, where she completed a thesis project as part of the Eckardt Scholars Program in the lab of Dr. Colin Saldanha, Ph.D. There she studied sex differences in the response to brain injury in songbirds under the supervision of Dr. Kelli Adams Duncan, Ph.D., and became interested in further exploring cellular mechanisms underlying brain diseases. She enrolled in the Neuroscience program at Weill Cornell Graduate School of Medical Sciences, and joined the laboratory of Giovanni Manfredi, M.D. Ph.D. in the Feil Family Brain and Mind Research Institute, where she has been studying the role of mitochondrial dysfunction in neurodegenerative disease and stroke.

Dedicated to Hyun Jeong Kim

ACKNOWLEDGEMENTS

First, I would like to thank my mentor, Dr. Giovanni Manfredi for supporting me in becoming an independent scientist and critical thinker, and for being an excellent role model. I am extremely grateful for the current and past members of the Manfredi lab, and the entire “MitoLab”, who have taught me everything that I know about mitochondria and have become wonderful friends. In particular, the experiments described in this work would not have been possible without the expertise of Dr. Hyun Jeong Kim, Dr. Anatoly Starkov, Dr. Liping Qian, Dr. Ping Zhou, Dr. Federica Valsecchi, and Dr. Hibiki Kawamata. Thank you to my thesis committee: Dr. Gary Gibson, Dr. Teresa Milner, and Dr. Anatoly Starkov, for their mentorship and support. I would also like to thank our collaborators at external institutions: Dr. Antoni Barrientos and Dr. Myriam Bourens at University of Miami, Dr. Cathleen Lutz at The Jackson Laboratories, and Dr. Doris Germain and Dr. Amanjot Riar at Mount Sinai School of Medicine. I must also thank the Weill Cornell Electron Microscopy Core (Dr. Leona Cohen-Gould), the Neuroanatomy EM Core (Dr. Teresa Milner), and the Cornell University Proteomics Core (Dr. Sheng Zhang). This work was made possible by my funding source, NIH F31 pre-doctoral fellowship NS090715. I would like to thank my peers and faculty members in the graduate school and neuroscience program for making this experience so rewarding. Finally, I would also like to thank my incredible partner in crime, parents, sister, and my family and friends for supporting me throughout graduate school and always.

TABLE OF CONTENTS

LIST OF FIGURES

LIST OF TABLES

LIST OF ABBREVIATIONS

17βE	17β-estradiol
AD	Alzheimer's Disease
ADP	Adenosine diphosphate
ALS	Amyotrophic lateral sclerosis
ATP	Adenosine triphosphate
COX	Cytochrome c oxidase
CsA	Cyclosporin A
CypD	Cyclophilin D
ΔΨm	Mitochondrial membrane potential
ERβ	Estrogen Receptor β
ERα	Estrogen Receptor α
FTD	Frontotemporal dementia
IM	Inner membrane
IMS	Intermembrane space
MICOS	Mitochondrial inner membrane cristae organizing system
MPT	Mitochondrial permeability transition
OGD	Oxygen glucose deprivation
OM	Outer membrane
OXPHOS	Oxidative phosphorylation
PD	Parkinson's Disease
RC	Respiratory chain
TH	Tyrosine hydroxylase
UPR^{mt}	Mitochondrial unfolded protein response

1. INTRODUCTION

1.1. Mitochondrial structure and function

The mitochondrion is a specialized double-membrane organelle in eukaryotic cells. Mitochondria form a dynamic, motile network that is a key player in many cellular processes, including ATP synthesis, fatty acid oxidation, calcium buffering, reactive oxygen species production, and apoptosis.

1.1.1. Mitochondrial structure

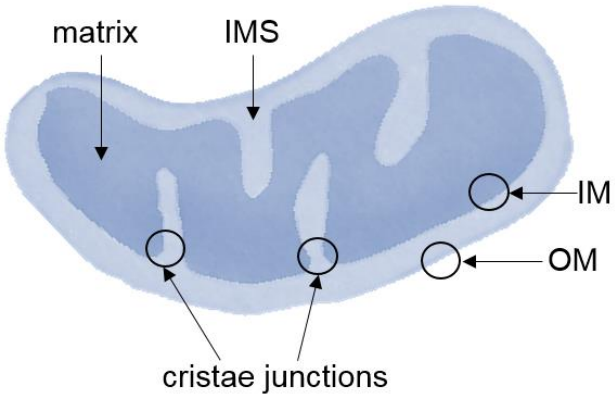

***Figure 1-1**. Mitochondrial structure*

Mitochondria have two membranes, the outer membrane (OM) and inner membrane (IM). The space between them is known as the intermembrane space (IMS), and the matrix is inside the IM. The folds in the IM form the highlighted cristae junctions.

Mitochondria are structured in subcompartments, which include outer membrane (OM), inner membrane (IM), intermembrane space (IMS) and mitochondrial matrix, as illustrated in Figure 1-1. The IM contains the subunits of the electron transport chain, and is folded into cristae, which increase the

surface area for oxidative phosphorylation (OXPHOS) to occur (Mannella, 2006). The mitochondrial matrix contains the mitochondrial DNA, which encodes 13 mitochondrial proteins, and 2 ribosomal and 22 transfer RNAs. Most mitochondrial proteins are encoded by nuclear genes, synthesized by cytoplasmic ribosomes, and then transported and folded into their final structures inside mitochondria.

1.1.2. Oxidative phosphorylation

Mitochondria have been called the “powerhouses of the cell” because one of their major functions is the production of cellular energy in the form of adenosine triphosphate (ATP). OXPHOS is the aerobic process that generates ATP in eukaryotic mitochondria via the respiratory chain (RC) complexes (CI-

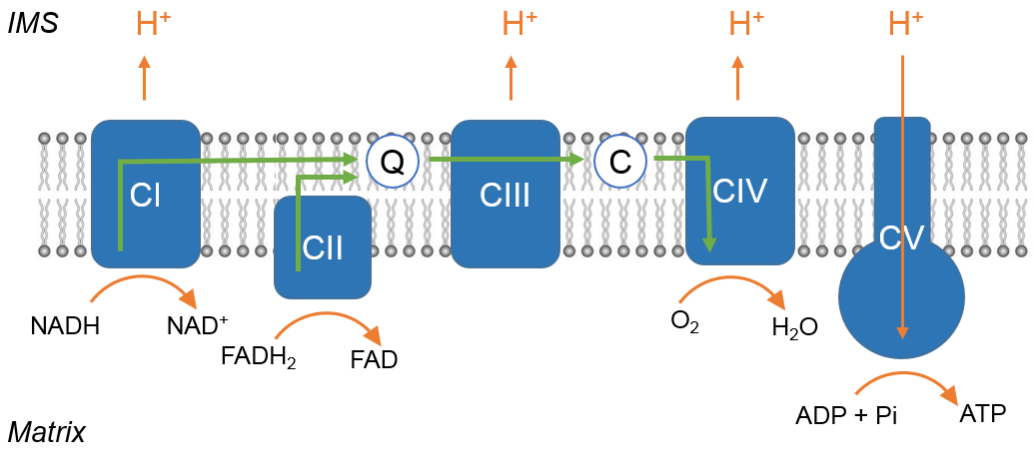

***Figure 1-2**. Respiratory chain*

Electrons are transferred (green arrows) from NADH-Q-oxidoreductase (CI) and succinate-Q reductase (CII) to coenzyme Q (Q, or ubiquinione), which carries the electrons to Q-cytochrome c-oxidoreductase (CIII). Cytochrome c transfers electrons to cytochrome c oxidase (CIV), what catalyzes the reduction of O2. Complexes I, III, and IV, pump protons into the intermembrane space (IMS), which creates an electrochemical proton gradient and drives ATP synthesis through ATP synthase (CV).

CIV) and the ATPase complex (CV). In eukaryotes, reduced electron carriers that are generated by the tricarboxylic acid cycle enter the RC. In a series of redox reactions, electrons are transferred from one RC complex to the next, and ultimately donated to molecular oxygen at complex IV to produce water. As a consequence of this electron transfer, protons are pumped from the matrix to the IMS. This generates an electrochemical gradient, and a proton-motive force, which is used to drive protons back into the matrix through CV, resulting in ATP generation from adenosine diphosphate (ADP) and inorganic phosphate. This process is illustrated in Figure 1-2. The ATP that is formed is transported across the mitochondrial IM by the adenine nucleotide translocator and through the OM into the cytosol.

1.1.3. Mitochondrial calcium handling

Mitochondria also play an important role in ion homeostasis. Mitochondrial calcium uptake buffers cytosolic calcium, and plays an important role in regulating bioenergetics, as several dehydrogenases in the mitochondrial matrix are regulated by calcium (McCormack et al., 1990). Mitochondrial calcium handling, illustrated in Figure 1-3, is a tightly regulated process involving many proteins, and varies greatly among tissues (Pizzo et al., 2012). Calcium enters the mitochondrial matrix through a mitochondrial calcium uniporter (Perocchi et al., 2010; Baughman et al., 2011; De Stefani et al., 2011), in a process modulated by several regulatory proteins, such as MICUs and EMRE (Perocchi et al., 2010; De Stefani et al., 2015; Kamer and Mootha, 2015). Calcium uptake requires the mitochondrial membrane potential ($\Delta\Psi m$) that is generated across the IM. Most of the calcium that enters

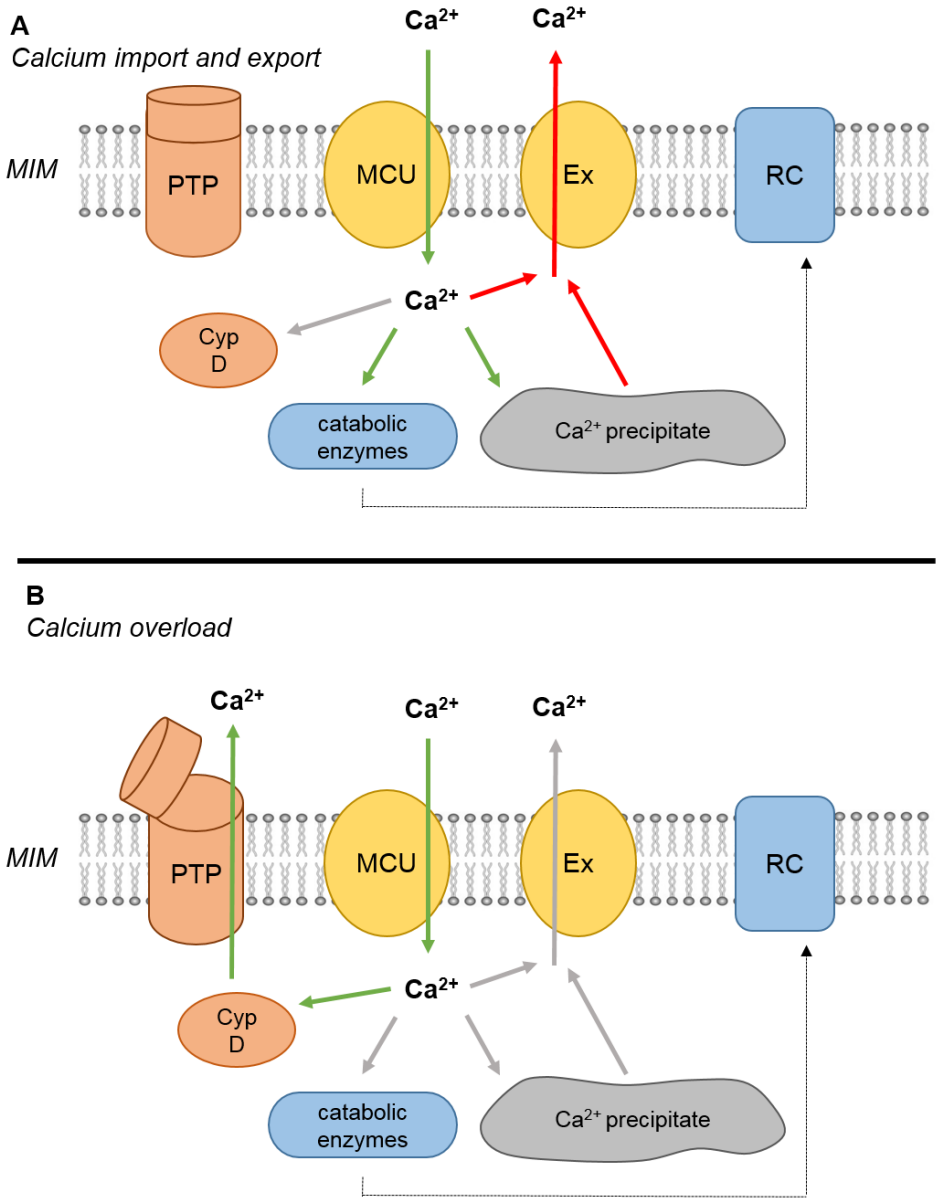

Figure 1-3. *Mitochondrial calcium handling*

A. In normal conditions, calcium enters mitochondria through the mitochondrial calcium uniporter (MCU), in the mitochondrial inner membrane (MIM). In the matrix, it forms precipitate and activates catabolic enzymes, which feed into the respiratory chain (RC). Calcium is slowly released via ion exchangers (Ex) in the MIM. **B**. Once calcium accumulation reaches a tissue-dependent threshold, it triggers cyclophilin D (CypD) translocation to the MIM and activates the opening of the permeability transition pore (PTP), allowing unregulated flow of calcium and small molecules.

precipitates in the matrix as calcium-phosphate (Kristian et al., 2007), keeping the concentration of free calcium fairly low. Free calcium is slowly released from mitochondria in excitable cells, such as neurons, via the Na^+/Ca^{2+} exchanger, or NCLX, in the IM (Palty et al., 2010). In other tissues, such as liver, the Ca^{2+}/H^+ exchanger is responsible for mitochondrial calcium extrusion (Jiang et al., 2009). When mitochondria are challenged with high calcium, mitochondrial permeability transition (MPT) occurs, resulting in swelling, OM rupture, and release of pro-apoptotic factors (Crompton et al., 1999; Hansson et al., 2011). MPT is the opening of a non-selective pore in the IM that results in unregulated flow of solutes and influx of water into the mitochondrial matrix. Calcium entry into mitochondria is a classic cause of MPT induction, however, MPT can also be induced by inorganic phosphate, oxidizing agents, reactive oxygen species, uncouplers, and other agents (Zoratti and Szabo, 1995).

1.2. Role of mitochondria in brain diseases

The brain has high energy demands, and relies on ion gradients and cellular signaling for neurotransmission (Attwell and Laughlin, 2001). Furthermore, the processes required to maintain calcium homeostasis in neurons are energetically costly (McCormack et al., 1990; Ivannikov et al., 2010). Given the critical role of mitochondria in these processes, it is not surprising that mitochondrial dysfunction is a key component of brain diseases.

1.2.1. Mitochondria in neurodegeneration

Mitochondrial dysfunction is a key component in the pathogenesis of neurodegenerative diseases. Many of these diseases develop in late

adulthood, and as reviewed in (Lin and Beal, 2006; Sun et al., 2016), a decline in mitochondrial function, increased mitochondrial DNA mutations, and elevated net reactive oxygen species production are associated with normal aging. Furthermore, many mutations in familial neurodegenerative diseases are in proteins with key mitochondrial involvement.

Many of the genes associated with familial Parkinson's Disease (PD), such as Parkin, Pink1 and DJ-1, are associated with mitochondrial quality control, oxidative stress and apoptosis. Use of the neurotoxin 1-methyl-4-phenyl-1,2,3,6-tetrahydropyridine (MPTP), induces a Parkinsonian syndrome and severe cell loss in the substantia nigra (Langston et al., 1983). This drug has been shown to decrease RC complex I activity, and RC complex I defects are also found in PD patients (Schapira et al., 1990).

Mitochondrial dysfunction also plays a role in Amyotrophic Lateral Sclerosis (ALS). Postmortem sporadic and familial ALS samples show defects in mitochondrial structure and function. Mutations in superoxide dismutase 1 (SOD1) were the first described in familial ALS, and are among the most common (Rosen et al., 1993). Animal models that overexpress the mutant human protein develop a disease phenotype, and have been used to demonstrate that mitochondrial energy production, calcium loading, and overall structure are impaired prior to neuronal death and disease onset (Kong and Xu, 1998; Mattiazzi et al., 2002; Damiano et al., 2006). Furthermore, while SOD1 is normally localized mainly in the cytosol, mutant SOD1 accumulates in mitochondria (Liu et al., 2004; Pasinelli et al., 2004; Vijayvergiya et al., 2005; Igoudjil et al., 2011).

Mitochondria are also connected to many other neurodegenerative diseases. In Alzheimer's Disease (AD), oxidative stress occurs early in

disease progression (Nunomura et al., 2001), and many implicated proteins such as Aβ and γ-secretase, which are found in the plasma membrane and other cellular compartments, also localize to the mitochondria (Hansson et al., 2004; Manczak et al., 2006). In Huntington's Disease (HD), defects in energy production have been demonstrated, and mitochondrial toxins that target CII induce a phenotype similar to HD (Brouillet et al., 1995; Gu et al., 1996).

1.2.2. Mitochondria in stroke

Mitochondria have been implicated in ischemic cell death via their role in energy production and in both necrotic and apoptotic cell death pathways. Within the ischemic core, the blood flow reduction during the ischemic period leads to impaired oxygen delivery and a rapid decline in ATP (Folbergrova et al., 1992). Cells may recover if the ischemic period is short, but if extended the major energy deficits in the ischemic core lead to necrosis (Sims and Muyderman, 2010). The penumbra, the region surrounding the core, also suffers from a rapid reduction in oxidative metabolism during ischemia but to a lesser extent. Energy metabolites and respiratory function can be temporarily restored briefly upon reperfusion, but a secondary decline occurs later in the reperfusion period. It is this later period of decline that is associated with massive neuronal death (Lust et al., 2002).

In addition to the role of mitochondrial energy deficits in stroke pathology, other mitochondrial phenomena are involved. The role of MPT was established by key studies demonstrating that both inhibition (Korde et al., 2007) and genetic ablation (Baines et al., 2005; Nakagawa et al., 2005; Schinzel et al., 2005) of the major pore regulator cyclophilin D (CypD) reduce necrosis following ischemia-reperfusion. Both MPT and the recruitment of pro-

apoptotic Bcl-2 family proteins to the mitochondrial OM are involved in the release of apoptogenic factors from mitochondria (Guegan and Sola, 2000; Gao et al., 2005).

1.3. Aims of thesis work

As summarized above, mitochondria are complex organelles that serve many functions, which are critical for cell viability, particularly in tissues with high energy demands, such as the brain and heart. Nevertheless, many aspects of mitochondrial function are not well understood, and many proteins that localize to mitochondria are not well characterized. The work described in this thesis aims to elucidate novel functions of two different proteins that are found in mitochondria in the central nervous system, and may play a role in disease pathogenesis.

The next chapter of this dissertation is focused on the role of estrogen receptor beta (ERβ) in mitochondria. Given the sex differences in stroke, and the importance of the MPT, we investigated the role of sex, as well as sex hormones and receptors in brain mitochondrial calcium-induced MPT.

The ERβ studies revealed a novel role in mitochondria for a protein that has well-characterized functions in the nucleus. However, the third chapter of this thesis is focused on another mitochondrial protein, coiled-coil-helix-coiled-coil-helix domain containing 10 (CHCHD10), on which no information was available at the start of this thesis work. Mutations in the gene encoding CHCHD10 were recently associated with ALS and other neuromuscular diseases, thus we were interested in uncovering the function of the protein in order to understand its role in disease.

Taken together, the studies in this dissertation revealed novel functions of two mitochondrial proteins, ERβ and CHCHD10, which can help to unravel cellular mechanisms underlying the pathogenesis of neurodegenerative disease and stroke.

2. ESTROGEN RECEPTOR BETA MODULATES PERMEABILITY TRANSITION IN BRAIN MITOCHONDRIA

2.1. Abstract

Recent evidence highlights a role for sex and hormonal status in regulating cellular responses to ischemic brain injury. A key pathological event in ischemic brain injury is the opening of a mitochondrial permeability transition pore (MPT) induced by excitotoxic calcium levels, which can trigger irreversible damage to mitochondria accompanied by the release of pro-apoptotic factors. Sex differences in MPT modulation in the brain have not been explored. Here, we show that mitochondria isolated from female mouse forebrain have a lower calcium threshold for MPT than male mitochondria, and that this sex difference depends on the MPT regulator, cyclophilin D (CypD). We also demonstrate that an estrogen receptor beta (ERβ) antagonist inhibits MPT and genetic ablation of ERβ decreases the sensitivity of mitochondria to the CypD inhibitor, cyclosporin A. These results suggest a functional relationship between ERβ and CypD in modulating MPT. Co-immunoprecipitation studies identified several ERβ binding partners in mitochondria. Among these, the mitochondrial ATPase was investigated as a putative site of regulation. We find that the known interaction between the ATPase subunit OSCP and CypD is decreased by ERβ knockout, providing a potential molecular mechanism of MPT regulation. Functionally, in a hippocampal slice oxygen glucose deprivation model, both CypD inhibition and ERβ knockout are protective exclusively in female slices. Taken together, these results identify a novel pathway for brain MPT regulation via ERβ that could contribute to sex differences in ischemic brain injury outcome.

2.2. Introduction

2.2.1. Sex differences in stroke

There is a growing body of evidence describing sex differences in ischemic brain injury. Many factors are thought to contribute to increased overall stroke risk and worse stroke outcome in women compared to men, including longer average life expectancy, post-menopausal hormonal changes, and hormonal replacement therapies (Writing Group et al., 2010). Furthermore, recent studies have highlighted cellular mechanisms, which differ between males and females, that may contribute to sex differences in stroke incidence and recovery (Spychala et al., 2017). For example, females have enhanced caspase activation compared to males in animal stroke models (Zhu et al., 2006; Liu et al., 2009). Conversely, stroke induced NAD+ depletion and caspase-independent nitric oxide and PARP-1 activation are prominent in males and ovariectomized females, but not in intact females (Siegel and McCullough, 2013). There are also more prominent increases in stroke-induced autophagy in females compared to males (Chen et al., 2013; Weis et al., 2014). While there have been some studies of sex differences in mitochondrial function in response to glutamate toxicity and oxidative stress (Chauhan et al., 2017), it is clear that further studies comparing sexes are needed to improve our understanding of the role of mitochondria in sex differences in stroke-induced cell death.

2.2.2. Mitochondrial permeability transition

One important cellular phenomenon in ischemic brain injury is mitochondrial permeability transition (MPT) (Starkov et al., 2004; Racay et al., 2009). MPT is the opening of a non-selective pore in the IM that results in

unregulated flow of solutes and influx of water into the mitochondrial matrix. MPT results in swelling of mitochondria, OM rupture, and release of pro-apoptotic factors (Crompton et al., 1999; Hansson et al., 2011). A key trigger for MPT pore opening is a high level of calcium in the mitochondrial matrix. Calcium enters mitochondria through the mitochondrial calcium uniporter (MCU) using $\Delta\Psi m$ as a driving force (De Stefani et al., 2011). A moderate calcium influx in mitochondria is critical for activation of matrix dehydrogenases of the TCA cycle, and boosts oxidative metabolism (McCormack et al., 1990). However, at high calcium concentrations, such as in ischemia reperfusion when neurons are flooded with calcium due to the opening of plasma membrane channels and release from internal calcium stores (Tymianski et al., 1993; Peng and Greenamyre, 1998), MPT occurs (Gouriou et al., 2011). It is important to note that alternatively to irreversible, damaging MPT, reversible and transient MPT can lead to opening of a low-conductance pore that may serve as a protective calcium extrusion mechanism (Bernardi and von Stockum, 2012).

The precise composition and mechanisms of regulation of the MPT pore remain controversial, although several candidates for structural and modulatory proteins have been proposed (reviewed in: (Bernardi and Di Lisa, 2015; Halestrap and Richardson, 2015)). Nevertheless, it is widely accepted that a key MPT modulatory protein is CypD, a matrix protein, which upon calcium influx translocates to the mitochondrial IM to promote MPT opening (Bernardi et al., 1994; Connern and Halestrap, 1994). In the absence of CypD (Basso et al., 2005; Schinzel et al., 2005) or under its pharmacological inhibition (Broekemeier et al., 1989; Szabo and Zoratti, 1991), MPT can still occur, but the calcium threshold for its activation is much higher.

Although sex differences in MPT have been observed in heart (Arieli et al., 2004; Milerova et al., 2016), the molecular mechanisms underlying these differences are unknown. Furthermore, whether males and females differ in brain MPT has not been explored.

2.2.3. Estrogen and estrogen receptors (ERs) in mitochondria

Sex hormones are clear potential candidates for modulators of mitochondrial functions. It is known that estrogens affect intracellular calcium dynamics (Zhao and Brinton, 2007; Zhang et al., 2010) and mitochondrial function (Nilsen et al., 2006), in both receptor dependent and independent manners (Simpkins et al., 2010). Two estrogen receptors, alpha (ERα) and beta (ERβ), were originally identified as nuclear receptors (Greene et al., 1986; Tremblay et al., 1997). Subsequently, both receptors have been shown to also localize to mitochondria (Chen et al., 2004), although for ERβ this has been more thoroughly characterized (Yang et al., 2004; Milner et al., 2005). Both male and female mouse brain contain ERβ in many regions, and some areas have more ERβ-containing cell profiles in females than in males (Milner et al., 2010), which may contribute to sex differences in MPT. However, despite the known effects of estrogen on mitochondrial function and the finding of ERs in mitochondria, until now the role of estrogen receptors in sex differences in MPT regulation has not been explored.

In this study, we investigated sex differences in calcium-induced MPT in mouse brain mitochondria, the mechanisms of ERβ and CypD MPT modulation, and the potential involvement of such mechanisms in ischemia reperfusion injury.

2.3. Materials and methods

2.3.1. Animals

CypDKO mice in the C57Bl/6J background have been described previously (Schinzel et al., 2005). CypDKO homozygotes are born at Mendelian frequency, do not display gross abnormal phenotypes, and are protected compared to controls in ischemia reperfusion injury (Schinzel et al., 2005). ERβKO mice in the C57Bl/6J background were from The Jackson Laboratories (strain B6.129P2-*Esr2*^{tm1Unc}/J). ERβKO homozygotes are born at Mendelian frequency, are normal in size, and do not have gross phenotypic abnormalities, though homozygote females are sub-fertile (Krege et al., 1998). CypDKO and ERβKO were crossed to obtain ERβ/CypD double KO animals. Heterozygote males and females were bred to obtain homozygote double KO animals. We performed all breeding and genotyping for these experiments at Weill Cornell Medicine. Adult animals (130 days of age) were used to isolate brain mitochondria for the calcium capacity and $\Delta\Psi$m measurements, and postnatal day 5 animals were used for the organotypic hippocampal slice cultures.

All experiments were approved by the Institutional Animal Care and Use Committee of the Weill Cornell Medicine and carried out in compliance with the National Institute of Health guidelines for the care and use of laboratory animals.

2.3.2. Preparation of mitochondria from brain

Purification of mouse forebrain non-synaptic mitochondria was performed as described in previous publications from our laboratory (Damiano et al., 2006; Kim et al., 2012). Mice were euthanized by decapitation, and the

forebrain removed and homogenized using a glass Dounce homogenizer on ice in ice-cold MS-EGTA buffer (225 mM mannitol, 75 mM sucrose, 5 mM HEPES, 1 mM EGTA, pH 7.4) containing 0.1 mg/ml fatty acid-free bovine serum albumin (BSA). All centrifugation steps were performed using a Type 70.1 Ti rotor in a Beckman Optima XE-90 centrifuge. The homogenates were centrifuged at 2,000 g for 5 minutes; the supernatant was collected and centrifuged at 12,000 g for 10 minutes. The pellet was suspended in 1 mL MS-EGTA (without BSA), layered on top of isolation buffer containing 23% Percoll. The gradient was centrifuged at 40,000 g for 12 minutes and then the interphase layer containing mitochondria was collected. The mitochondria were suspended in isolation buffer and centrifuged at 12,000 g for 10 minutes, three times. The pellet containing purified mitochondria was resuspended in MS-EGTA and protein concentration was calculated using a BCA assay kit (Pierce).

2.3.3. Calcium capacity and membrane potential measurements

Mitochondria (0.1 mg protein/mL) were subjected to 25 µM pulses of calcium every 150 seconds in the spectrofluorimeter cuvette in the presence of 125 mM KCl, 20 mM HEPES, 1 mM $MgCl_2$ (pH 7.2), 4 mM KH_2PO_4, 0.2 mM ATP, 1 µM rotenone and 5 mM succinate. Fura-FF (0.2 µM, Life Technologies) was used to measure calcium uptake using 340/380 nm excitation and 510 nm emission. A final addition of EGTA (1 mM) was added. Fluorescence traces over time were obtained and calcium capacity, the point at which mitochondria start to lose the ability to take up all of the calcium in the buffer, was calculated. The fluorescence levels measured at 75 seconds after each calcium addition were plotted and the inflection point was determined. To

correlate the inflection point to a calcium concentration, calcium standards of known concentration were added to create a calibration curve and calculate mitochondrial calcium capacity (nmol Ca^{2+}/mg protein). In some experiments, the CypD inhibitor cyclosporin A (CsA, 1 μM) was added to mitochondria prior to the first calcium addition. CsA binds to CypD and inhibits MPT pore formation (Broekemeier et al., 1989; Griffiths and Halestrap, 1991). CsA has also immunosuppressant and nephrotoxic effects as a result of the inhibition of calcineurin (Liu et al., 1991). However, in experiments in isolated mitochondria it is frequently used to study calcium-dependent MPT (Broekemeier et al., 1989).

Mitochondrial calcium capacity measurements were performed in absence or presence of the ERβ inhibitor 4-[2-Phenyl-5,7-*bis*(trifluoromethyl)pyrazolo[1,5-*a*]pyrimidin-3-yl]phenol (PHTPP, Tocris Bioscience) or the ERα inhibitor 1,3-*Bis*(4-hydroxyphenyl)-4-methyl-5-[4-(2-piperidinylethoxy)phenol]-1*H*-pyrazole dihydrochloride (MPP, Tocris Bioscience), added prior to calcium additions. PHTPP is 36-fold selective for ERβ in binding, and was fully effective as an ERβ antagonist in a transcription based assay, with no effect on ERα (Compton et al., 2004). MPP is a highly selective ERα antagonist with >200-fold binding selectivity for ERα over ERβ, and demonstrated selectivity in transcription-based assays (Sun et al., 2002).

Safranin O (2 μM, Sigma) was used to measure $\Delta\Psi m$ using 495 nM excitation and 586 nm emission, in the conditions described above. Following sequential calcium boluses, antimycin A (1 μg/mL) was added to inhibit the RC and induce maximal depolarization. The percent of maximal depolarization for each calcium addition was plotted in order to determine the amount of calcium required to induce 50% of the maximal achievable depolarization (Δψm50). To

test the ability of mitochondria to generate Δψm, sequential additions of the uncoupler SF6847 (2 nM each, Malonoben, Tocris Bioscience) were made, and the decrease in Δψm after each addition was plotted.

Brain mitochondria were isolated and processed in pairs, with careful attention paid towards timing of the measurements in relation to mitochondrial isolation. Data are presented as mean values and standard error of the mean. Differences between two groups were analyzed using Student's t-test with a 95% confidence interval.

2.3.4. Western blot

Brain mitochondria samples were prepared in Laemmli buffer with β-mercaptoethanol, then separated by SDS-PAGE on 12% Tris-acrylamide/bis-acrylamide gels and transferred to polyvinylidene fluoride membranes (BioRad). Membranes were probed overnight with the following primary antibodies: anti-Tim23 (BD Transduction Laboratories), anti-mitochondrial calcium uniporter (MCU, Sigma), anti-voltage dependent anion channel (VDAC, Abcam), anti- mitochondrial calcium uptake 1 (MICU1, Abcam), and anti-CypD (Mitoscience). Membranes were incubated with horseradish peroxidase-conjugated secondary antibodies (Jackson ImmunoResearch) and detected via chemiluminescence.

2.3.5. Hippocampal slice culture preparation and oxygen glucose deprivation

Hippocampal slice cultures (coronal slices, 350μm thick) were prepared as previously described (Gahwiler et al., 2001; Zhou et al., 2012a), and cultured on Millicell CM membrane inserts (Millipore). After 14 days in culture, slices were imaged for three consecutive days after staining with propidium iodide (PI) in the culture medium (5 μg/mL). On the first day, baseline PI

images were captured (Fl_{basal}) in a transmission fluorescence microscope with a 2X objective, and then oxygen glucose deprivation (OGD) was performed. Briefly, slices were washed in OGD buffer (125 mM NaCl, 5 mM KCl, 1.2 mM Na_2PO_4, 26 mM $NaHCO_3$, 1.8 mM $CaCl_2$, 0.9 mM $MgCl_2$, 10 mM HEPES, pH 7.4), and then incubated in OGD buffer without glucose in an anoxic gas chamber (Billups-Rothenberg, Inc.) for one hour, and then returned to normal culture medium, containing 5 mg/mL glucose. Anoxia was achieved by bubbling the OGD buffer without glucose with 95% N_2/5% CO_2 before the start of the OGD, and by flushing the sealed gas chamber with 95% N_2/ 5% CO_2 upon starting the OGD. On the second day, post-OGD PI images were captured (Fl_{OGD}). Then, slices were treated with 1 mM *N*-Methyl-D-aspartic acid (NMDA) for 24 hours. On the third day, post-NMDA PI images were captured, representing the maximum death in each slice (Fl_{max}). The same imaging settings were used at all time points, and images from the CA1 hippocampal region were used to calculate the proportion of OGD-induced death using the formula $(Fl_{OGD} – Fl_{basal})/(Fl_{max} – Fl_{basal})$ x 100%.

2.3.6. Cell culture, transfection, and FLAG co-immunoprecipitation

COS-7 cells were cultured in high-glucose (4.5 g/L) Dulbecco's modified Eagle's medium (DMEM, Life Technologies) supplemented with 5% fetal bovine serum (Atlanta Biologicals) and 1% antibiotic-antimycotic (Life Technologies). Cells were transfected with the ERβ-Flag construct (Addgene #35562) using the Lonza Nucleofector device according to the manufacturer's instructions. Enriched mitochondrial fractions were prepared from transfected cells. Briefly, cells were harvested and homogenized in MS-EGTA with BSA, and centrifuged at 4°C at 800 g for 5 minutes. Supernatants were centrifuged

at 10,000 g for 10 minutes, and pellets washed in BSA-free MS-EGTA buffer and then resuspended in MS-EGTA. Protein concentrations were quantified using a BCA assay kit (Pierce).

Co-Immunoprecipitation (Co-IP) experiments were performed on mitochondrial fractions using a Co-Immunoprecipitation kit (Pierce). Briefly, FLAG antibody (Sigma F1804) or normal mouse IgGs (ThermoFisher) were covalently coupled to IP resins. Mitochondria (0.5 mg) were suspended in Co-IP lysis/wash buffer and incubated with the resins overnight. Proteins were eluted in elution buffer and eluates neutralized with Tris-HCl pH 8.5. Western blot using FLAG antibody was performed to confirm the presence of ERβ-Flag in the Co-IP eluates. Each Co-IP was repeated and representative Western blots are shown.

2.3.7. Protein extraction, digestion and Tandem Mass Tag (TMT) labeling

Proteins were denatured in 200 mM triethylammoniumbicarbonate, 7 M urea, 2 M thiourea and 0.2% SDS, pH 8.5 for 1 hour. Each sample (2 µg) was reduced with 11.9 mM tris(2-carboxyethyl) phosphine for 1 hour at 37°C, alkylated with 20 mM iodoacetamide for 1 hour in the dark and quenched with 20 mM dithiothreitol (DTT). The proteins were precipitated with acetone and frozen overnight, reconstituted in 90 µL of 100 mM triethylammoniumbicarbonate and digested with 0.2 µg trypsin for 18 hours at 37°C. The TMT 6-plex labels were reconstituted with 45 µL of anhydrous ACN and added to each of the digest samples for 1 hour at room temperature. The peptides from the 6 samples were mixed with each tag: 126-tag (mock IP #1), 127-tag (ERβ-FLAG IP #1), 128-tag (ERβ-FLAG + 17βE #1) 129-tag (mock IP #2), 130-tag (ERβ-FLAG IP #2), and 131-tag (ERβ-FLAG + 17βE #2). The six

samples were pooled, evaporated to dryness and subjected to cation exchange chromatography fractionation using a PolyLC strong cation-exchange cartridge (PolyLC Inc. Columbia, MD). The pooled peptides were then reconstituted with 3 mL of loading buffer (10 mM potassium phosphate pH 3.0, 25% ACN), and the pH adjusted to 3.0 with formic acid. After conditioning of the strong-cation exchange (SCX) cartridge (PolySULFOETHYL A, 10 mm id x 14 mm, particle size 12 µm, pore size 300 Å), the sample was loaded and washed with an additional 2 mL of loading buffer. The peptides were eluted in three isocratic steps by 1 mL of loading buffer containing 50 mM, 150 mM and 500 mM KCl for each step. Desalting of SCX fractions was carried out using solid phase extraction (SPE) on Sep-Pak® Cartridges (Waters, Milford, MA) and the eluted peptides were evaporated to dryness.

2.3.8. Nano-scale reverse phase chromatography and tandem mass spectrometry (nanoLC-MS/MS)

Each fraction was reconstituted in 15 µL 0.5% FA, and nanoLC-ESI-MS/MS analysis was carried out using an Orbitrap Elite (Thermo-Fisher Scientific, San Jose, CA) mass spectrometer equipped with a “CorConneX” nano ion source device (CorSolutions LLC, Ithaca, NY). The Orbitrap was interfaced with a Dionex UltiMate3000RSLCnano system (Thermo, Sunnyvale, CA). Each sample was injected onto a PepMap 100 C-18 RP nano trap column (5 µm, 100 µm × 20 mm, Thermo) with nanoViper Fittings at 20 µL/min flow rate and then separated on a PepMap C-18 RP nano column (3 µm, 75 µm x 15 cm), and eluted in a 120 min gradient of 5% to 38% acetonitrile (ACN) in 0.1% formic acid at 300 nL/min., followed by a 5-min ramping to 95% ACN-

0.1% FA and a 5-min hold at 95% ACN-0.1% FA. The Orbitrap Elite was operated in positive ion mode (nano spray voltage 1.6 kV, source temperature at 250°C). The instrument was operated in data-dependent acquisition (DDA) mode using FT mass analyzer for one survey MS scan for selecting top 15 precursor ions followed by data-dependent HCD-MS/MS scans on the precursor peptides with multiple charged ions above a threshold ion count of 8000 with normalized collision energy of 37%. MS survey scans at a resolution of 60,000 (fwhm at *m*/*z* 400), for the mass range of m/z 375-1600, and MS/MS scans at 15,000 resolution for the mass range, m/z 100-2000. Dynamic exclusion parameters were set at repeat count 1, an exclusion list size of 500, 50 s exclusion duration with ±10 *ppm* exclusion mass width. The activation time was 0.1 ms for HCD analysis. All data were acquired under Xcalibur 2.2 operation software (Thermo-Fisher Scientific).

All MS and MS/MS raw spectra from TMT experiments were processed using Proteome Discoverer 1.4 (PD1.4, Thermo) and the spectra used for subsequent database search using Mascot Daemon (version 2.3.02, Matrix Science, Boston, MA). The human RefSeq sequence plus Chlorocebus_aethiops_plus_flander_virus database containing 37,469 sequence entries was downloaded on August 28, 2013 from NCBInr and used for database searches. The default search settings used for 6-plex TMT quantitative processing and protein identification in Mascot server were: two mis-cleavages for full trypsin with fixed carbamidomethyl modification of cysteine, fixed 6-plex TMT modifications on lysine and N-terminal amines and variable modifications of methionine oxidation, and deamidation on asparagines/glutamine residues. The peptide mass tolerance and fragment mass tolerance values were 15 ppm and 100 mDa. The significant scores at

95% confidence interval for the peptides defined by a Mascot probability analysis (www.matrixscience.com/help/scoring_ help.html#PBM) greater than “identity” were used as filters along with a p value of < 0.05 (expectation value). The resulting peptides are considered to be confidently identified peptides with at least 2 unique peptides per protein. Intensities of the reporter ions from TMT tags upon fragmentation were used for quantification of peptides.

2.3.9. OSCP co-immunoprecipitation

Enriched mitochondrial fractions from HEK293 cells or purified brain mitochondria were prepared as described above. The OSCP antibody (Santa Cruz #sc-365162) or normal mouse IgGs (ThermoFisher) were coupled to the resin provided in the co-immunoprecipitation kit (Pierce) and co-IP of mitochondrial preparations (0.5 mg) was performed overnight in the following buffer: 50mM Tris-HCl, 150mM NaCl, 1mM EDTA, 0.1% NP-40, pH 7.4 (Beck et al., 2016). Proteins were eluted from the resin using the provided buffer and samples subjected to Western blot, as described above.

2.4. Results

2.4.1. Sex difference in brain mitochondria calcium capacity depends on CypD

To investigate sex differences in calcium-induced MPT we used mitochondria freshly isolated from adult mouse forebrain (130 days of age). Mitochondria were prepared via centrifugation of forebrain homogenates in a Percoll gradient. Calcium capacity, defined as the maximal amount of calcium that mitochondria could take up before undergoing MPT, was measured with a

fluorimetric approach. Mitochondria were resuspended in buffer containing respiratory substrates and the ratiometric calcium probe Fura-FF, and sequential calcium boluses (25 μM each) were added to the cuvette.

Mitochondrial calcium uptake was indicated by a deflection in the fluorescence ratio trace. The calcium concentration was increased until uptake was no longer observed, indicating MPT. Representative traces of calcium uptake show that female brain mitochondria (gray trace) take fewer calcium additions than males (black trace), before undergoing calcium-induced MPT (Figure 2-1 A). Calcium capacity was calculated by correlating the inflection point of the fluorescence ratio trace to a standard curve obtained with calcium standards. The quantification of MPT threshold demonstrated that calcium capacity was significantly lower in female mitochondria compared to male mitochondria (p=0.012, n=8, Figure 2-1 B).

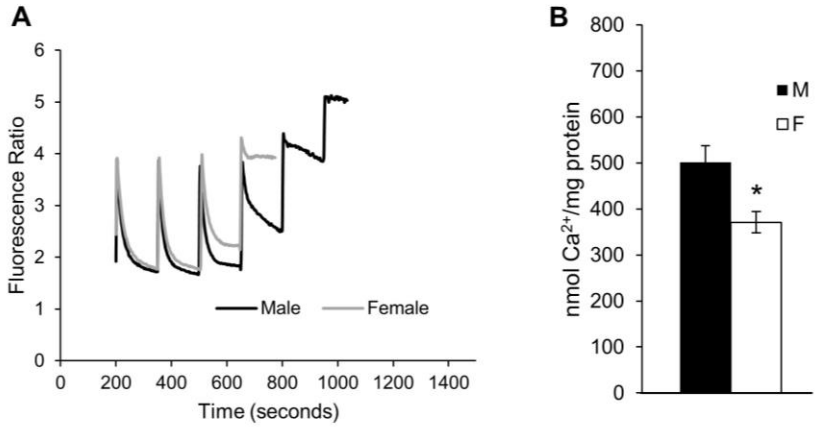

***Figure 2-1**. Sex difference in brain mitochondrial calcium capacity*

A. Representative fluorimetric traces of calcium uptake in mitochondria purified from male (black line) and female (gray line) adult (130 days of age) mouse mouse forebrain. **B**. Quantification of brain mitochondrial calcium capacity in wild type males and females. n = 8 animals per group; * $p<0.05$.

In order to understand the mechanism underlying the sex difference in brain mitochondrial calcium capacity MPT, we investigated the involvement of the well-known pore regulator CypD. The classical CypD inhibitor cyclosporin A (CsA, 1 μM), added to the cuvette immediately prior to the start of the

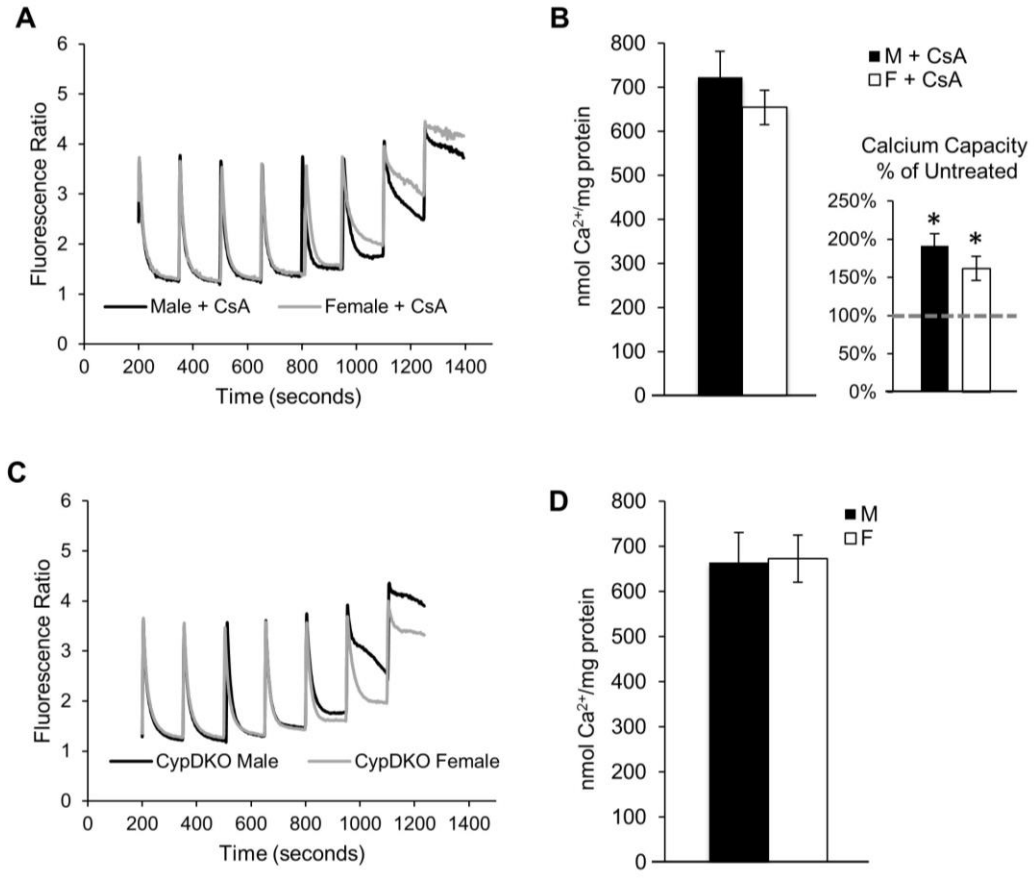

***Figure 2-2**. Sex difference is cyclophilin D dependent*

A. Representative fluorimetric traces of calcium uptake in the presence of CsA (1 μM) in mitochondria purified from male (black line) and female (gray line) adult mouse forebrain. **B**. Quantification of calcium capacity in male and female brain mitochondria in the presence of CsA. Calcium capacity in CsA treated mitochondria shown as percentage of vehicle treated calcium capacity (dashed line) in the figure inset. * $p<0.05$ vs. untreated; n = 4 animals per group. **C**. Representative fluorimetric traces of calcium uptake in mitochondria purified from male (black line) and female (gray line) adult CypDKO mouse forebrain. **D**. Quantification of brain mitochondrial calcium capacity in CypDKO mice. n = 8 animals per group.

calcium boluses, increased calcium capacity in both male and female brain mitochondria (by 91 ± 16 % and 62% ± 6, respectively, n=4, p=0.001 and p=0.0085, Fig. 2B inset), and abolished the sex difference (p=0.72, Figure 2-2 A, B). Importantly, we further established the role of CypD by studying brain mitochondrial calcium capacity in males and females with genetic ablation of CypD (CypDKO). CypDKO also increased calcium capacity in both male and female brain mitochondria, and abolished the sex difference (n=8, p=0.93, Figure 2-2 C,D). Taken together, pharmacological and genetic evidence indicate that CypD is required for the sex difference in mouse brain mitochondrial calcium capacity.

2.4.2. ERβ modulates brain MPT in a CypD-dependent manner

Because of the sex difference in brain mitochondrial calcium capacity and the localization of ERs in brain mitochondria, we examined the possibility that selective antagonists of ERβ or ERα modulate brain mitochondrial calcium capacity. Mitochondria were treated with 5 μM of the ERβ inhibitor PHTPP or the ERα inhibitor MPP, prior to calcium additions. Calcium capacity was markedly increased by PHTPP treatment to approximately the same extent in both male and female brain mitochondria relative to untreated mitochondria (respectively by 62% ± 3, p=0.004 and 57% ± 15, p=0.005, n=3, Figure 2-3 A) and eliminated the sex difference (p=0.78). This finding was particularly interesting, as molecules that increase the calcium threshold for MPT are under investigation as a therapeutic strategy to prevent apoptosis induction (Argaud et al., 2005; Le Lamer et al., 2014; Martin et al., 2014b; Warne et al., 2016). Furthermore, because PHTPP affected calcium capacity within minutes in purified mitochondria, any transcriptional effects of the drug could virtually

be excluded, suggesting that ERβ in mitochondria could act as an MPT regulator. On the other hand, the ERα antagonist MPP had no significant effects on calcium capacity (respectively, p=0.51 and 0.15, n=4), suggesting that ERα in mitochondria is not involved in modulating calcium capacity (Figure 2-3 B).

To further examine the role of ERβ in brain MPT we utilized ERβKO mice. Similar to wild type mice, ERβKO brain mitochondria calcium capacity was lower in females than in males (p=0.004, n=8, Figure 2-4 A), suggesting that ERβ is not required for the sex difference. Nevertheless, addition of PHTPP to ERβKO mitochondria failed to increase calcium capacity in males and females (respectively, p=0.83 and p=0.51, n=3, Figure 2-4 B), indicating that the increase of calcium capacity by PHTPP observed in wild type mice (Figure 2-3 A) requires ERβ, and therefore it is not an off-target effect of the

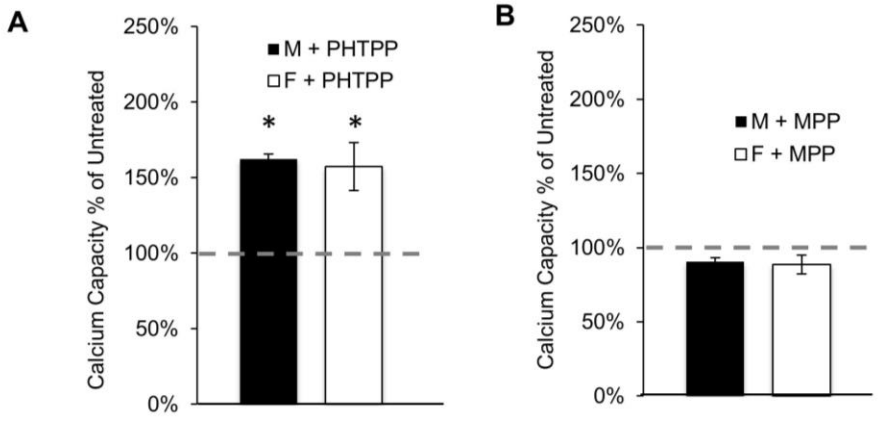

Figure 2-3. *Pharmacological inhibition of estrogen receptors*

A. Quantification of calcium capacity in wild type mitochondria treated with the ERβ antagonist PHTPP (5 μM). Data are represented as percent of calcium capacity of respective vehicle-treated mitochondria (dashed line). * $p<0.05$ vs. untreated; n = 3. **B**. Quantification of mitochondrial calcium capacity of wild type mitochondria treated with ERα antagonist MPP (5 μM). Data are represented as percent of calcium capacity of respective vehicle-treated mitochondria. n = 4.

drug. Unlike the effect of CsA on wild type mitochondria (Figure 2-3 B inset), CsA modestly increased calcium capacity in both male and female ERβKO mitochondria (Figure 2-4 C), and the effect failed to reach statistical significance (respectively, 38% ± 6, p=0.24 and 24% ± 6, p=0.23, n=6). Nevertheless, as in wild type mitochondria (Figure 2-2 B), the sex difference in mitochondrial calcium capacity was abolished by CsA in ERβKO mice (p=0.41, Figure 2-4 C).

To further explore the functional interaction between ERβ and CypD in the handling of mitochondrial calcium, we compared the depolarization of mitochondria in response to calcium accumulation in wild type and ERβKO mice, in the presence or absence of CsA. We used Safranin O to assess changes in Δψm (Akerman and Wikstrom, 1976). Specifically, we measured the mitochondrial depolarization following sequential bolus calcium additions (25 μM each), equivalent to those used for Fura-FF measurements. Since mitochondrial calcium uptake uses the force of Δψm, each calcium addition followed by uptake results in a decrease of Δψm.

Ultimately, maximal loss of Δψm occurs when mitochondria undergo MPT. Example traces of Safranin O fluorescence upon sequential calcium additions for wild type and ERβKO mitochondria are shown in figure 2-4 D and 2-4 E, respectively. In wild type mitochondria, on average CsA doubled the amount of calcium required to induce 50% of the maximal achievable depolarization (Δψm50, Figure 2-4 F). However, in ERβKO mitochondria CsA only increased the amount of calcium required for Δψm50 by 1.5 fold (p=0.02, n=6). Lastly, we tested brain mitochondrial calcium capacity in ERβ/CypD double KO female mice compared to CypDKO female mice to assess whether

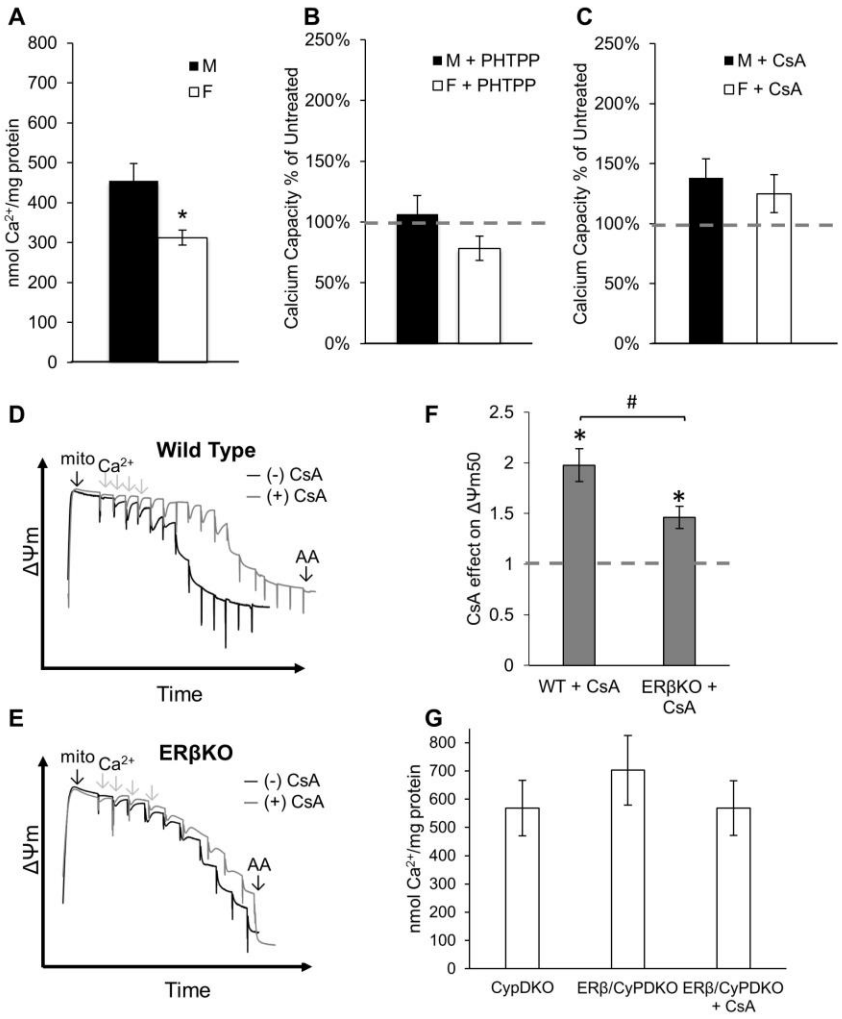

Figure 2-4*. ERβKO mitochondria have decreased CsA sensitivity.*

A. Quantification of calcium capacity in male and female ERβKO brain mitochondria. * $p<0.05$; n = 8 animals per group. **B**. Quantification of mitochondrial calcium capacity of ERβKO mitochondria treated with PHTPP (5 μM). Data are represented as percent of calcium capacity of respective vehicle-treated mitochondria (dashed line). n = 3 animals per group. **C**. Quantification of calcium capacity of ERβKO mitochondria treated with CsA (1 μM). Data are represented as percent of calcium capacity of respective vehicle-treated mitochondria. n = 6 animals per group. **D**. Representative trace of Δψm in wild type (WT) brain mitochondria with and without CsA (1 μM). Sequential calcium additions and final addition of antimycin A (AA) are indicated with arrows. **E**. Representative trace of Δψm in ERβKO brain mitochondria with and without CsA treatment. **F**. Quantification of half-maximum Δψm in the presence of CsA, normalized by vehicle-treated, in WT and ERβKO. * $p<0.05$ vs. vehicle-treated; # $p<0.05$; n = 6 animals per group. **G**. Quantification of female brain mitochondrial calcium capacity in CypDKO and ERβ/CypDKO, and ERβ/CypDKO treated with CsA. n = 3 animals per group.

the absence of ERβ modifies the effect of CypDKO. Calcium capacity was not significantly different in the two genotypes (p=0.44, n=3, Fig. 2-4 G).

Taken together, these data indicate that there is a functional relationship between ERβ and CypD in modulating calcium-induced MPT in brain, and since ERβKO did not affect calcium capacity in CypDKO mitochondria, we concluded that that ERβ was functionally upstream of CypD in regulating MPT.

2.4.3. ERβKO does not affect mitochondrial calcium-related protein expression or bioenergetics

ERβ was first identified as a nuclear receptor that regulates the expression of an estrogen-responsive transcriptional program (Mosselman et al., 1996; Tremblay et al., 1997). However, here we showed that the ERβ antagonist PHTPP affects mitochondrial calcium capacity within minutes, suggesting fast-acting mechanisms by which ERβ modulates MPT. To exclude that changes in calcium handling were caused by altered levels of proteins involved in calcium fluxes in mitochondria, we compared protein expression in wild type and ERβKO brain mitochondria. The levels of calcium handling proteins were assessed by Western blot of purified brain mitochondrial extracts. The intensities of the immunoreactive bands for the mitochondrial calcium uniporter (MCU), voltage-dependent anion channel (VDAC), mitochondrial calcium uptake 1 (MICU1), CypD, and integral IM protein Tim23 used as loading reference, were unchanged in ERβKO mitochondria relative to wild type (Figure 2-5 A). Furthermore, no differences were observed in the levels of these proteins between sexes.

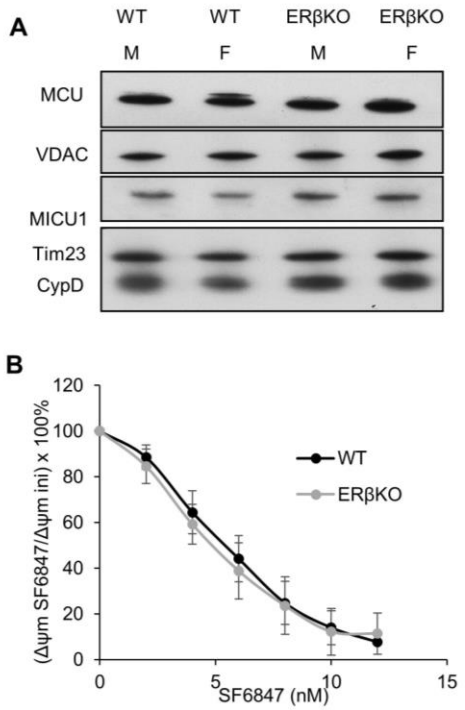

Figure 2-5*. Western blot and uncoupler titration in ERβKO*

A. Representative Western blot of MCU, VDAC, MICU1, CypD, and Tim23 as mitochondrial protein loading control in wild type (WT) and ERβKO male and female mouse brain mitochondria. **B**. Depolarization of wild type and ERβKO mitochondria in response to sequential additions (2nM each) of uncoupler SF6847. Data are calculated as the percentage of the initial membrane potential. n = 4 animals per group.

Mitochondrial calcium buffering ability is closely tied to Δψm, as calcium uptake via the MCU requires Δψm, and saturation of mitochondrial calcium uptake leads to loss of Δψm (Nicholls and Crompton, 1980). Thus, we determined whether differences in the ability to generate $\Delta\Psi$m existed between wild type and ERβKO brain mitochondria. To this end, we added sequential boluses (2 nM each) of the uncoupler SF6847 to purified brain mitochondria, and assessed mitochondrial depolarization upon each addition using the Safranin O fluorescence method. Upon addition of the uncoupler,

mitochondria attempt to maintain their Δψm by enhancing electron transfer and proton pumping in the RC. Therefore, the rate of depolarization can be taken as a measure of respiratory competence. Results indicated that wild type and ERβKO mitochondria did not differ in their ability to generate Δψm (n=4, Figure 2-5 B), because the rate of depolarization in response to SF6847 was virtually identical in the two genotypes. Together, these data excluded that the modulation of brain MPT by ERβ was due to effects on the expression of key mitochondrial calcium proteins or changes in mitochondrial bioenergetics.

2.4.4. ERβKO and CypD inhibition decrease cell death in female hippocampal slices exposed to oxygen glucose deprivation

Since calcium-induced MPT plays a role in ischemic brain injury (Starkov et al., 2004; Racay et al., 2009) and sex differences in ischemia-reperfusion injury have been extensively reported (Recently reviewed in (Girijala et al., 2016; Spychala et al., 2017)) we hypothesized that modulation of the ERβ-CypD axis of MPT could be involved in the pathogenic process.

To address this hypothesis, we used organotypic hippocampal slice cultures prepared from postnatal day 5 wild type or ERβKO littermates. Slices were treated with propidium iodide (PI) to label dead cells, and images were captured before and 24 hours after exposure to anoxic and glucose-free buffer (oxygen glucose deprivation, OGD). Throughout the OGD, slices were treated with either vehicle or CsA (1 μM). After assessing cell death induced by OGD, the same slices were treated with NMDA (1 mM) to induce maximal cell death.

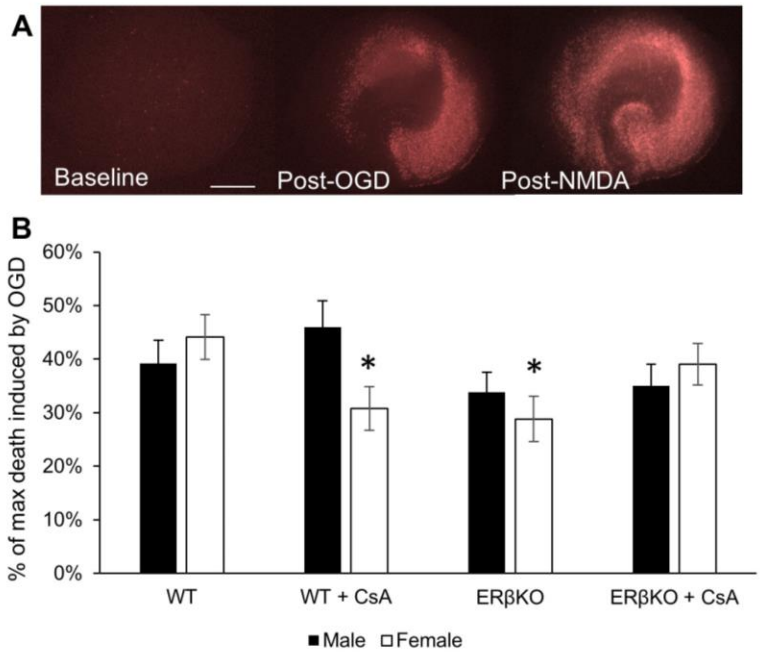

Figure 2-6*.Oxygen glucose deprivation in hippocampal slices*

A. Representative images of hippocampal slice cultures stained with propidium iodide (PI) (indicating cell death) at baseline, 24 hours post-oxygen glucose deprivation (OGD), and 24 hours post- treatment with 1 mM NMDA. Bar = 50 μm. **B**. Quantification of the percentage of PI fluorescence 24 hours post-OGD over the percentage of PI fluorescence post-NMDA treatment, with subtraction of fluorescence prior to any treatment. n = 24, 41, 5, 27, 32, 22, 27, 24 slices per group over 8 experiments; * $p < 0.05$ vs. wild type (WT) female.

A representative set of images of hippocampal slices subjected to this protocol is shown in Figure 6A. In slices from male mice, neither treatment with CsA nor genetic ablation of ERβ had any effect on cell death induced by OGD (Figure 2-6 B). However, in females, ERβKO had less OGD-induced cell death, when compared to wild type slices. Moreover, CsA treatment was protective in wild type female slices, but not in ERβKO slices (Figure 2-6 B). These data suggest that mechanisms underlying the pathological responses to

ischemic injury differ in males and females, and that the mitochondrial ERβ-CypD axis exerts modulatory effects on cell death only in females.

2.4.5. ERβ interacts with mitochondrial proteins in an estrogen-dependent manner

To begin investigating the mechanism of ERβ modulation on MPT we designed a cell-based system to identify ERβ binding partners in mitochondria using an unbiased approach based on co-immunoprecipitation (co-IP) and protein mass spectrometry (MS). Since the specificity of commercially available antibodies against ERβ is highly controversial (Snyder et al., 2010), we used a recombinant FLAG-tagged human ERβ DNA construct to express the full-length, 59 kDa protein (ERβ-FLAG) in COS-7 cells. COS-7 cells were utilized for this experiment, because they are efficiently transfected, allow for high expression of the transgene due to episomal replication of plasmids, and divide rapidly (18 hours), providing large number of cells for mitochondria isolation. Western blot using anti-FLAG antibody allowed for both the detection and the IP of the expressed protein. The recombinant ERβ-FLAG protein was detected in whole cell homogenates, as well as in the cytosolic and enriched mitochondrial fractions, confirming that the protein localizes to multiple cellular compartments, including mitochondria.

To address the role of the ERβ ligand estrogen in regulating its interactions with mitochondrial proteins, COS-7 cells were transfected with ERβ-FLAG and enriched mitochondria fractions were extracted 48 hours after transfection. Mitochondria were incubated with estrogen (17βE, 10 μM) or vehicle for 10 minutes and throughout all steps of protein co-IP. A FLAG antibody covalently bound to resins was used to co-IP proteins. As negative

control, cells mock transfected with empty plasmid were used. Finally, proteins were eluted and subjected to MS. Two independent experiments were conducted and only proteins that were detected and identified with high confidence (95%) were considered. Among these, we selected only proteins known to reside in mitochondria, which were >2 fold enriched in ERβ expressing cells treated with 17βE relative to mock and were not enriched in cells treated with vehicle. MS of proteins that Co-IP with ERβ identified a relatively small number of peptides that fulfilled the enrichment criteria described above (Table 1).

Table 1*. Peptides identified by mass spectrometry of proteins eluted after Co-IP with ERβ-FLAG.*

Numbers indicate the ratio of the abundance of the peptides enriched in FLAG Co-IP in either the presence or the absence of 17βE, normalized by the peptide abundance in the Co-IP eluate from mock transfected cells.

	FLAG Co-IP + 17βE / mock	***FLAG Co- IP / mock***
HADHB (mito trifunctional protein)	3.9	0.9
Calmodulin 2	3.1	0.8
Hsp10	2.5	0.9
Ribsomal protein L34	3.3	1.1
Ribosomal protein L30	6.9	1.1
Ribosomal protein L35	5.2	0.9
Ribsomal protein L13	7.4	0.9
Ribosomal protein S10	5.1	0.8
ATPase subunit α (F1)	2.6	0.9
ATPase subunit c (F0)	3.3	0.9

One of them was the trifunctional protein b (HADHB), an enzyme that catalyzes three steps of β-oxidation and interacts with complex I of the RC in the IM. Calmodulin, hsp10, and several of the mitochondrial ribosome protein components were also identified among ERβ interactors in mitochondria. In addition, the co-IP revealed subunit c of the F_0 ATPase and subunit α of the F_1 ATPase as ERβ binding partners, which was particularly intriguing because ATPase was previously identified as an ERβ binding partner in rat brain (Alvarez-Delgado et al., 2010). Furthermore, both the β subunit (Giorgio et al., 2013) and the c ring (Alavian et al., 2014) of the ATPase were proposed to be structural components of the MPT pore, and the ATPase complex was found to be a binding partner of CypD (Giorgio et al., 2009; Chinopoulos et al., 2011).

Since it was shown that CypD binds the ATPase complex at the level of the oligomycin sensitivity conferring protein (OSCP) in the lateral stalk of the complex (Giorgio et al., 2009; Beck et al., 2016), we investigated whether ERβ-FLAG could bind directly to OSCP. We transfected HEK293 cells with ERβ-FLAG or empty vector (pcdna) and treated them with either vehicle (ethanol) or 10μM 17βE for 24 hours. The presence of ERβ-FLAG in the mitochondrial fractions was confirmed by Western blot (Figure 2-7 A, left panel). Samples were subjected to co-immunoprecipitation using an antibody against OSCP or an IgG control and eluates were probed for OSCP, FLAG and CypD. OSCP was successfully pulled down in all samples (Figure 2-7 A, right panel), but we did not detect ERβ-FLAG interacting with OSCP. This result was in agreement with the ERβ-FLAG co-IP mass spectrometry data, as OSCP was not identified. Although a small amount of CypD was found in the

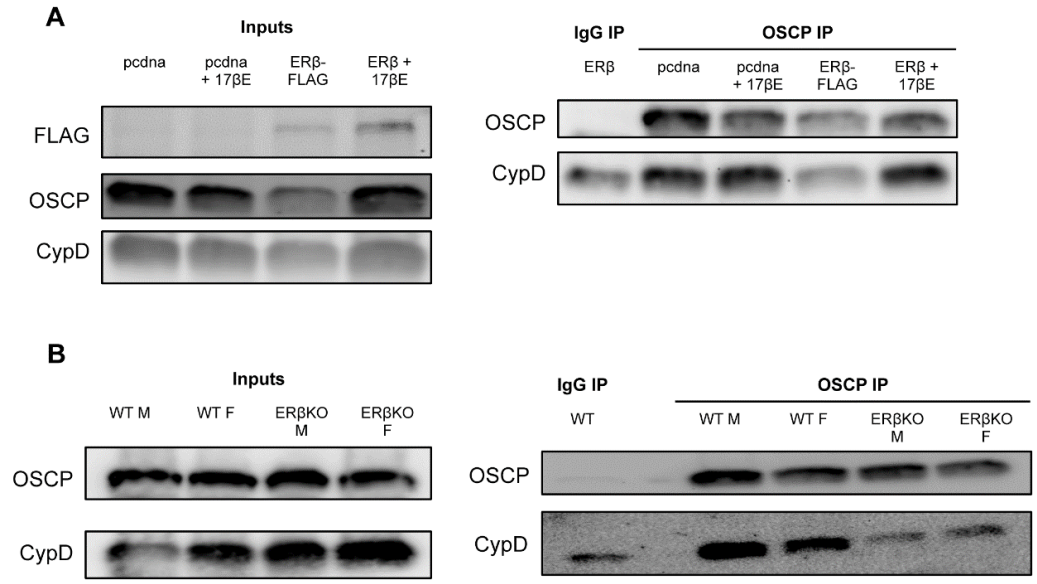

***Figure 2-7**. Protein-protein interactions*

A. Left: Western blot of FLAG, OSCP and CypD in enriched mitochondrial fractions from HEK293 cells expressing empty vector (pcdna) or ERβ-FLAG, with and without 17βE treatment. Right: Western blot of co-IP eluate from IgG IP or OSCP co-IP. **B**. Left: Western blot of OSCP and CypD in purified brain mitochondria from wild type (WT) and ERβKO males and females. Right: Western blot of co-IP eluate from IgG IP or OSCP co-IP.

IgG co-IP, indicating non-specific binding, it was clearly enriched in the OSCP co-IP, confirming previous observations (Giorgio et al., 2009; Beck et al., 2016).

Therefore, we tested the hypothesis that in mouse brain ERβ could modulate the interaction between OSCP and CypD. We performed co-IP of OSCP in purified brain mitochondria from wild type and ERβKO male and female mice. Western blot indicated that expression of OSCP and CypD did not differ among samples (Figure 2-7 B, left panel). Interestingly, co-IP of OSCP in these samples revealed that the interaction between OSCP and

CypD was greatly reduced in male and female ERβKO mitochondria, to levels comparable to the non-specific IgG control (Figure 2-7 B).

2.5. Discussion

We have identified a novel pathway for MPT modulation in brain that can contribute to sex differences in ischemic brain injury. We first demonstrated a sex difference in brain mitochondrial calcium capacity whereby female brain mitochondria undergo MPT at a lower calcium concentration than male mitochondria. Decreased mitochondrial calcium capacity reflects an increased propensity for calcium-dependent MPT pore opening. The consequences of increased MPT sensitivity depend on the properties of the pore opening. MPT may represent an irreversible permeabilization event resulting in mitochondrial swelling and release of solutes, including calcium and pro-apoptotic factors (Crompton et al., 1999; Hansson et al., 2011) or it could be a reversible, limited permeabilization event that can facilitate calcium release from the mitochondrial matrix and prevent calcium overload (Bernardi and von Stockum, 2012). Previous studies in rat heart show that female mitochondria are more resistant to calcium-induced swelling following a single calcium bolus than male mitochondria (Milerova et al., 2016), and have improved recovery from calcium-induced depolarization (Arieli et al., 2004). Furthermore, in heart mitochondrial calcium overload is a key cellular event following ischemia reperfusion, which profoundly affects the outcome of ischemia (Halestrap and Richardson, 2015). Taken together, this evidence suggests that sex differences in calcium-induced MPT can be linked to the differences observed in heart ischemia (Ostadal and Ostadal, 2014).

Little is known about the mechanisms of sex differences in ischemic brain injury and its potential links to MPT. However, because of the increased stroke risk in females, particularly in early menopause (Writing Group et al., 2010), it is possible that sex hormones and their receptors play a role in influencing stroke incidence by modulating brain MPT. Therefore, it could be hypothesized that decreased calcium capacity in female brain mitochondria is involved in increased susceptibility to stroke. On the other hand, a protective reversible MPT cannot be completely ruled out, since our experimental paradigm with consecutive boluses of calcium is designed to force brain mitochondria into irreversible pore opening. Future experiments with different conditions will be needed to address this possibility.

The isolated brain mitochondria used in these studies were prepared by a modified version of the original protocols developed by Sims, utilizing a Percoll gradient (Sims, 1990; Sims and Anderson, 2008). These mitochondria are considered non-synaptic mitochondria derived from post-synaptic neurons and glia. Synaptic mitochondria can be generated by Ficoll or Percoll gradients combined with digitonin or nitrogen cavitation, and are derived primarily from presynaptic terminals (Lai and Clark, 1979; Brown et al., 2004). Synaptic and non-synaptic mitochondria differ in morphology (Muller et al., 2005), MPT sensitivity to calcium (Brown et al., 2006), CypD content (Naga et al., 2007), and overall proteome (Stauch et al., 2014). The methods to prepare synaptic mitochondria can disrupt mitochondria and interfere with calcium-induced MPT (Brustovetsky et al., 2002), hence non-synaptic mitochondria are more frequently used to study MPT and were prepared for our studies. Mitochondria-associated ERβ has been identified in both dendrites and terminals, though its distribution varies between sub-regions. For example, in

some regions such as the hippocampus, only approximately 25% of ERβ immunoreactivity is found in axon terminals (Milner et al., 2005). Future work exploring the possible role of this ERβ-CypD axis specifically in synaptic mitochondria could also be interesting.

We used pharmacological and genetic approaches to begin to address the mechanisms underlying sex differences in brain MPT. We found that both inhibition and deletion of CypD eliminated the sex differences in mitochondrial calcium capacity, suggesting that CypD is a necessary component of the mechanism underlying sex differences. We also demonstrated that the ERβ antagonist PHTPP increased mitochondrial calcium capacity and eliminated sex differences. These findings were particularly intriguing, because they suggested a functional link between ERβ and CypD. Since MPT inhibition has been explored as a therapeutic target (Sileikyte and Forte, 2016), but its use has been traditionally challenging due to off target effects of CypD inhibition (Laupacis et al., 1982), we deemed that this finding could have applications in modulating MPT in conditions of brain calcium overload, such as ischemia. This led us to further investigate the role of ERβ in MPT.

We found that ERβ modulated sensitivity to CsA, as the inhibitory effect of CsA on MPT in brain mitochondria was attenuated by ERβKO, in both males and females. These data further confirmed the functional relationship between ERβ and CypD in modulating calcium capacity. However, since sex differences persisted in the calcium capacity of ERβKO brain mitochondria, we concluded that ERβ could not be the only molecular determinant of the sex differences.

Similar to our results in brain mitochondria, it was previously shown that male and female cardiac mitochondria also contain similar amounts of

CypD, VDAC and ATP synthase (Milerova et al., 2016), highlighting a role for protein-protein interaction, rather than protein expression levels, as the putative mechanism causing a blunted CsA effect in ERβKO brain mitochondria. Therefore, using co-IP of mitochondrial proteins with a tagged ERβ followed by unbiased MS approach, we searched for candidates for ERβ protein interactors in mitochondria. Interestingly, one of the identified proteins, HADHB, was previously shown to bind ERβ (Zhou et al., 2012b). Although the involvement of HADHB in MPT is still unknown, its location and interactions with IM components and ERβ, as well as its effects on cardiolipin (Taylor et al., 2012), make it an intriguing candidate for MPT regulation. The list also included Calmodulin (Toledo et al., 2014) and hsp10 (He and Lemasters, 2003), which have been implicated in MPT regulation, although the mechanisms of action are not yet known, and further studies will be needed to determine how these proteins affect MPT in brain.

Several of the mitochondrial ribosome protein components were also identified. The strong enrichment of the interaction of these proteins with ERβ by estrogen is surprising and the functional meaning unclear, especially in relationship to MPT. However, it is possible that ERβ in mitochondria has other functions, and the interactions with mitochondrial ribosomal proteins may suggest that ERβ and estrogen are involved in the regulation of mitochondrial protein synthesis.

The co-IP followed by mass spectrometry also revealed subunit c of the F_0 ATPase and subunit α of the F_1 ATPase as ERβ binding partners. This was a particularly interesting result for three reasons. First, the ATPase was previously identified as an ERβ binding partner in rat brain (Alvarez-Delgado et al., 2010). Second, both dimers of the β subunit (Giorgio et al., 2013) and

the c ring (Alavian et al., 2014) of the ATPase were proposed to be structural components of the MPT pore. Third, the ATPase was found to be a binding partner of CypD at the OSCP subunit of the complex (Giorgio et al., 2009; Chinopoulos et al., 2011; Beck et al., 2016). We performed co-IP studies using OSCP antibody in cultured cells and in brain mitochondria, which did not detect a physical interaction between ERβ and OSCP. However, ERβKO decreased the binding of OSCP to CypD in brain mitochondria, which could explain the decreased sensitivity to CsA in ERβKO mitochondria. Therefore, modulation of the interaction between OSCP and CypD could be the mechanism of MPT regulation by ERβ in brain mitochondria. Future work will take a closer look at these protein-protein interactions and their possible modulation by calcium or sex hormones by using genetic and pharmacological tools in cell culture models.

To seek proof of principle that ERβ and CypD play a role in modulating the sex differences in the outcome of ischemic injury we used an organotypic hippocampal slice culture OGD system. We tested the effects of CsA and ERβKO using male and female-derived slices, since previous reports showed that female-derived cultures were less susceptible to OGD injury than males (Li et al., 2005). We found the same baseline susceptibility to hippocampal cell death induced by OGD in male and female slices. However, female-derived slices were protected by CsA addition or by ERβKO, while male-derived cultures were not. This result supports the concept that ERβ and CypD play a role in modulating sex differences in ischemia. It also contributes to an increasing body of evidence on the role of ERβ in neuronal vulnerability, since it was shown that ERβKO is protective under oxidative stress in primary neuronal culture models (Yang et al., 2009), and human studies indicate that

males and females respond differently to stroke therapies (Dotson and Offner, 2017; Sohrabji et al., 2017).

In conclusion, this work identified new molecular players involved in sex differences in brain MPT regulation and mitochondrial calcium capacity. Importantly, the modulation of brain MPT may also be pathologically relevant to other sex biased brain degenerative conditions, in which mitochondrial calcium handling is altered, such as ALS (Damiano et al., 2006; Kim et al., 2012), AD (Supnet and Bezprozvanny, 2010) and PD (Martin et al., 2014a). Taken together, these findings suggest that the function of ERβ in modulating MPT could become a therapeutic target in neurodegeneration.

3. FUNCTION OF MITOCHONDRIAL PROTEIN CHCHD10

3.1. Abstract

Mutations in CHCHD10 are associated with myopathy, motor neuron disease, dementia, and Parkinson's disease. CHCHD10 is a conserved mitochondrial protein with yet unknown function. Here, we investigate CHCHD10 properties and the effects of its downregulation in cellular and mouse models. CHCHD10 associates with membranes in the mitochondrial intermembrane space (IMS) and its mitochondrial localization depends on cysteine residues in the twin CX_9C domain. Moreover, CHCHD10 interacts with a closely related IMS protein, CHCHD2. Both CHCHD10 and CHCHD2 interact with P32/GC1QR, a protein with various intra and extra-mitochondrial functions. CHCHD10 and CHCHD2 have short half-lives, suggestive of regulatory rather than structural functions. Acute silencing of CHCHD10 induces apoptosis in proliferating cultured cells, unrelated to bioenergetic defects, which is attenuated by recombinant CHCHD10 or CHCHD2. However, upon chronic CHCHD10 silencing, selected cells adapt to survive, suggesting that compensatory mechanisms exist. In vivo, CHCHD10 is expressed in many mouse tissues, most abundantly in heart, skeletal muscle, and liver, and in specific brain regions, notably the substantia nigra. Homozygote CHCHD10 knockout mice are born at Mendelian ratio, have no gross phenotypes, no mitochondrial bioenergetic defects or mitochondrial ultrastructure abnormalities in brain, heart or skeletal muscle, indicating that compensatory mechanisms occur in vivo. In summary, we describe novel CHCHD10 binding partners and show that while CHCHD10 prevents apoptosis, its loss can be compensated for by adaptive mechanisms. Taken

together, these results strongly indicate that the process leading to CHCHD10-linked human diseases are not based on loss of normal function of the protein.

3.2. Introduction

3.2.1. Mutations in CHCHD10 in disease

ALS, also known as Lou Gehrig's disease or motor neuron disease, is a rapidly progressing, fatal neurodegenerative disease characterized by loss of motor neurons. It is more recently thought that ALS and frontotemporal dementia (FTD) are at either end of a disease spectrum termed FTD-ALS, as there is overlap of cognitive and motor defects found in both diseases, and they are thought to share genetic mutations and pathogenic mechanisms (Lattante et al., 2015). About 5-10% of ALS cases are considered familial, while the majority are sporadic, meaning that they arise from unknown causes. Mutations in many of the genes associated with familial ALS have been identified, the most common being C9ORF72 and SOD1. Other disease associated mutations are in genes involved in protein degradation, RNA processing, trafficking, and several other functions (Robberecht and Philips, 2013; Therrien et al., 2016). Complex pathogenic mechanisms are involved in both the sporadic and familial forms of FTD-ALS (Peters et al., 2015). One of the major pathogenic mechanisms associated with ALS mitochondrial dysfunction (Damiano et al., 2006; Magrane et al., 2009; Kawamata and Manfredi, 2010; Palomo and Manfredi, 2015; Manfredi and Kawamata, 2016).

In recent years, several mutations in the gene encoding Coiled-Coil-Helix-Coiled-Coil-Helix Domain Containing 10 (CHCHD10) have been identified in families with ALS or FTD-ALS (Bannwarth et al., 2014; Johnson et

al., 2014; Muller et al., 2014; Dols-Icardo et al., 2015; Ronchi et al., 2015; Zhang et al., 2015; Perrone et al., 2017). Mutations in this gene have also been associated with several other diseases (Pasanen et al., 2016) including FTD (Jiao et al., 2016), mitochondrial myopathy (Ajroud-Driss et al., 2015), spinal muscular atrophy (Penttila et al., 2015), Charcot-Marie-Tooth disease (Auranen et al., 2015), late onset AD (Xiao et al., 2016) and PD (Rubino et al., 2017). Table 2 lists all reported CHCHD10 mutations associated with disease.

Table 2. *CHCHD10 disease mutations*

Mutation	***Disease***	***Reference***
Pro12Ser	ALS	Dols-Icardo, 2015
Arg15Ser (in cis G58R)	Mitochondrial myopathy	Arjoud-Driss, 2015
Arg15Leu	ALS	Müller, 2014; Johnson, 2014; Zhang, 2015
His22Tyr	FTD	Jiao, 2016
Pro23Thr	FTD	Zhang, 2015
Pro23Ser	FTD	Jiao, 2016
Ala32Asp	FTD	Jiao, 2016
Pro34Ser	FTD-ALS, ALS, PD	Chaussenot, 2014; Ronchi, 2015; Chiò, 2015; Perrone, 2017; Rubino, 2017
Ala35Asp	FTD, Late Onset AD	Zhang, 2015; Xiao, 2016
Val57Glu	FTD	Jiao, 2016
Gly58Arg	Mitochondrial myopathy	Arjoud-Driss, 2015
Ser59Leu	Mitochondrial myopathy, FTD-ALS	Bannwarth, 2014; Chaussenot, 2014
Gly66Val	ALS, Spinal muscular atrophy Jokela type, Charcot-Marie-Tooth disease type 2	Müller, 2014; Penttilä, 2015; Auranen, 2015; Pasanen, 2016
Pro80Leu	ALS, FTD-ALS	Ronchi, 2015; Zhang, 2015; Perrone, 2017
Gln82*	FTD	Dols-Icardo, 2015
Pro96Thr	FTD-ALS	Perrone, 2017
Gln108*	FTD, PD	Perrone, 2017

CHCHD10 is a 142 amino acid, nuclear-encoded, mitochondrial protein, and the first mitochondrial proteins to be associated with familial ALS. CHCHD10 is encoded by a highly conserved gene, which contains four exons (Figure 3-1 Top). The protein has two predicted domains, a mitochondrial targeting signal at the N-terminus, and a coiled-coil-helix-coiled-coil-helix domain at the C terminus (Figure 3-1 Bottom). Between these two domains is a hydrophobic alpha helix region, lacking a predicted functional or structural connotation. Despite ample evidence that mutations in CHCHD10 cause diseases in humans, the function of the protein remains unknown.

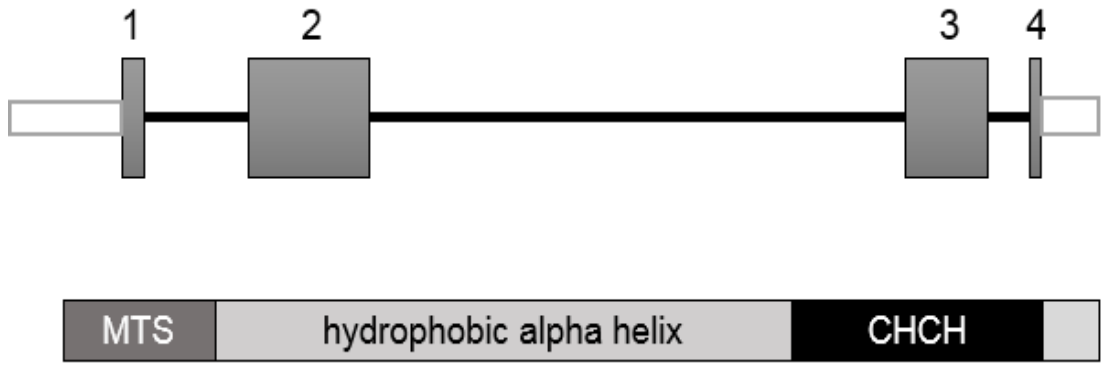

Figure 3-1*. CHCHD10 structure*

Top. CHCHD10 gene consists of 4 exons (grey boxes). Bottom. CHCHD10 protein contains a mitochondrial-targeting signal (MTS), a coiled-coil-helix-coiled-coil-helix domain (CHCH) separated by a hydrophobic amino acid stretch of unknown function.

3.2.2. Twin CX_9C proteins

CHCHD10 contains a twin CX_9C domain, which is characterized by two pairs of cysteines separated by nine amino acids that fold to form a coiled-coil-helix-coiled-coil-helix domain. CX_nC domains are found in many different proteins, and twin CX_9C domains are present in several proteins localized in mitochondria. In mitochondria, twin CX_9C proteins are typically retained in the IMS or IM after import through the action of the Mia40-Erv1 disulfide relay system, which is illustrated in Figure 3-2 (Hell, 2008; Koehler and Tienson,

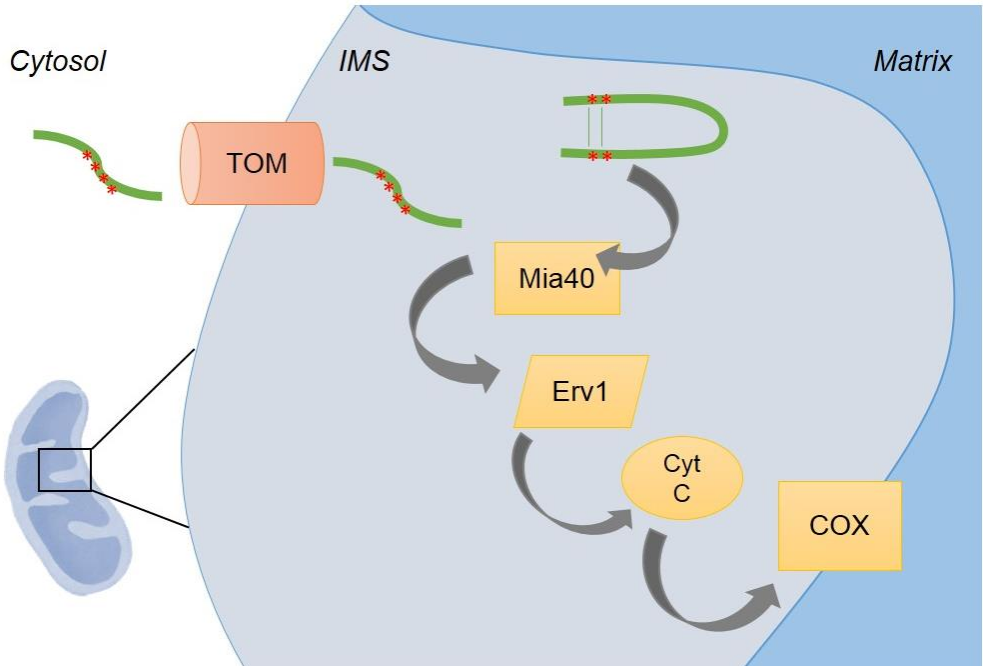

***Figure 3-2**. Mia40-Erv1 disulfide relay system*

Mitochondrial precursor proteins (green) enter the IMS via the TOM complex. In the IMS, they transiently bind to Mia40 via disulfide bonds between intramolecular cysteines (red asterisks). This results in the release of the CX_9C protein in an oxidized folded state, trapping it in the IMS. In this process, Mia40 is reduced, and it is reoxidized by Erv1, which donates its electrons to cytochrome c, feeding into the RC at cytochrome c oxidase (COX).

2009). The IMS was thought to be a reducing environment not conducive to disulfide bond formation, however, the discovery of Mia40 led to the identification of a protein import pathway that relies on thiol-disulfide exchange reactions occurring in the IMS (Stojanovski et al., 2008). Mitochondrial compartments contain several proteins that regulate the redox state and allow for oxidative protein folding, including thioredoxins and glutaredoxins, and the existence of a protein import pathway that relies on disulfide bonding highlights the importance of maintaining mitochondrial redox state (Chatzi et al., 2016).

A genome-wide analysis of eukaryotic twin CX_9C proteins revealed that these proteins have many functions and could be involved in the structural organization of molecular scaffolds in mitochondria (Longen et al., 2009; Cavallaro, 2010). Mia40 itself contains a twin CX_9C domain, which is thought to stabilize the protein in the IMS, where it interacts with newly imported IMS proteins (Chacinska et al., 2004). CHCHD1 is a component of the mitochondrial ribosome (Koc et al., 2013). The twin CX_9C proteins, NDUFS5, NDUFB7, and NDUFA8 serve as accessory subunits of RC complex I (Brandt, 2006; Cavallaro, 2010). Most twin CX_9C proteins with described functions are RC complex IV (cytochrome c oxidase, COX) assembly factors. For example, COX17 is a well-characterized mitochondrial copper chaperone containing a twin CX_9C domain which supplies copper to COX (Arnesano et al., 2005; Banci et al., 2008). The twin CX_9C proteins COX19 and CMC1 are also involved in copper trafficking to COX (Rigby et al., 2007; Horn et al., 2008; Horn et al., 2010).

The mitochondrial twin CX_9C proteins CHCHD3 (Li et al., 2016) and CHCHD6 (Ding et al., 2015) are components of the mitochondrial contact site

and cristae organizing system (MICOS). Sequence analysis of CHCHD3 and CHCHD6 predicts that they arose from a gene duplication event before the speciation of *Homo sapiens* and *Mus musculus*, and that they serve similar, but non-overlapping roles (Cavallaro, 2010). This study also predicated a similar gene duplication event for another pair of proteins CHCHD10 and CHCHD2, and suggested that these two proteins may have similar non-overlapping roles.

The functions of CHCHD10 and CHCHD2 are still in the early stages of investigation. Deletion of Mic17, the yeast homolog of CHCHD10 and CHCHD2, did not significantly affect mitochondrial respiration or structure (Longen et al., 2009). Until recently, very little has been published on the function of human CHCHD10 in mitochondria. One study in patient fibroblasts containing the S59L mutation in CHCHD10 suggested that this mutation in CHCHD10 altered mitochondrial cristae structure maintenance, because of faulty interactions with the major component of MICOS, mitofilin, and with CHCHD3 and CHCHD6 (Genin et al., 2016).

CHCHD2 (also called MNNR1), has several proposed functions, including regulating complex IV of the RC via a nuclear and mitochondrial localization (Aras et al., 2015), modulating cellular susceptibility to apoptosis (Liu et al., 2015), promoting cell migration (Seo et al., 2010; Wei et al., 2015), and priming cell differentiation (Zhu et al., 2016).

The sequence alignment of human proteins CHCHD10, CHCHD2, CHCHD3, and CHCHD6 is shown in Figure 3-3. This alignment highlights the evidence for the two gene duplications that gave rise to CHCHD3 and CHCHD6 or CHCHD2 and CHCHD10, respectively (Cavallaro, 2010). CHCHD10 and CHCHD2 are highly homologous (58% identity), while CHCHD3 and CHCHD6 are also homologous (35% identity), but there is no significant similarity between the two pairs. The only similarity resides in the twin CX_9C domain near the C terminus. This highlights the importance of investigating the functions of CHCHD10 and CHCHD2 in parallel, and

```
CHCHD10  ----------------------MPRG---SRSAASRPAS----------RPAAPSAHP 23
 CHCHD2  ----------------------MPRG---SRSRTSRMAPPASRAPQMRAAPRPAPVAQP 34
 CHCHD3  MGG--TTSTRRVTFEADENENITVVKGIRLSENVIDRMKESSP--------------SG 43
 CHCHD6  MGSTESSEGRRVSFGVDEEERVRVLQGVRLSENVVNRMKEPSS--------------PP 45

CHCHD10  PAHPP-PSAAAPAPAP----------------SGQPGLMAQMATTA------------ 52
 CHCHD2  PAAAP-PSAVGSSAAA----------------PRQPGLMAQMATTA------------ 63
 CHCHD3  SKSQRYSGAYGASVS-------DEELKRRVAEE----LALEQAKKES-----EDQKRLKQ 87
 CHCHD6  PAP--TSSTFGLQDGNLRAPHKESTLPRSGSSGGQQPSGMKEGVKRYEQEHAAIQDKLFQ 103

CHCHD10  -A--GVAVGSAVGHVMGSALTGAFSGGSSE---------------PSQPAVQQAPTPAA 93
 CHCHD2  -A--GVAVGSAVGHTLGHAITGGFSGGSNA--------------EPARPDITYQEPQGT 105
 CHCHD3  AKELDRERAAANEQLTRAILRERICSEEERAKAKHLARQLEEKDRVLKKQDAFYKEQLAR 147
 CHCHD6  VA--KREREAATKHSKASLPTGEGSISHEEQKSVRLARELESREAELRRRDTFYKEQLER 161

CHCHD10  -------------------------P-QPLQMGPCAYEIRQFLDCSTT-QSDLSLCEGF 125
 CHCHD2  -------------------------Q-PAQQQQPCLYEIKQFLECAQN-QGDIKLCEGF 137
 CHCHD3  LEERSSEFYRVTTEQYQKAAEEVEAKFKRYESHPVCADLQAKILQCYRENTHQTLKCSAL 207
 CHCHD6  IERKNAEMYKLSSEQFHEAASKMESTIKPRRVEPVCSGLQAQILHCYRDRPHEVLLCSDL 221

CHCHD10  SEALKQCKYYHGLSSLP--- 142
 CHCHD2  NEVLKQCRLANGLA------ 151
 CHCHD3  ATQYMHCVNHAKQSMLEKGG 227
 CHCHD6  VKAYQRCVSAAHKG------ 235
```

***Figure 3-3**. Protein sequence alignment*

Human CHCHD2, CHCHD10, CHCHD3 and CHCHD6 sequences were aligned using Protein Blast (NCBI).

suggests that their function may not overlap with the MICOS proteins CHCHD3 and CHCHD6, as previously suggested (Genin et al., 2016). Moreover, mutations in CHCHD2, like in CHCHD10, have been associated with familial PD (Ogaki et al., 2015; Shi et al., 2016), suggesting that the dysfunction of these two proteins may be involved in the pathways underlying neurodegenerative diseases.

The mitochondrial field has characterized the functions of many twin CX_9C proteins, but is currently in the very early stages of uncovering the function of CHCHD10 and CHCHD2. Here, we explore the physiological role of CHCHD10 in vitro and in vivo.

3.3. Material and Methods

3.3.1. Animals

CHCHD10 knockout animals in the C57Bl/6J background were generated using CRISPR/Cas9 technology (Yang et al., 2014) by The Jackson Laboratories. Plasmids encoding a signal guide RNA designed to introduce a mutation (a single nucleotide insertion of an A residue within exon 2, P16fs46ter) in the *Chchd10* gene and the *cas9* nuclease were introduced into the cytoplasm C57BL/6J-derived fertilized eggs with well recognized pronuclei. Correctly targeted embryos were transferred to pseudopregnant females. Correctly targeted pups were identified by sequencing and PCR and further bred to C57BL/6J (Stock No. 000664) to develop the colony. Animals were genotyped using the TransnetYX automated genotyping service, which uses a TaqMan-based, real-time PCR assay. Heterozygote males and females were bred to obtain CHCHD10KO animals and littermate controls, which were born

according to Mendelian ratio. Generation of founder mice was performed at The Jackson Laboratories, and all subsequent breeding for the described experiments was performed at Weill Cornell Medicine.

All experiments were approved by the Institutional Animal Care and Use Committee of the Weill Cornell Medicine and carried out in compliance with the National Institute of Health guidelines for the care and use of laboratory animals.

3.3.2. Cell culture

HEK293 cells were cultured in high-glucose Dulbecco's modified Eagle's medium (DMEM, Life Technologies) supplemented with 5% fetal bovine serum (Atlanta Biologicals) and 1% antibiotic-antimycotic (Life Technologies). To investigate protein turnover in cell culture, HEK293 cells were treated with cycloheximide (50 µg/mL, Sigma) in the culture medium. Cell number was determined by aspirating culture medium, washing twice with PBS to remove floating cells, and by trypsinizing and counting attached cells using a Beckman Coulter cell counter. HEK293 cells were selected for these experiments, as they are highly transfectable, allow for high expression of the transgene, and divide rapidly, providing large number of cells for mitochondria isolation.

Protein lysates or enriched mitochondrial fractions were prepared from cells where indicated. To prepare total lysates, cells were harvested in RIPA buffer (50 mM Tris-HCl (pH 7.4), 50 mM NaCl, 1% Triton-X, 5 mM EDTA, 10 mM $Na_4P_2O_7$, 50 mM NaF) for 30 minutes on ice and then centrifuged 13,000 rcf for 10 minutes at 4°C to obtain protein supernatants. To prepare the enriched mitochondrial fractions, cells were harvested and homogenized in

mannitol-sucrose buffer (225 mM mannitol, 75 mM sucrose, 5 mM HEPES, 1 mM EGTA, 1 mg/mL fatty-acid free BSA, pH 7.4), and centrifuged at 4°C at 800 rcf for 5 minutes. Supernatants were centrifuged at 10,000 rcf for 10 minutes, and pellets washed in BSA-free mannitol-sucrose buffer and then resuspended in mannitol-sucrose buffer. Protein concentrations were quantified using a BCA assay kit (Pierce).

3.3.3. Co-Immunoprecipitation

Co-Immunoprecipitation (Co-IP) experiments were performed on HEK293 cell mitochondrial fractions using a co-Immunoprecipitation kit (Pierce). Briefly, indicated antibody or normal mouse IgGs (ThermoFisher) were covalently coupled to IP resins. Mitochondria (0.5 mg) were resuspended in Co-IP lysis/wash buffer and incubated with the resins overnight. Proteins were eluted in the provided elution buffer and eluates neutralized with Tris-HCl pH 8.5. Western blot was performed to confirm the presence of the target protein in the Co-IP eluates. Results of Co-IP experiments were reproduced at least three times and representative Western blots are shown.

3.3.4. Western blot

Samples were prepared in Laemmli buffer with β-mercaptoethanol, then separated by SDS-PAGE on AnyKD Tris-acrylamide/bis-acrylamide gels (BioRad) and transferred to polyvinylidene fluoride membranes (BioRad) using the Trans Blot Turbo Transfer System. Membranes were probed overnight with the following primary antibodies: CHCHD10 (Sigma), CHCHD2 (Proteintech), OXPHOS subunit cocktail (MitoSciences), P32 (Abcam, used on cell lysates), P32 (Cell Signaling, used on mouse tissue), mitofilin (Thermo), Tim23 (BD Transduction Laboratories), and β-actin (Sigma). The specificities

of the CHCHD10 and CHCHD2 antibodies were confirmed by the absence of a band in the immunoblots following siRNA treatment. CHCHD10 antibody specificity was also demonstrated in the CHCHD10KO Western blots and immunohistochemistry experiments. Membranes were incubated with secondary antibodies (anti-mouse or anti-rabbit IgG (H+L), 1:10,000, LiCOR), and signal was detected using the Odyssey CLX Imager (LiCOR).

3.3.5. Blue native page

HEK293 were harvested by trypsinization, washed twice with ice cold PBS and resuspended in ice-cold PBS (100 µl). To obtain an enriched mitochondrial fraction, cells were incubated with 4 mg/ml digitonin (Sigma) in a final volume of 200 µl for 10 min on ice. Next, the cells were centrifuged (10 min, 10,000 g, 4 °C) and mitochondrial pellets were washed twice with 1 ml ice-cold PBS. Pellets were solubilized in 100 µl “ACBT buffer” containing 1.5M aminocaproic acid (Sigma) and 75 mM Bis-Tris (Sigma). To isolate mitochondrial OXPHOS complexes 20 µl 10% (w/v) β-lauryl maltoside (Sigma) was added and the solution was incubated for 10 minutes on ice. Following centrifugation (30 min, 10,000 g, 4 °C), the protein concentration was determined using a protein assay (Pierce) and gels were loaded with 20 µg of mitochondrial protein.

BN-PAGE was performed using a native page TM 4–16% Bis-Tris Gel (Invitrogen). Immunodetection was carried out by incubating PVDF membranes transferred using the Trans Blot Turbo Transfer System (BioRad), with antibodies directed against the NDUFA9 subunit of CI (CI-39; Abcam), the 70 kDa subunit of CII (CII-70, Invitrogen), the core2 subunit of CIII (CIII-core2; Abcam), subunit 2 of CIV (CIV-2; Abcam) and the α subunit of CV (CV-α;

Abcam). The secondary antibody consisted of IRDye 800CW Conjugated Goat Anti-mouse IgG (H+L), Highly Cross Adsorbed (LiCOR, 1:10,000). Fluorescence scanning was performed using an Odyssey Imaging system (LiCOR) and fluorograms were inverted for visualization purposes.

3.3.6. Plasmids, siRNA, and transfection

CHCHD10 silencing was achieved using three different Silencer Select siRNAs from Life Technologies: s53405 (A, in the 3' untranslated region), s196436 (B, in the 3' untranslated region), s226550 (C, in coding sequence), and the Silencer Select scrambled negative control (#4390846). CHCHD2 silencing was achieved using two different Silencer Select siRNAs: s224192 (A, in the 3' untranslated region), s56012 (B, in the 3' untranslated region). Transient transfection was performed using Lipofectamine RNAiMAX (ThermoFisher) according to manufacturer's instructions. HEK293 cell lines with CHCHD10 stable knockdown were created by generating lentiviral particles with the Mission shRNA CHCHD10 silencing construct (Sigma, SHCLNG-NM_213720) and selecting for transduced clones using puromycin (1 µg/mL) in the culture medium.

CHCHD10-FLAG (Vigene) and CHCHD2-FLAG (Sino Biological Inc.) overexpression plasmids with c-terminal FLAG tags were commercially available. The CHCHD10-myc plasmid was generated by mutagenizing the c-terminus of the FLAG construct to replace the tag (Agilent QuickChange II Site-Directed Mutagenesis Kit). Transient transfection and rescue experiments using both siRNA and overexpression plasmids were performed using Lipofectamine 2000 according to manufacturer's instructions. Stable cell lines with CHCHD10 or CHCHD2 overexpression were generated by transfecting

HEK293 cells and selecting for clones using puromycin (1 μg/mL) or G418 (500 μg/mL) in the culture medium.

3.3.7. Protease Protection Assay and Alkaline Extraction

For the protease protection assay, mitochondria were resuspended in 10 mM Tris-HCl pH 7, 10 mM KCl, 0.15 mM $MgSO_4$ with 0.25 M sucrose, or the same buffer without sucrose in order to cause swelling and produce mitoplasts. Mitochondria, mitoplasts, and sonicated mitochondria were treated with 0.62 μg/mL proteinase K for 20 minutes on ice and then centrifuged at 50,000 g for 15 minutes at 4°C.

For alkaline extraction, mitochondria were first ruptured by sonication. Soluble and insoluble fractions were obtained by centrifugation at 50,000 g for 15 minutes at 4°C. The pellet (insoluble fraction) was resuspended in 0.1 M Na_2CO_3 pH 11, and kept on ice for 30 minutes. The sample was centrifuged at the same speed in to separate the membrane associated (supernatant) and membrane embedded (pellet) proteins. Protein samples were analyzed by Western blot. These experiments were repeated at least three times and representative Western blots are shown.

3.3.8. Immunocytochemistry

Coverslips were washed with PBS, fixed in 4% paraformaldehyde for 20 minutes and washed with 20 mM glycine in PBS (PBS-glycine). Next, cells were permeabilized with 0.1% Triton X-100, washed with PBS-glycine, and blocked in 0.5% BSA in PBS-glycine. Coverslips were incubated in primary antibody for 45 minutes at 37°C, washed in PBS glycine, and incubated in secondary antibody (Cy2 or Cy3, Jackson ImmunoResearch) for 45 minutes at 37°C. Primary antibodies were used for CHCHD10 (Sigma), myc (Abcam),

cytochrome c (BioLegend), and Tom20 (SantaCruz FL-145). Coverslips were washed with PBS-glycine and mounted using Fluoromount-G (SouthernBiotech).

3.3.9. Quantification of mitochondrial TMRM accumulation

TMRM (tetramethyl rhodamine methyl ester) accumulation was used to measure $\Delta\Psi m$. Microscopy images of HEK293 cells stained with 10 nM TMRM (Invitrogen) were acquired using a TCS SP5 Confocal Microscope (Leica Microsystems) with an oil-immersion 40 × lens. Cells were washed twice and then imaged in HEPES-Tris (HT) imaging buffer (in mM: 132 NaCl, 4.2 KCl, 1 $MgCl_2$, 5.5 D-glucose, 10 HEPES, 1 $CaCl_2$, pH 7.4 with Tris base) at 37°C. The intensity for the region of interest was background corrected using a nearby extracellular region of identical size. At the end of the experiment, cells were treated with FCCP (1 µM) to determine the lowest fluorescence intensity and to prove that the loading of TMRM was comparable in different samples.

3.3.10. Caspase activity

Cells were homogenized in lysis buffer (25 mM HEPES pH 7.4, 0.1% Triton X-100, 5 mM $MgCl_2$, 2mM DTT, 1.5 mM EDTA, 1X protease inhibitor cocktail), incubated on ice for 10 minutes, and centrifuged at 13,000 g for 5 minutes. The supernatant was mixed with equal volume 2X assay buffer (20 mM HEPES pH 7.4, 100 mM NaCl, 1 mM EDTA, 0.1% CHAPS, 10% sucrose, 10 mM DTT), containing ac-DEVD-afc for caspase-3 or Ac-LEHD-afc for caspase-9 (each 5 µM, Cayman). Samples were incubated for 1 hour at 37°C and read in a plate reader with 405 nm excitation, 505 nm emission

wavelengths. Data were expressed as relative fluorescence intensity per mg protein (quantified from supernatant).

3.3.11. Mitochondrial isolation from tissue

Isolation and purification of mouse forebrain mitochondria was performed using a Percoll gradient as previously described (Damiano et al., 2006; Kim et al., 2012). The muscle (gastrocnemius) was mashed with scissors in a petri dish on ice. The tissue was homogenized with a glass-glass homogenizer on ice (30 times loose pestle, 30 times tight pestle) in MS-EGTA BSA buffer (210 mM mannitol, 70 mM sucrose, 1 mM EGTA, 5 mM HEPES, 0.5% fatty acid free BSA). The homogenate was filtered with gauze in order to remove fat and fibrous tissue and then was centrifuged at 600 g for 10 minutes at 4°C. The supernatant was collected and the pellet was homogenized a second time. The combined supernatants were finally centrifuged at 12,000 g for 10 minutes at 4°C. Heart mitochondria were prepared by homogenizing tissue with a Teflon-glass drill homogenizer on ice for 1 minute in MS-EGTA BSA (0.1%) buffer and spinning at 1000 g for 10 minutes at 4°C. The supernatant was centrifuged at 8000 g for 10 minutes at 4°C, and pellet resuspended in MS-EGTA and centrifuged again. The final mitochondrial pellets were resuspended in MS-EGTA without BSA and protein concentration was determined using a BCA Assay Kit (Pierce).

3.3.12. Measurement of COX activity

Cytochrome c oxidase (COX) enzymatic activity was measured spectrophotometrically (at 550 nm) using a previously described assay in isolated mitochondria from tissue or from cells permeabilized with n-dodecyl-maltoside (Birch-Machin and Turnbull, 2001). Sample was suspended in

10mM KH_2PO_4 (pH 7.4), and reduced cytochrome c (0.025 mM) was added to the cuvette. The rate of decrease of absorbance was calculated as nmol cytochrome c/min/million cells or mg protein using the extinction coefficient E=0.0195 x uM^{-1} x cm^{-1}.

3.3.13. Measurement of oxygen consumption

HEK293 cells were trypsinized, washed and resuspended in 100 µl of MS-EGTA buffer. Part of this suspension (3 µl) was used for protein concentration determination and the rest was added to the chamber. O_2 consumption was measured at 37 °C using polarographic oxygen sensors in a two-chamber Oxygraph (OROBOROS Instruments, Innsbruck, Austria). After the recording of the endogenous respiration in the presence of pyruvate (5mM), maximal O_2 consumption was determined by adding carbonyl cyanide 4-(trifluoromethoxy)phenylhydrazone (FCCP, 1 µM). At the end of the experiment, potassium cyanide (KCN, 1 mM) was added to completely inhibit the respiration.

Oxygraphic measurements of isolated mitochondria from brain, muscle and heart were performed using specific buffers and substrates: pyruvate (5 mM) and malate (2 mM) in MS-EGTA buffer with 4 mM H_2KPO_4, 1 mM $MgCl_2$ for brain; pyruvate (5 mM), malate (2 mM) and glutamate (5 mM) in KCl buffer (125 mM KCl, 20 mM HEPES, 4 mM H_2KPO_4, 1 mM $MgCl_2$, pH 7.2) for muscle; malate (2 mM) and glutamate (5 mM) in MS-EGTA buffer with 4 mM H_2KPO_4, 1 mM $MgCl_2$ for heart. Mitochondrial proteins (125 µg) were loaded in the chamber in the presence of substrates to determine non-stimulated, State 2 respiration rate. After addition of 0.5 mM ADP, stimulated State 3 respiration rate was assessed. The ATPase inhibitor carboxiactrattilosite (CATR, 1 µM)

was then added to inhibit mitochondrial respiration. To determine the maximal respiration, 2,4-Dinitrophenol (DNP, 40 µM) was added at the end of the experiment. Data analysis was performed using the Oroboros O2k DatLab software.

3.3.14. Measurement of ATP synthesis

ATP synthesis in HEK293 digitonin permeabilized cells (1.5 million), or mitochondria freshly isolated from tissues (20-60 µg) was measured using a rapid kinetic luminescence assay, as described in detail previously (Vives-Bauza et al., 2007). This assay monitors continuous ATP synthesis using a luciferase-luciferase system. Measurements were performed in buffer containing 5mM pyruvate and malate and expressed as nmol ATP/min/million cells or nmol ATP/min/mg protein.

3.3.15. Calcium capacity measurement

Calcium capacity was measured fluorimetrically using the ratiometric probe Fura-FF. Methods are described in Chapter 2 in more detail. In these studies, calcium capacity in cells was measured in buffer containing 125 mM KCl, 20 mM HEPES, 1 mM $MgCl_2$ (pH 7.2), 200 µg/mL fatty-acid free BSA, 4 mM KH_2PO_4, 0.2 mM ATP, 1 µM rotenone and 5 mM succinate. In brain, mitochondrial calcium capacity was measured using the same buffer and substrates described for brain mitochondrial oxygen consumption experiments above (with 25 µM EGTA, 200 µg/mL fatty-acid free BSA and 0.2 mM ATP). A single 25 µM calcium addition followed by consecutive 10µM additions were added to 0.15 mg mitochondria in the presence of Fura-FF (0.2 µM, Life Technologies).

3.3.16. Electron microscopy

Preparation of cell cultures for electron microscopy is described in (Cohen-Gould, 2013). Cells were washed with serum-free media or appropriate buffer then fixed with a modified Karnovsky's fix of 2.5% glutaraldehyde, 4% parafomaldehyde and 0.02% picric acid in 0.1 M sodium cacodylate buffer at pH 7.2 (Ito and Karnovsky, 1968). Following a secondary fixation in 1% osmium tetroxide, 1.5% potassium ferricyanide (de Bruijn, 1973), samples were dehydrated through an ethanol series, and embedded in situ in LX-112 resin (Ladd Research Industries). En face ultrathin sections were cut using a Diatome diamond knife (Diatome, USA, Hatfield, PA) on a Leica Ultracut ultramicrotome (Leica, Vienna, Austria). Sections were collected on copper grids and further contrasted with lead citrate (Venable and Coggeshall, 1965).

Perfusion of animals and fixation of tissue in 3.75% acrolein and 2% paraformaldehyde in 0.1M phosphate buffer was performed as described in detail in (Milner et al., 2011). Immunohistochemistry was performed on coronal brain sections (40 µM thick). Sections were coded by animal using punch codes and pooled together to ensure equal treatment throughout the procedure. Briefly, sections were incubated in 1% sodium borohydride in 0.1 M phosphate buffer, washed in 0.1 M Tris Saline, blocked in 0.5% BSA, and incubated in primary antibody in 0.1% BSA while shaking. Next, sections were washed and incubated in biotinylated secondary antibody and ABC Solution (Vector Laboratories) prior to 3,3’-Diaminobenzidine peroxidase labeling. Primary antibodies used in this study were anti-CHCHD10 (rabbit, Sigma) for light microscopy, and anti-Tyrosine Hydroxylase (sheep, Millipore) for electron microscopy.

To prepare tissue sections for electron microscopy, they were fixed with 2% glutaraldehyde, post-fixed in 2% osmium tetroxide, dehydrated in an ethanol series, flat embedded in Embed812 resin (Electron Microscopy Sciences, Hatfield, PA), cut (60-70 nm) using a Diatome diamond knife on a Leica Ultracut ultramicrotome (Leica Microsystems) and collected on grids. Sections were counterstained with uranyl acetate (5% brain, 1.5% muscle and heart) and Reynolds lead citrate, and viewed in a Tecnai (FEI) or JEM 1400 (JEOL, USA, Inc.) transmission electron microscope.

3.4. Results

3.4.1. CHCHD10 is a membrane-associated protein in the mitochondrial intermembrane space

CHCHD10 localizes to mitochondria, as illustrated by a double label immunocytochemistry experiment in HEK293 cells in which CHCHD10 fluorescence signal completely overlaps with that of the mitochondrial protein cytochrome c (Figure 3-4 A). To investigate the submitochondrial localization of CHCHD10, a protease protection assay was performed by our collaborators at University of Miami. Whole mitochondria, mitoplasts (mitochondria lacking the OM), and lysed mitochondria were prepared from HEK293 cells and treated with either vehicle or proteinase k to digest exposed proteins. Samples were loaded in a Western blot and membranes probed using antibodies against CHCHD10 or representative proteins for the mitochondrial IM and matrix. Upon protease treatment of whole mitochondria, only OM proteins were degraded (Figure 3-4 B). Upon protease treatment of mitoplasts, IM and

IMS proteins were digested. Proteins from all mitochondrial compartments were digested upon protease treatment of lysed mitochondria.

CHCHD10 was protected from digestion in whole mitochondria, but not in the mitoplast fraction, suggesting it localizes in the IMS or in the outer layer of the IM.

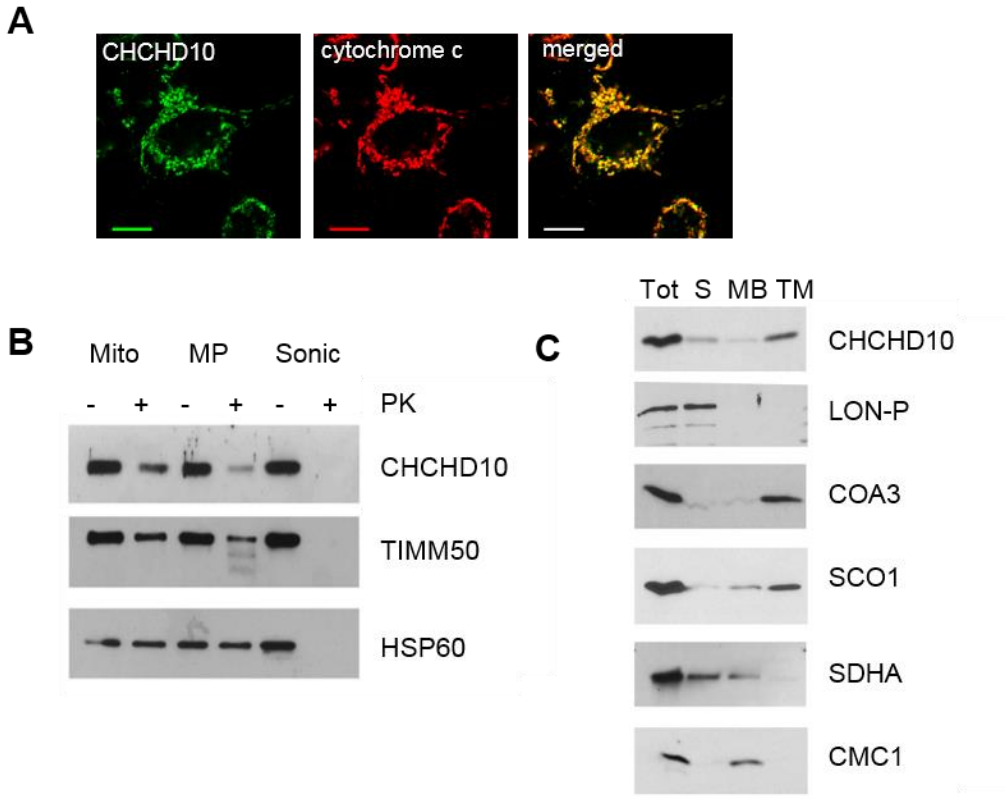

***Figure 3-4**. Mitochondrial localization of CHCHD10*

A. Immunocytochemistry of HEK293 cells stained with anti-CHCHD10 (green) and anti-cytochrome c (red) antibodies. Bar = 10 µm. **B**. Western blot of mitochondria (M), mitoplasts (MP) and sonicated mitochondria (Sonic) from HEK293 cells in the absence or presence of proteinase K (PK). Western blot of control proteins: TIMM50 (inner membrane), an HSP60 (matrix). **C**. Western blot of HEK293 mitochondria subjected to alkaline extraction using sodium carbonate. Western blot of control proteins: LON-P (soluble), COA3 (1 transmembrane domain), SCO1 (1 transmembrane domain), SDHA (loosely bound to membrane) and CMC1 (membrane bound). Total (Tot), soluble (S), membrane bound (M, and transmembrane (TM) fractions.

Next, we subjected mitochondrial fractions from HEK293 cells to sodium carbonate treatment followed by a high speed centrifugation to separate membrane bound and soluble proteins. Western blot of total mitochondrial protein, the soluble protein fraction, membrane associated fraction, and integral membrane associated fractions revealed that CHCHD10 was found in several fractions. While a fraction of the protein was soluble, a large portion appeared to be associated with mitochondrial membranes (Figure 3-4 C).

The twin CX_9C protein CHCHD2 is imported via the Mia40-Erv1 system, as a mutation of any one cysteine in this domain prevents CHCHD2 mitochondrial localization (Aras et al., 2015). To investigate whether CHCHD10 also requires the twin CX_9C domain for its mitochondrial localization, we generated a plasmid expressing CHCHD10 with a C-terminal myc tag (CHCHD10-myc) and a plasmid with a Cys to Ser mutation at position

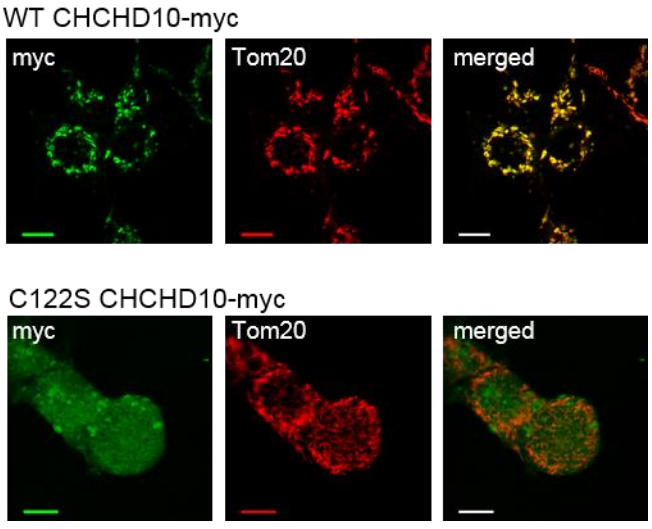

Figure 3-5*. CHCHD10 cysteine mutagenesis*

Representative images of immunocytochemistry of HEK293 cells transfected with WT CHCHD10-myc or C122S CHCHD10-myc. Coverslips stained with anti-myc (green) and anti-Tom20 (red) antibodies. Bar = 10 µm.

122 (C122S CHCHD10-myc). While CHCHD10-myc colocalized by immunostaining with the mitochondrial marker cytochrome c, C122S CHCHD10-myc showed a diffuse cytosolic staining, indicating that the Cys at position 122 is required for the mitochondrial localization of CHCHD10 (Figure 3-5). This confirmed that the twin CX_9C domain integrity is critical for mitochondrial import or retention, presumably by the Mia40-Erv1 system.

3.4.2. CHCHD10 and CHCHD2 are homologous binding partners that also bind P32

A previous study suggested that CHCHD10 interacts with mitofilin (IMMT), together with CHCHD3 and CHCHD6, in the mitochondrial inner membrane cristae organizing system (MICOS) (Genin et al., 2016). We sought to reproduce this interaction. We transfected HEK293 cells with a CHCHD10 construct containing a C-terminal FLAG tag (CHCHD10-FLAG) or empty vector, and prepared enriched mitochondrial fractions to be used for co-immunoprecipitation (Co-IP) of CHCHD10 and associated proteins using a

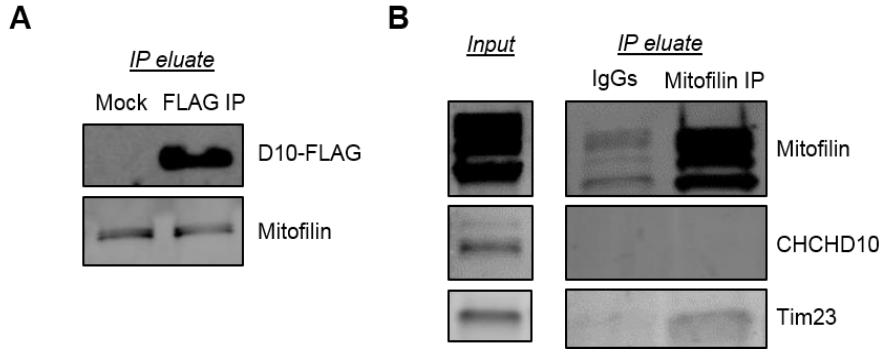

***Figure 3-6**. CHCHD10 and mitofilin do not interact.*

A. Mitochondria from empty vector (mock) or CHCHD10-FLAG transfected cells were subjected to Co-IP with FLAG antibody. Western blot of Co-IP eluate probed with FLAG and mitofilin antibodies. **B**. Mitochondria from HEK293 cells were subjected to Co-IP with mitofilin antibody or control IgG. Western blot of input and Co-IP eluate probed with mitofilin, CHCHD10, and Tim23 antibodies.

FLAG antibody. The Western blot confirmed the presence of CHCHD10-FLAG in the eluate (Figure 3-6 A). However, when we pulled down CHCHD10-FLAG, we detected mitofilin in the IP eluate, but mitofilin was also detected in the control IgG, indicating non-specific binding of mitofilin to IgGs (Figure 3-6 A). Therefore, we performed reverse Co-IP and pulled down mitofilin (Figure 3-6 B). We did not detect CHCHD10 in the mitofilin Co-IP eluate, but we were able to detect Tim23, which was previously shown to interact with mitofilin (Ding et al., 2015). Overall, our results indicated that CHCHD10 does not interact with mitofilin. Retrospectively, this result was not completely surprising, because the CHCHD10 sequence is highly dissimilar to the MICOS proteins CHCHD3 and CHCHD6 (Figure 3-3). Furthermore, CHCHD10 was not identified in a recent study that used crosslinking and mitofilin Co-IP followed by mass spectrometry (Janer et al., 2016).

Since we were unable to confirm the interactions with mitofilin, to search for new potential binding partners of CHCHD10 we used a candidate approach. Because CHCHD10 and CHCHD2 are homologous, we explored the possibility that they may physically interact. We performed Co-IP using mitochondria fractions from HEK293 cells expressing CHCHD10-FLAG and detected CHCHD2 in the FLAG Co-IP eluate, but not in the IgG control Co-IP indicating that the two proteins interact (Figure 3-7 A). We confirmed this interaction by performing the reverse Co-IP, in which cells were transfected with CHCHD2-FLAG and Co-IP performed with either FLAG antibody or control IgG, and identified CHCHD10 in the FLAG Co-IP eluate (Figure 3-7 B).

Next, we investigated whether CHCHD10 could also bind to itself to form homo-oligomers. Because of the C-terminal tags in the CHCHD10 construct, we could distinguish the recombinant CHCHD10 from the

endogenous, as it migrates higher in an SDS-PAGE gel. When we performed Co-IP of CHCHD10-FLAG using FLAG antibody, we did not detect endogenous CHCHD10 in the Co-IP eluate, indicating that CHCHD10-FLAG does not bind to endogenous CHCHD10 (Figure 3-7 C).

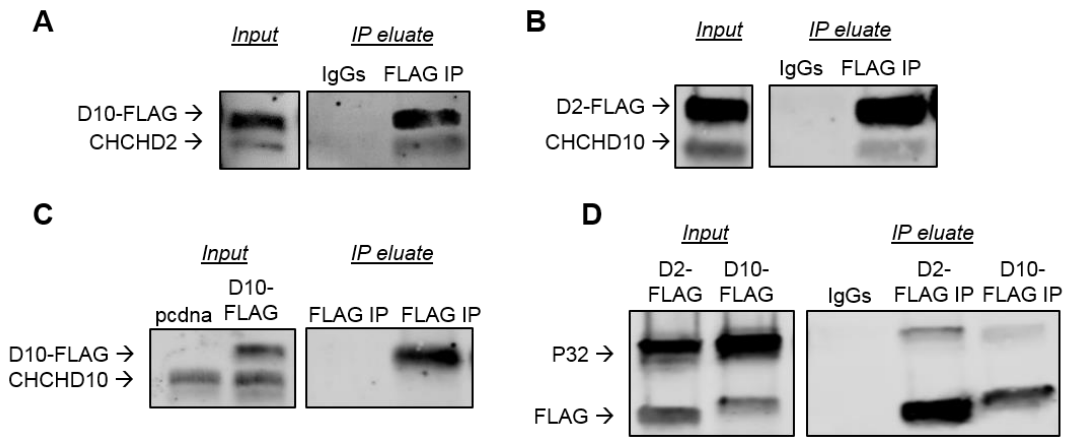

***Figure 3-7**. CHCH1D10, CHCHD2 and P32 Co-IP*

HEK293 cells were transfected with indicated plasmids and enriched mitochondrial fractions were prepared (Input). Co-IP with either FLAG antibody or control IgGs was performed (IP eluate) and samples were ran in Western blot. Membranes were probed with FLAG and additional antibody for indicated proteins.

A. Co-IP, CHCHD10-FLAG transfected cells. **B**. Co-IP, CHCHD2-FLAG transfected cells. **C**. Empty vector (pcdna) or CHCHD10-FLAG transfected cells, each used for Co-IP with FLAG antibody. **D**. Co-IP, CHCHD2-FLAG or CHCHD10-FLAG cells.

CHCHD2 was shown to bind to a protein named P32 (Seo et al., 2010), otherwise known as HABP1, C1QBP, and GC1QR. Because of the sequence homology and physical interaction between CHCHD10 and CHCHD2, we investigated whether CHCHD10 also interacted with P32. We transfected HEK293 cells with either CHCHD2-FLAG or CHCHD10-FLAG, prepared mitochondrial fractions, and performed Co-IP using a FLAG antibody. We confirmed the previously reported interaction between CHCHD2 and P32, and

also detected P32 in the CHCHD10-FLAG Co-IP eluate, but not in the control IgG eluate, indicating that P32 and CHCHD10 physically interact in mitochondria (Figure 3-7 D). Taken together the Co-IP experiments suggested the existence in mitochondria of a protein complex containing CHCHD10, CHCHD2, and P32.

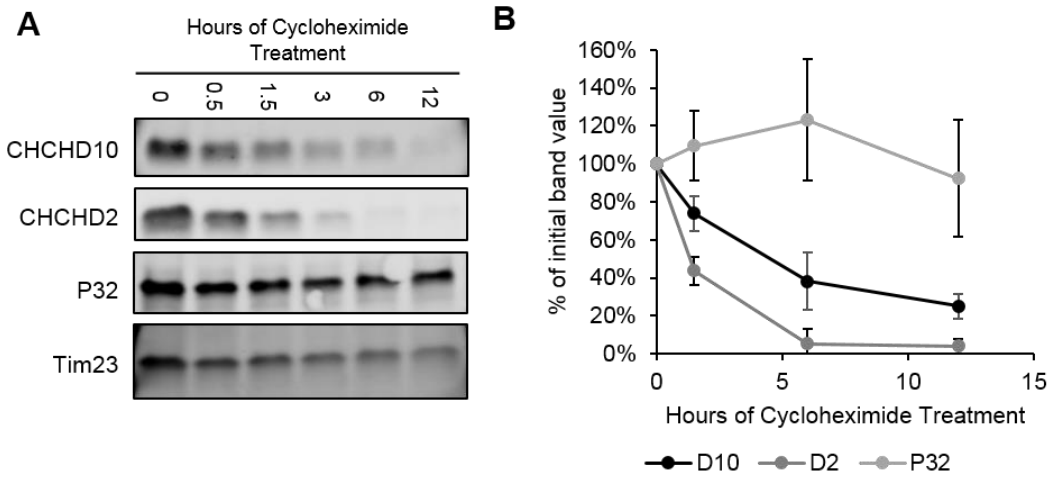

***Figure 3-8**. Cycloheximide treatment*

A. HEK293 cells were treated with cycloheximide for indicated number of hours and harvested for Western blot using antibodies against CHCHD10, CHCHD2, P32 and Tim23 (IM protein). **B**. Quantification of band intensity following, 1.5, 6 or 12 hours of cycloheximide treatment. Data are expressed as percentage of the band intensity at 0h for each protein. n = 3 experiments, 2 samples per time point.

Next, to further characterize the properties of these interacting proteins we investigated the turnover of endogenous CHCHD10, CHCHD2, and P32 in HEK293 cells. We treated cells with cycloheximide to inhibit protein translation for 0.5, 1.5, 3, 6 and 12 hours. Western blot of whole cell homogenates was used to examine the turnover of these proteins over time (Figure 3-8 A). We observed that CHCHD10 and CHCHD2 levels decreased rapidly (Figure 3-8), while P32 and Tim23 (IM CX_3C protein) had a much slower decline,

suggesting that both CHCHD10 and CHCHD2 are rapidly degraded proteins. Moreover, the turnover of CHCHD2 was faster than that of CHCHD10 (Figure 3-8 B), suggesting that the degradation of these two proteins can be differentially regulated, and that CHCHD10 and CHCHD2 can exist independently.

3.4.3. Transient silencing of CHCHD10 decreases cell number

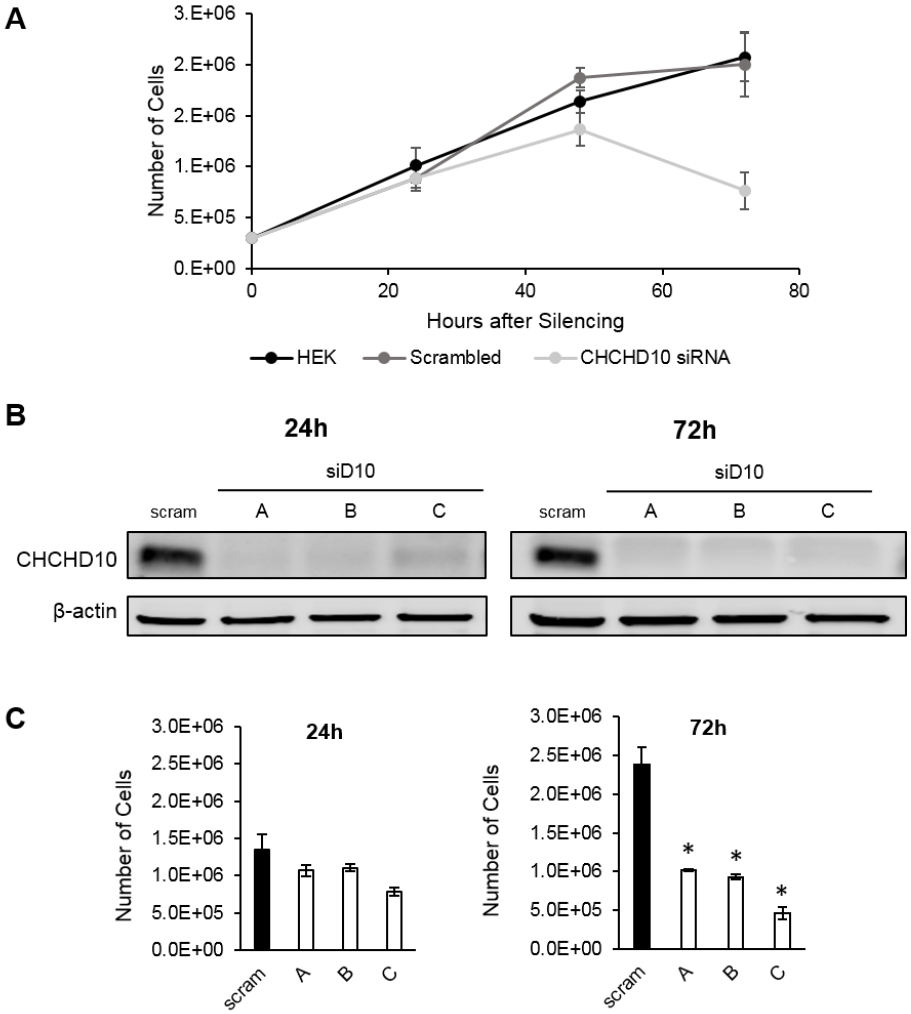

***Figure 3-9**. CHCHD10 siRNA in HEK293 cells*

A. HEK293 cell number in untreated (HEK), or following 24, 48 and 72 hour treatment with scrambled or CHCHD10 siRNA. n = 3. **B**. Western blot of cell homogenates and following 24 or 72 hours of treatment with scrambled (scram) siRNA or CHCHD10 (siD10) siRNAs. **C**. Quantification of HEK293 cell number following 24 or 72 hours siRNA treatment. * $p < 0.05$ vs. scram, n = 3 wells each.

To start exploring the function of CHCHD10, we transfected HEK293 cells with a siRNA against CHCHD10, and noticed a decrease in cell number in silenced cells following 72 hours of siRNA treatment(Figure 3-9 A). We repeated this experiment with two more unique siRNAs (called B and C), each targeting a different region of the CHCHD10 mRNA sequence. All three siRNAs caused a rapid and almost complete silencing of CHCHD10 expression after 24 hours of treatment that persisted at 72 hours, as demonstrated by Western blot (Figure 3-9 B). After 24 hours of siRNA treatment, no differences in the cell number were observed. However, 72 hours after silencing, a significant decrease in cell number was observed in cells silenced with all three CHCHD10 siRNAs (Figure 3-9 C).

We also silenced CHCHD2 using two different siRNAs (Figure 3-10 A) directed against different regions of the mRNA. After 24 or 72 hours of siRNA treatment, we did not observe differences in the number of cells (Figure 3-10 B). Furthermore, transient simultaneous silencing of both CHCHD2 and CHCHD10 (Figure 3-10 C) induced a decrease in cell number similar to that of CHCHD10 silencing alone (Figure 3-10 D), suggesting that there were no additive effects of co-silencing.

Next, we investigated whether overexpression of a CHCHD10 or CHCHD2 could rescue the loss of cell viability induced by CHCHD10 siRNA treatment. We co-transfected HEK293 cells with plasmids (pcDNA empty vector, WT CHCHD10-myc or CHCHD2-FLAG) and siRNA (scrambled or siD10 A). We chose siD10A because it targets the 3'UTR of the mRNA, which is not present in the recombinant CHCHD10-myc construct, and therefore does not silence it. Western blot confirmed the expression of the recombinant proteins (Figure 3-11 A). After 72 hours, expression of CHCHD10 or CHCHD2

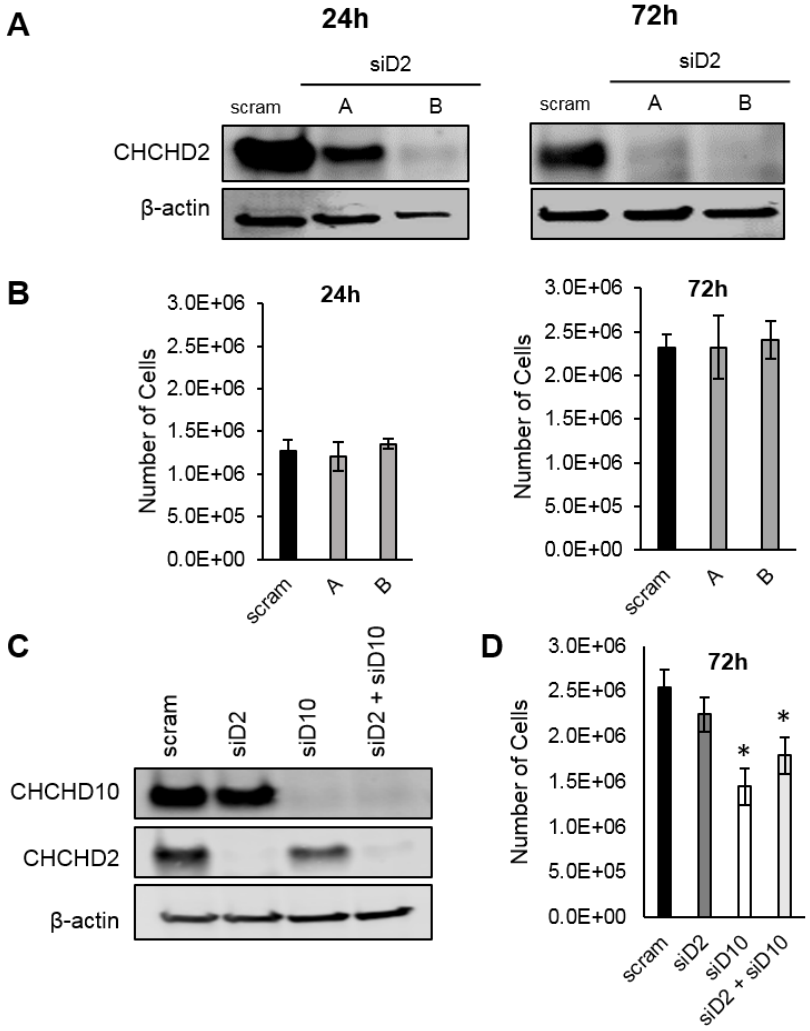

Figure 3-10. *CHCHD2 siRNA in HEK293 cells*

A. Western blot of cell homogenates and following 24 or 72 hours of treatment with scrambled (scram) siRNA or CHCHD2 (siD2) siRNAs. **B**. Quantification of HEK293 cell number. n = 3 wells each. **C**. CHCHD2 and CHCHD10 combination silencing Western blot. **D**. Quantification of cell number. * $p < 0.05$ vs. scram, n = 6 wells each.

constructs had no effect on cell number in cells treated with the scrambled siRNA. However, both constructs resulted in a partial rescue of cell number in cells treated with CHCHD10 siRNA (Figure 3-11 B). This indicates that, while silencing CHCHD2 does not result in loss of cell viability, its expression is able

to cross-complement the effects of CHCHD10 silencing, suggesting that some functional overlap exists between CHCHD10 and CHCHD2.

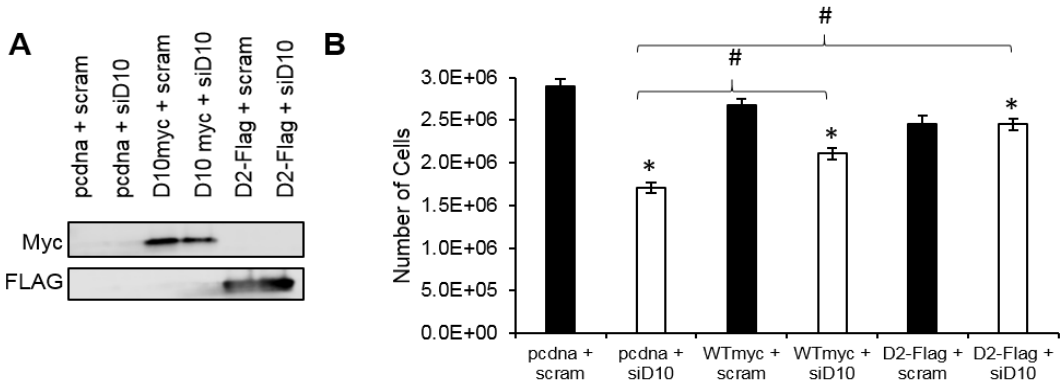

***Figure 3-11**. Rescue of cell number loss induced by CHCHD10 silencing*

A. Western blot of HEK293 transfected with scrambled or CHCHD10 siRNA (siD10 A) and empty vector (pcdna), CHCHD10-myc, or CHCHD2-Flag, overexpression plasmids. **B**. Quantification of cell number after 72 hours of treatment with siRNA and/or pcdna, CHCHD10-myc, or CHCHD2-FLAG overexpression plasmids. * $p < 0.05$ vs. pcdna + scram, # $p < 0.05$ between groups, n = 8 wells each.

3.4.4. CHCHD10 silencing triggers apoptosis.

To understand the nature of the cell viability loss induced by CHCHD10 silencing, we examined the mitochondria-dependent apoptosis using a variety of approaches.

The ability to maintain $\Delta\Psi m$ is usually compromised when cell undergo apoptosis (Zamzami et al., 1995) and a decline in $\Delta\Psi m$ indicates mitochondrial dysfunction. Therefore, we examined $\Delta\Psi m$ using the potentiometric probe TMRM at 24, 48, and 72 hours after treatment with CHCHD10 siRNA (Figure 3-12 A). Despite effective protein silencing at 24 hours (Figure 3-9 A) $\Delta\Psi m$ was maintained (Figure 3-12 A). However, there

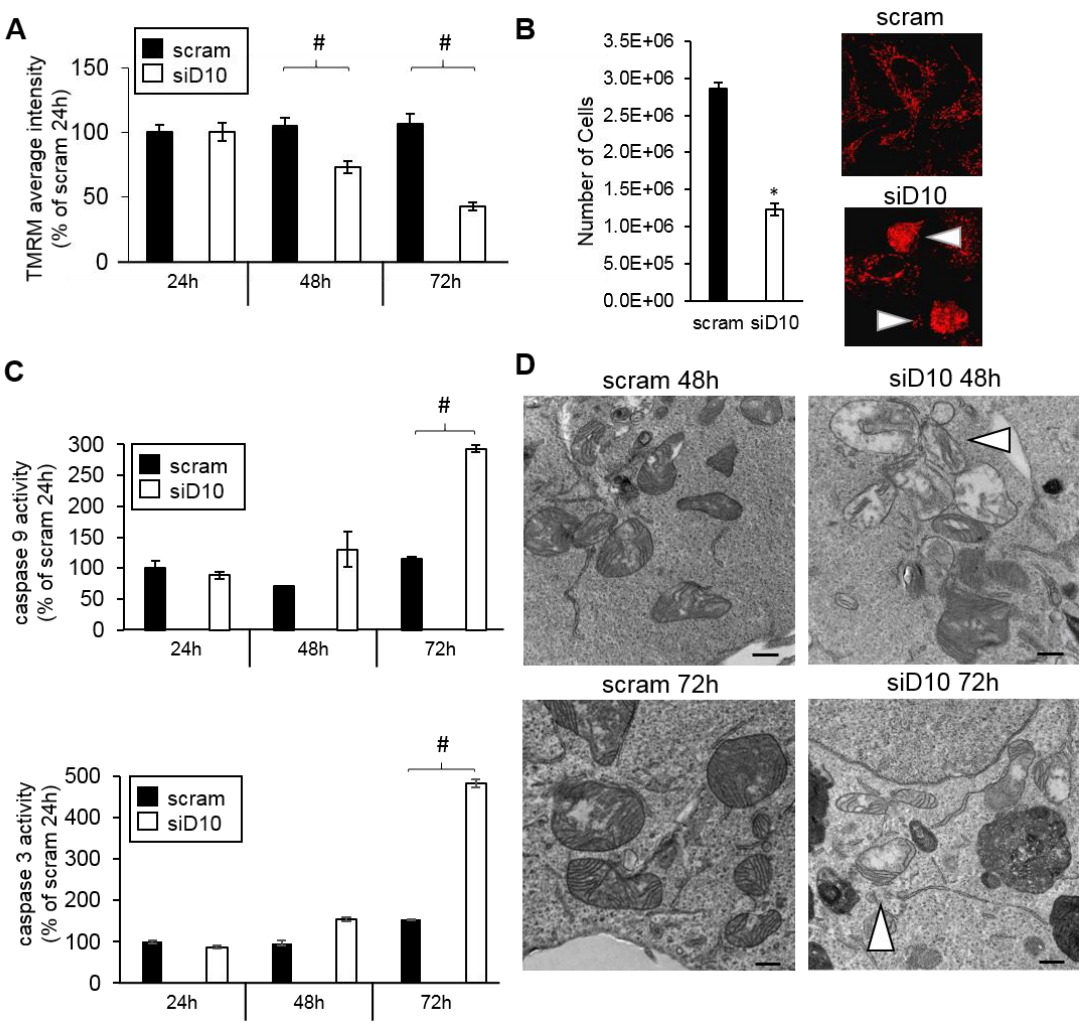

***Figure 3-12**. CHCHD10 silencing and apoptosis*

A. Mitochondrial membrane potential measured by average TMRM intensity in cells treated with scrambled or CHCHD10 siRNA for 24, 48 or 72 h. Data are represented as the percentage of the TMRM intensity of cells treated with scram siRNA for 24h. **B**. Quantification of HeLa cell number after 96h of scram or siD10 siRNA treatment. * $p < 0.05$, $n = 3$. Immunocytochemistry of cytochrome c in HeLa cells after 72h. Arrowheads indicate cells with diffuse staining, indicating cytochrome c release from mitochondria into the cytosol. **C**. Caspase 9 activity in cells treated with scrambled or CHCHD10 siRNA for 24, 48 or 72h. Data are represented as percentage of the cells treated with scram siRNA for 24h. # $p < 0.05$, $n = 3$ experiments in triplicate. Caspase 9 activity in cells treated with scrambled or CHCHD10 siRNA for 24, 48 or 72h. Data are represented as percentage of cells treated with scrambled siRNA for 24 hours. # $p < 0.05$, $n = 3$ experiments in triplicate. **D**. Electron micrographs of HEK293 cells 48 or 72h after treatment with scrambled or CHCHD10 siRNAs. Arrows indicate mitochondria with abnormal cristae. Bar = 500 nm.

was a significant $\Delta\Psi m$ decrease in silenced cells at 48 hours, which further declined at 72 hours (Figure 3-12 A). This indicated that in silenced cells mitochondria are unable to maintain normal $\Delta\Psi m$ in the period preceding the time of decline in cell number (i.e., 72 hours).

We then investigated cytochrome c release from mitochondria by immunocytochemistry, as indicated by diffuse cytochrome c staining, which is a marker of activation of the mitochondrial apoptotic pathway (Kluck et al., 1997; Kluck et al., 1999; Goldstein et al., 2000). For this experiment we used HeLa cells, which have a larger size and a flatter morphology than HEK293 cells, which allows for better imaging. HeLa cells treated with scrambled and CHCHD10 siRNA also showed a decrease in cell number, although it reached statistical significance at 96 hours, slightly later than HEK293 cells (Figure 3-12 B). Cytochrome c release was detected in HeLa cells after 72 hours of CHCHD10 silencing, but not in cells transfected with scrambled siRNA (Figure 3-12 B), suggesting that the loss of cell number was caused by apoptotic cell death.

To further investigate apoptotic event in CHCHD10 silenced HEK293 cells, we measured caspase 9 and caspase 3 activities using a fluorimetric assay. Both caspase activities were significantly increased 72 hours after CHCHD10 silencing compared to scrambled control (Figure 3-12 C), confirming the activation of the mitochondrial apoptotic pathway.

Since mitochondrial apoptosis is usually associated with alterations in mitochondrial structure, notably loss of cristae integrity (Scorrano et al., 2002; Scorrano, 2009), we studied the mitochondrial cristae structure by electron microscopy in cells treated with CHCHD10 siRNA or a scrambled control

siRNA. Abnormal mitochondrial ultrastructure, characterized by swelling of the matrix space and cristae disruption, was evident in CHCHD10 silenced cells at 48 and 72 hours (Figure 3-12 D). Taken together, this evidence indicates that transient silencing of CHCHD10 triggers a pro-apoptotic cascade, likely initiated in mitochondria, which also results in loss of $\Delta\Psi m$ and mitochondrial integrity.

Since OXPHOS is a critical mitochondrial function and some twin CX9C proteins participate in RC complex assembly (Horn et al., 2008; Horn et al., 2010), we investigated the RC in HEK293 cells upon CHCHD10 silencing. Using an antibody cocktail against one subunit of each of the five RC complexes, by Western blot we did not detect an effect of CHCHD10 silencing on the levels of these subunits after 72 hours of siRNA treatment (Figure 3-13 A). Furthermore, no differences were found in assembled RC complex levels, as assessed by blue native PAGE and Western blot (Figure 3-13 B). Functionally, there was a moderate decrease in COX activity (Figure 3-13 C). However, this moderate decrease did not result in respiration (Figure 3-13 D) in intact cells treated with CHCHD10 siRNA compared to scrambled siRNA, nor did it result in ATP synthesis defects, measured by a kinetic luminescence-based assay in permeabilized cells (Figure 3-13 E). Taken together, these results indicate that apoptotic cell death following CHCHD10 transient silencing was not directly caused by inability of mitochondria to produce ATP.

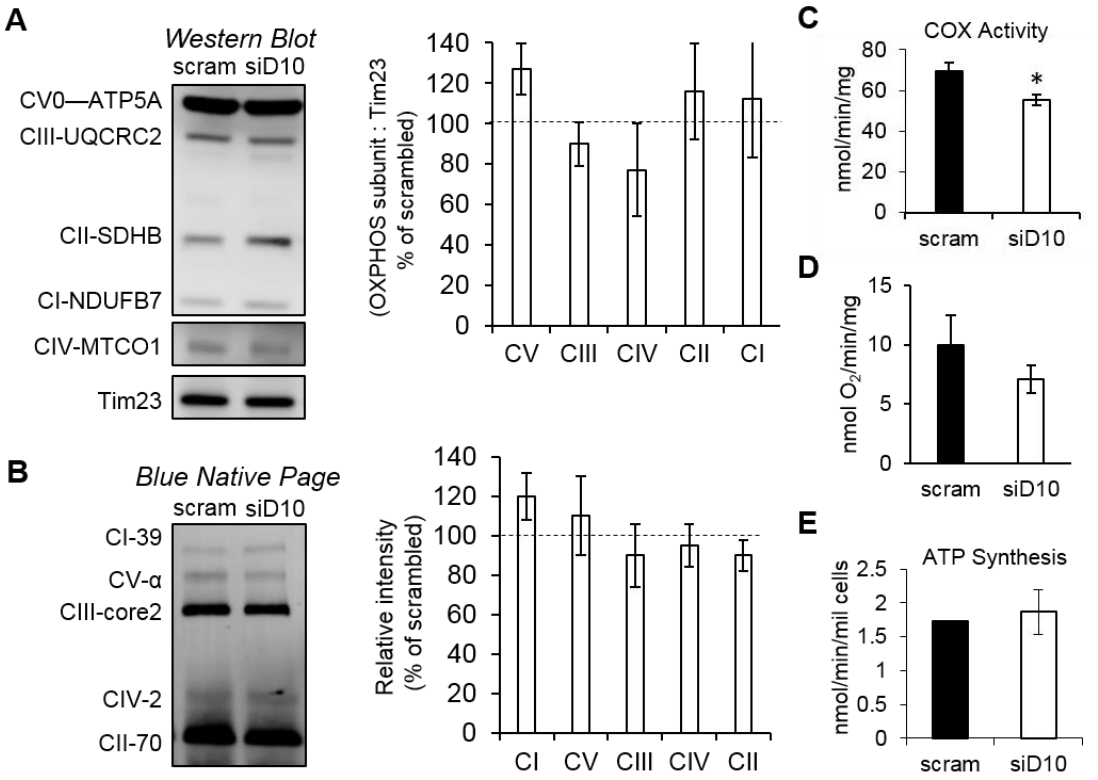

***Figure 3-13**. CHCHD10 and OXPHOS complexes in HEK293 cells.*

A. Representative Western blot and quantification of OXPHOS complex subunits and Tim23 (mitochondrial loading control) in HEK293 cell homogenate after 72h of treatment with scrambled (scram) or CHCHD10 siRNA (siD10). Data are represented as percentage of scram control. **B**. Representative blue native gel and quantification of OXPHOS complex subunits in HEK293 cell homogenate after 72h of treatment with scram or siD10 siRNA. Data are represented as percentage of scram control. n = 3 wells each. **C**. Cytochrome c oxidase (COX) activity in cells treated for 48h with scram or siD10 siRNA. * $p < 0.05$, n = 6 wells in triplicate. **D**. Oxygen consumption in intact cells treated for 48h with scram or siD10 siRNA. n = 6 experiments. **E**. ATP synthesis in permeabilized cells treated for 48h with scram or siD10 siRNA. n = 3 wells each in duplicate.

3.4.5. HEK293 cells with stable knockdown of CHCHD10 are viable

To address the effects of chronic CHCHD10 silencing, we generated stable cell lines, in which CHCHD10 was knocked down. HEK293 cells were transduced with lentivirus expressing either a CHCHD10 shRNA or a scrambled shRNA, and clones were selected in puromycin. All stable clones generated showed approximately 80% CHCDH10 silencing (Figure 3-14 A). However, no clones with complete CHCHD10 silencing were identified (out of 8 clones). Similar to CHCHD10 transient silencing, stable CHCHD10 silencing did not affect CHCHD2 and P32 expression levels (Figure 3-14 A). However, unlike the transiently silenced cells, the stable CHCHD10 shRNA cell lines showed no loss of viability and no growth differences compared to scrambled shRNA (Figure 3-13 B). Furthermore, no defects in COX activity (Figure 3-14 C) or ATP synthesis (Figure 3-14 D) were observed in the stable CHCHD10 shRNA lines.

The CHCHD10 and CHCHD2 binding partner P32 was proposed as a MPT pore candidate (Starkov, 2010), Thus, we measured the calcium capacity of mitochondria extracted from control and CHCHD10 knockdown HEK293 stable lines. Calcium capacity was measured fluorimetrically using the ratiometric calcium probe Fura-FF. Mitochondria were subjected to repeated bolus calcium additions, until they were no longer able to take up the added calcium, suggesting the occurrence of MPT. Calcium traces were virtually identical in control and knockdown mitochondria (Figure 3-14 E), suggesting that CHCHD10 silencing does not affect calcium uptake and calcium-induced MPT in HEK293 cells.

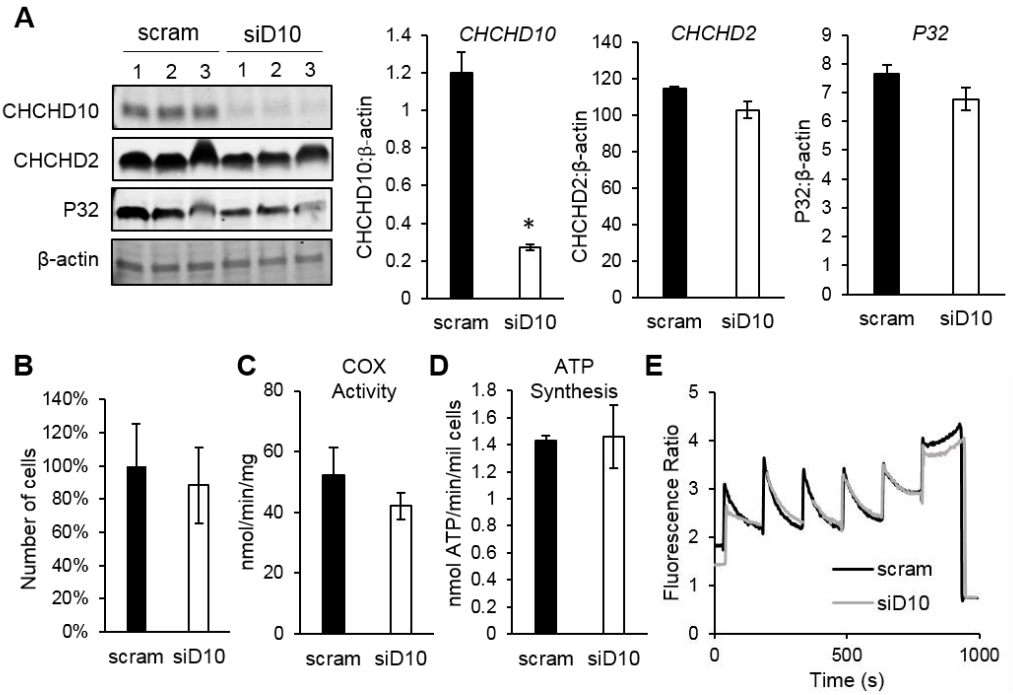

Figure 3-14*. CHCHD10 stable knockdown HEK293 cell lines*

A. Western blot of CHCHD10, CHCHD2, P32, and β-actin of homogenates (50 µg) of 3 cells lines stably expressing scrambled shRNA (scram) and 3 cell lines stably expressing CHCHD10 shRNA (siD10). Quantification of band intensity normalized by β-actin loading control. **B**. Number of cells 48 hours after seeding either scram or siD10 stable HEK293 line. Data are expressed as percentage of scram. n = 3 samples each. **C**. COX activity in scram or siD10 stable line. n = 3 experiments in triplicate. **D**. ATP synthesis in a scram or siD10 stable line measured using a luciferase-based assay. n = 3 experiments in duplicate. **E**. Representative Fura-FF calcium capacity traces of scram and siD10 HEK293 cells with one 25 µM calcium addition and sequential 10 µM calcium additions followed by a final addition of 1 mM EGTA.

Taken together, these results demonstrated that stably silenced HEK293 cells can survive with low levels of CHCHD10, and that chronic CHCHD10 reduction does not disrupt mitochondrial function. This indicates that upon selection cells are able to adapt to CHCHD10 decrease and that this

adaptation does not involve compensation by increased expression of CHCHD2.

3.4.6. CHCHD10 and CHCHD2 in mouse tissue

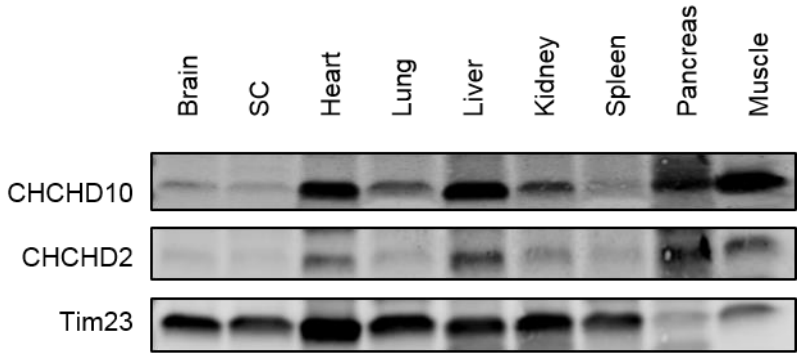

***Figure 3-15**. Western blot of CHCHD10 in mitochondria from mouse tissue.*

Representative Western blot using antibodies against CHCHD10, CHCHD2, and Tim23 (as mitochondrial loading control), in crude mitochondrial extracts prepared from indicated wild type mouse tissues. 50 µg protein was loaded per sample. SC = spinal cord.

In order to understand the function of CHCHD10 and CHCHD2 in the context of an organism, we examined its expression and function in mouse tissues. We generated crude mitochondrial fractions from brain, spinal cord, heart, lung, liver, kidney, spleen, pancreas and skeletal muscle (gastrocnemius) from a wild type adult C57Bl6J mouse, and analyzed CHCHD10 and CHCHD2 expression by Western blot (Figure 3-15). CHCHD10 and CHCHD2 were expressed in all tissues examined, but the levels were highest in heart, liver, pancreas and skeletal muscle. Moreover, the patterns of tissue expression of CHCHD10 and CHCHD2 were similar, consistent with the hypothesis that they participate in a common function.

We also investigated the physical interaction between CHCHD10, CHCHD2 and P32 in mouse heart, which has high CHCHD10 and CHCHD2 expression. Mitochondrial proteins from heart were subjected to Co-IP with antibodies against CHCHD10, CHCHD2 or control IgG. As in the cell culture Co-IP experiment using tagged constructs, we were able to demonstrate interactions between endogenous mouse CHCHD10, CHCHD2 and P32 in heart (Figure 3-16), suggesting that these interactions occur in vivo and are probably involved in the functions of the proteins. Furthermore, we did not identify a specific interaction between CHCHD2 or CHCHD10 with mitofilin.

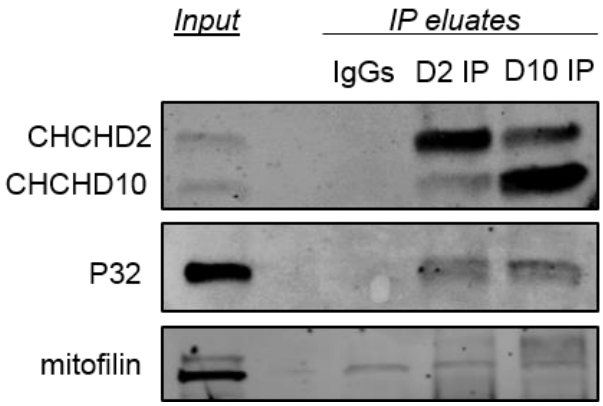

***Figure 3-16**. CHCHD10, CHCHD2, P32 Co-IP in heart*

Mitochondria from mouse heart (Input) were subjected to Co-IP either with CHCHD2 antibody, CHCHD10 antibody or control IgGs (IP eluate) and samples were run in Western blot. Membranes were probed with CHCHD2, CHCHD10, P32, and mitofilin antibodies.

3.4.7. CHCHD10 knockout animals are viable and do not exhibit gross phenotypic or mitochondrial abnormalities

We generated a CHCHD10 knockout animal (CHCHD10KO) in collaboration with The Jackson Laboratories to investigate the function of CHCHD10 in vivo. Using CRISPR/Cas9, we introduced a single adenine nucleotide in exon 2 of CHCHD10 (Figure 3-17 A), which resulted in a frameshift mutation and premature stop codon. Breeding of heterozygote animals resulted in homozygote KO animals born at Mendelian ratios. We confirmed the absence of CHCHD10 expression by Western blot of homogenates from various tissues of CHCHD10 homozygote KO mice, including brain, skeletal muscle and heart (Figure 3-17 B). Heterozygote and homozygote males and females were viable and did not exhibit any gross phenotypic abnormalities from birth through early adulthood (up to 200 days of age).

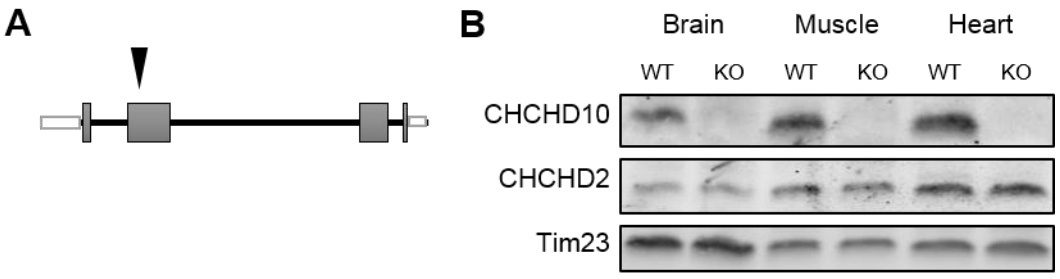

Figure 3-17*. CHCHD10KO mice*

A. Four exons of CHCHD10 are indicated in grey. Black arrowhead indicates location of single nucleotide insertion in CHCHD10KO. **B**. Representative Western blot of brain, skeletal muscle (gastrocnemius) and heart homogenate from adult wild type (WT) and CHCHD10KO (KO) mice. 100 µg protein was loaded per sample. Membrane was probed with antibodies against CHCHD10, CHCHD2 and Tim23 (mitochondrial loading control).

Since it was previously suggested that CHCHD10 plays a role in mitochondrial cristae maintenance using cultured cells from patients affected by CHCHD10 mutations (Genin et al., 2016), we wanted to investigate cristae morphology and overall mitochondrial ultrastructure by electron microscopy in vivo in the CHCHD10KO tissues. First, we performed immunohistochemistry with CHCHD10 antibodies in wild type and CHCHD10KO brain sections **to**

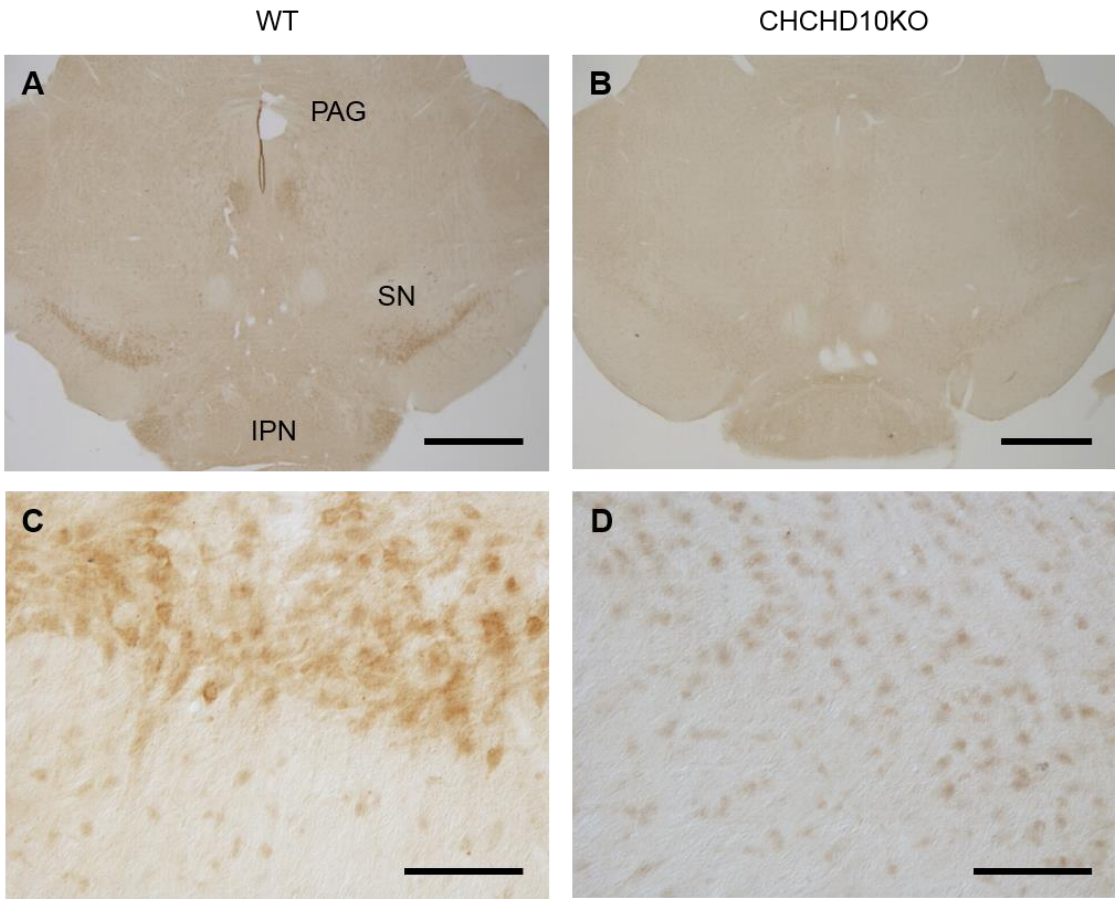

***Figure 3-18**. CHCHD10 immunohistochemistry*

A. CHCHD10 immunoreactivity in brain section containing substantia nigra (SN) region from wild type (WT) mouse. **B**. CHCHD10 immunoreactivity in brain section containing SN from CHCHD10KO mouse. Representative images in A and B captured at 2X magnification. Bar = 50 µm. PAG = periaqueductal gray, IPN = interpeduncular nucleus. **C**. CHCHD10 immunoreactivity in SN from WT mice. **D**. CHCHD10 immunoreactivity in SN from CHCHD10KO mouse. Representative images in C and D captured at 20X magnification. Bar =10 µm.

determine in which brain regions CHCHD10 is expressed. CHCHD10 staining was not homogeneous in the brain; rather, it was confined to particular brain regions, including the deep cerebellar nuclei, the ventricular lining, and most remarkably the substantia nigra (Figure 3-18 A, C). CHCHD10KO brain was used to confirm the specificity of the CHCHD10 antibody staining (Figure 3-18 B, D). Because of the specific expression of CHCHD10 in this area, and because of the association of CHCHD10 and CHCHD2 with PD (Ogaki et al., 2015; Shi et al., 2016; Rubino et al., 2017), we examined the substantia nigra of 100 days old wild type and CHCHD10KO mice by electron microscopy. Dopaminergic neuronal processes were identified by tyrosine hydroxylase (TH) immunoreactivity. We did not detect mitochondrial ultrastructural abnormalities in dopaminergic processes or in the other cell types in this brain region (Figure 3-19). In wild type and CHCHD10KO adult mouse skeletal muscle (soleus, Figure 3-20 A) and heart (Figure 3-20 B), where the protein is highly expressed (Figure 3-15), we did not observe abnormal cristae or other mitochondrial structural abnormalities. In heart, however, we noticed dark, electron dense round structures (Figure 3-20 B) localized in the region between sarcomeres, which contain heart mitochondria. These nature of these structures remains to be elucidated, but the morphology suggests that they could be lysosomes. Interestingly these structures were not connected with mitochondrial membranes, but were always in very close proximity to mitochondria.

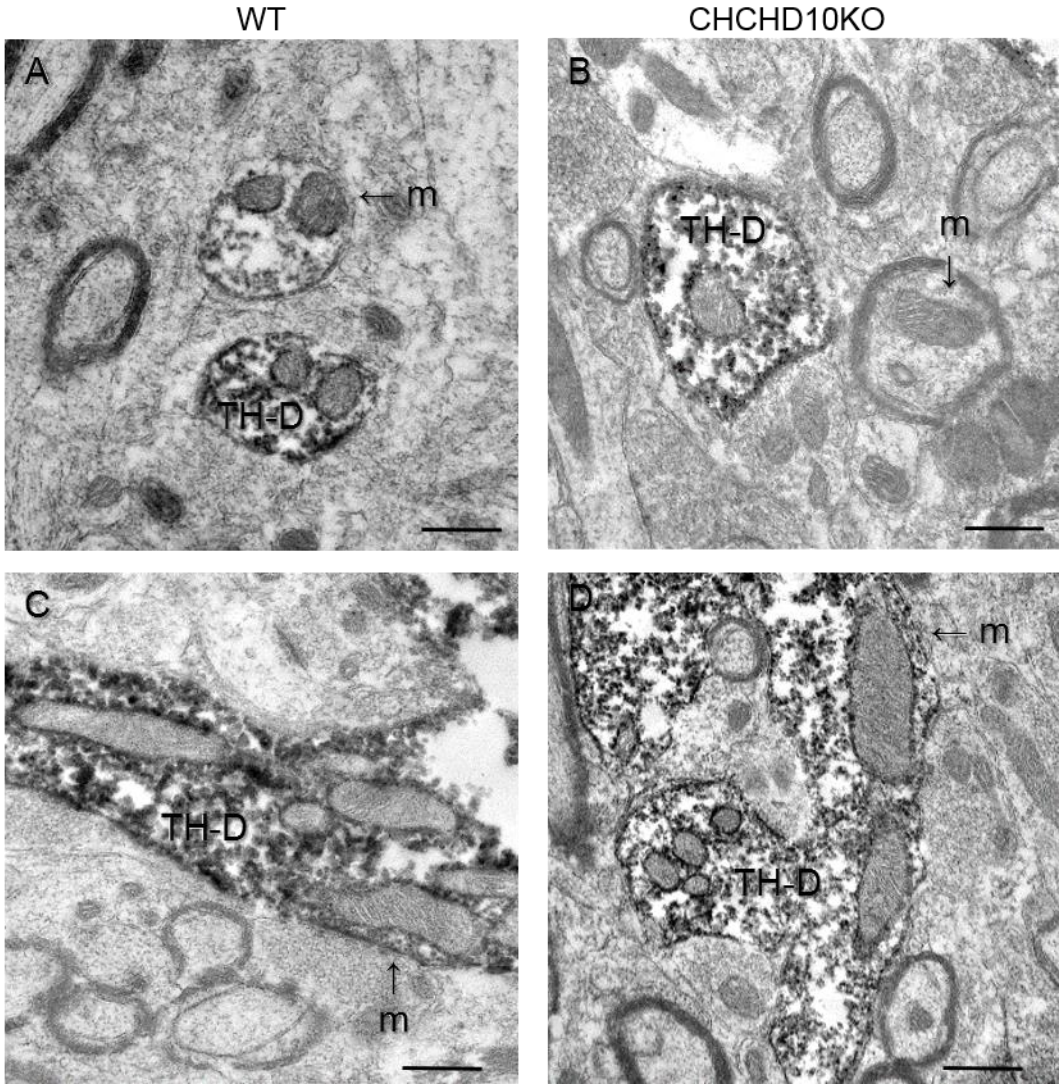

***Figure 3-19**. CHCHD10KO brain electron microscopy*

Representative electron micrographs of WT (A, C) and CHCHD10KO (B, D) substantia nigra, showing TH-immunoreactive dendrites (TH-D). m = example mitochondria. Bar = 500 nm.

We also studied mitochondrial bioenergetics in the brain, skeletal muscle, and heart of CHCHD10KO at 100 days of age. Mitochondria isolated from forebrain did not display differences in oxygen consumption (Figure 3-21 A), COX activity (Figure 3-21 B), or ATP synthesis (Figure 3-21 C), in CHCHD10KO compared to wild type. Also, brain mitochondrial calcium

capacity of control and CHCHD10KO was similar (Figure 3-21 D). Mitochondria isolated from skeletal muscle (gastrocnemius) had decreased ADP-stimulated respiration (Figure 3-21 E), but not COX activity (Figure 3-21 F) or ATP synthesis (Figure 3-21 G) differences relative to wild type. There were no differences in respiration (Figure 3-21 H) or ATP synthesis (Figure 3-21 I) between heart mitochondria from CHCHD10KO and wild type controls.

Taken together, these data suggest that CHCHD10KO has tissue specific effects, resulting in a moderate decline in respiration in skeletal muscle, but not in other tissues examined. This decline in muscle, however, did not result in an ATP synthesis defect. Importantly, while there was an abnormal accumulation of electron-dense structures in CHCHD10KO heart, the lack of changes in mitochondrial ultrastructure in any tissue studied does not support the hypothesis that CHCHD10 is required for mitochondrial cristae maintenance.

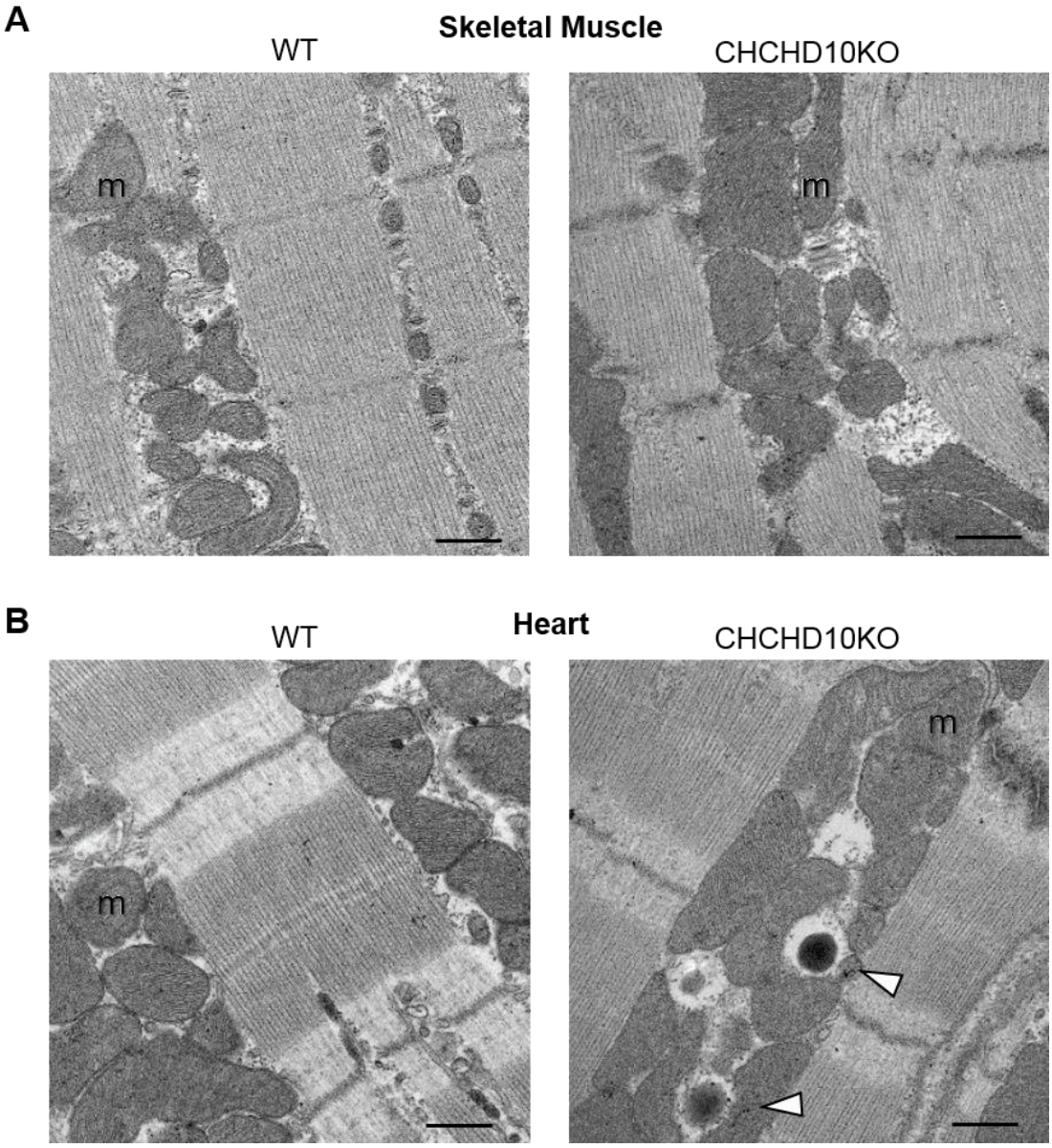

Figure 3-20. *CHCHD10KO skeletal muscle and heart electron microscopy*

A. Representative electron micrograph of WT and CHCHD10KO skeletal muscle (soleus). **B**. Representative electron micrograph of WT and CHCHD10KO heart right ventricle wall. Arrowheads indicate round structures present in CHCHD10KO. m = mitochondria. Bar = 500nm.

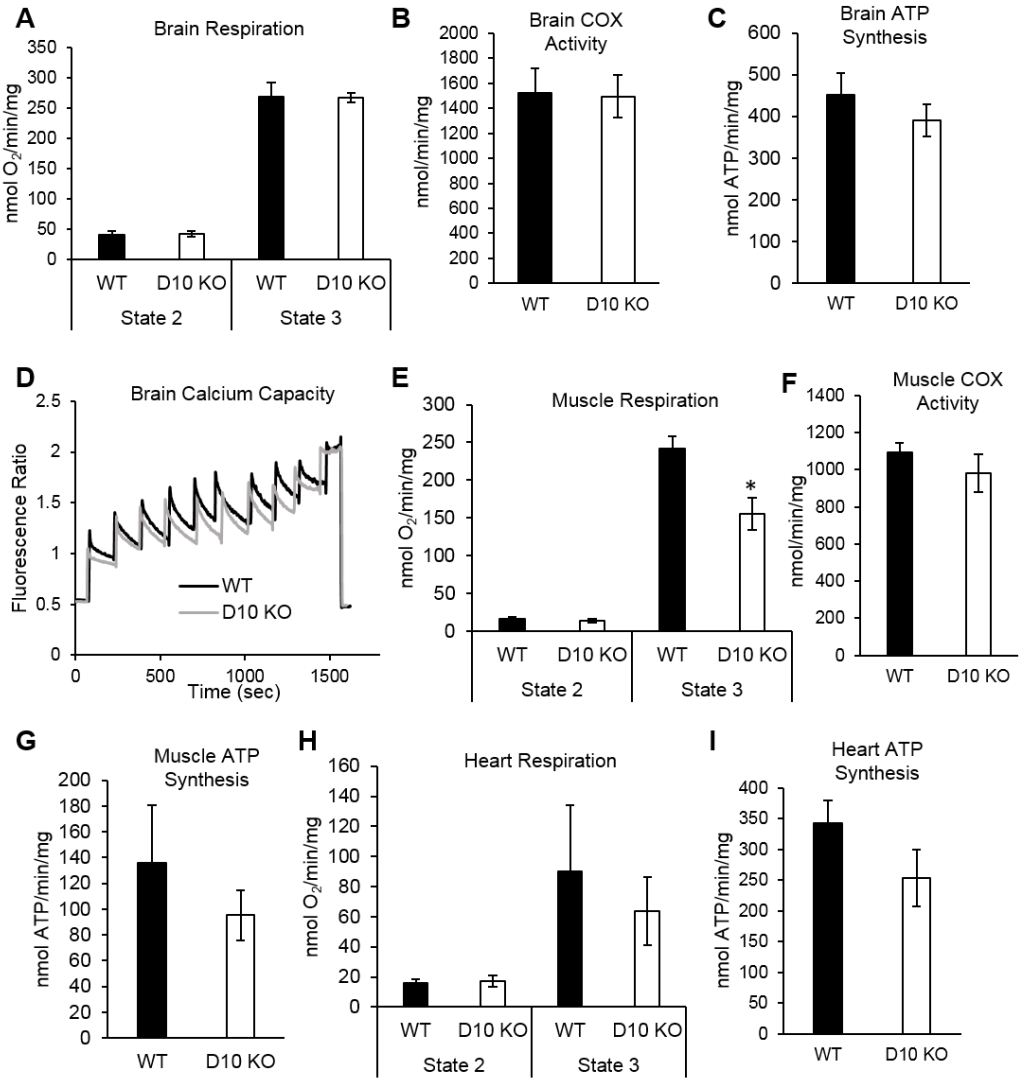

Figure 3-21*. CHCHD10KO mouse bioenergetics*

A. Oxygen consumption rate of wild type (WT) and CHCHD10KO brain mitochondria before (State 2) and after (State 3) ADP stimulation. n = 3 animals per group. **B**. COX activity of WT and CHCDH10KO brain mitochondria. n = 3. **C**. ATP synthesis rate of WT and CHCDH10KO brain mitochondria. n = 3. **D**. Representative Fura-FF calcium capacity traces of WT and CHCHD10 KO brain mitochondria with one 25μM calcium addition and sequential 10μM calcium additions followed by a final addition of 1mM EGTA. **E**. Oxygen consumption rate of WT and CHCHD10KO skeletal muscle mitochondria. * $p < 0.05$, n = 7. **F**. COX activity in WT and CHCHD10KO skeletal muscle mitochondria. n = 3. **G**. ATP synthesis rate of WT and CHCDH10KO skeletal muscle mitochondria. n = 7. **H**. Oxygen consumption rate of WT and CHCHD10KO heart mitochondria. n = 4. **I**. ATP synthesis rate of WT and CHCDH10KO heart mitochondria. n = 4.

3.5. Discussion

This study identified a functional and physical relationship between the mitochondrial IMS twin CX_9C proteins CHCHD10 and CHCHD2 and examined the consequences of modulating their expression in vitro and in vivo. We first confirmed the mitochondrial intermembrane space localization of CHCHD10, and found that similarly to other mitochondrial twin CX_9C proteins it requires the cysteine(s) in the C terminus for its mitochondrial localization. Surprisingly, we demonstrated that, in addition to the being soluble in the IMS, as previously reported (Bannwarth et al., 2014), CHCHD10 also associates with mitochondrial membranes. Interestingly, the TMpred software (Hofmann and Stoffel, 1993) for prediction of membrane-spanning regions of proteins, predicates one transmembrane region of CHCHD10 in exon 2, which is part of a highly conserved region containing many disease-associated mutations.

The homology between CHCHD10 and CHCHD2 led us to investigate their relationship. We found that these proteins bind to each other, and to the mitochondrial protein P32. It is important to note, however, that P32 is abundantly expressed, and only a small portion is pulled down with either CHCHD10 or CHCHD2. Since CHCHD10 and CHCHD2 are found in the mitochondrial IMS and P32 localizes to the mitochondrial matrix (Muta et al., 1997), it is possible that they may interact while P32 is en route to the matrix, or that they may interact through the IM since P32 can associate with membranes (Jiang et al., 1999). Although we did not find evidence that modulating the expression of CHCHD10 or CHCHD2 affects the levels of P32 in cells, we cannot yet exclude that it may affect its localization and function. The former will be investigated in vitro and in vivo by fractionating cells and tissue to assess the distribution of P32. The latter is complicated by the

multiplicity of proposed functional roles of P32, which range from complement response in immunity to apoptosis.

We demonstrated that acute loss of CHCHD10 in immortalized cells, such as HEK293 and HeLa cells, causes apoptosis independently of mitochondrial bioenergetic failure. Conversely, silencing of CHCHD2 did not induce death, confirming previously reported findings in lung cancer cells (Liu et al., 2015). Furthermore, silencing of both CHCHD2 and CHCHD10 did not have additive effects on cell death. This suggests that the two proteins do not overlap functionally, despite their sequence similarity and interaction. Interestingly, however, apoptotic cell death following CHCHD10 siRNA could be partially rescued by overexpressing either CHCHD10 or CHCHD2. Therefore, while the two proteins have different functions, they appear to participate in a common pathway.

Relative to other mitochondrial proteins, CHCHD10 and CHCHD2 are rapidly turned over, with a half-life of less than a few hours. This observation does not support a structural role for either protein. Instead, it suggests that they could serve as chaperones, either for protein import, similar to other CX_nC Tim proteins (Curran et al., 2002; Mesecke et al., 2005) or for metal transport, such as the CX_nC proteins involved in copper transport and RC assembly (Horn et al., 2008; Horn et al., 2010). In addition or alternatively, CHCHD10 and CHCHD2 could be involved in signaling processes, as suggested by the nuclear translocation of CHCHD2 under hypoxic conditions to regulate COX isoforms (Aras et al., 2015).

CHCHD10 silencing by siRNA induces apoptosis in both HEK293 and HeLa cells, yet stable knockdown HEK293 cell lines with about 20% remaining protein and CHCHD10KO mice are viable. These results clearly indicate that

both immortalized cells in culture and differentiated cells in vivo can activate compensatory mechanisms to adapt to the loss of CHCHD10. Future work will investigate the functional consequences of CHCHD10 knockdown in additional cell lines and tissues. Gaining further insight into adaptive mechanisms that compensate for CHCHD10 loss will allow for a better understanding of CHCHD10 functions.

The expression of CHCHD10 in mouse tissues appears to be similar to what has been previously shown in human tissue, with high expression in heart and liver (Bannwarth et al., 2014). Because CHCHD10 and CHCHD2 mutations are associated with neurodegeneration, we were interested in exploring CHCHD10 expression in brain. This is particularly important because of the heterogeneity of the cellular composition of the brain. We demonstrated for the first time that CHCHD10 in the brain is localized to particular regions, including the substantia nigra, which is a vulnerable region in PD.

This study is the first to generate and describe a CHCHD10KO animal model. The CHCHD10KO mice do not display obvious motor symptoms reminiscent of PD or other human diseases, at least up to 200 days of age, the latest time at which we have observed their gross phenotype during breeding and handling for experiments. Longitudinal observations, pathology studies, and behavioral tests, such as for motor coordination, will be performed in collaboration with The Jackson Laboratories to determine whether these mice have more subtle behavioral phenotypes or develop age-related neurodegenerative phenotypes. Studies will also investigate CHCHD10KO responses to metabolic stress, such as high fat diet.

In brain, muscle, and heart of the CHCHD10KO mouse we did not detect mitochondrial cristae abnormalities that were described in mutant

CHCHD10 patient fibroblasts (Genin et al., 2016). However, the mutations may not cause a loss of function, especially because most of the familial forms of ALS, FTD, and myopathy reported were autosomal dominant with variable penetrance and phenotypes. Therefore, it is likely that the mutants act by disrupting mitochondrial functions and structure in a manner independent from the normal function of CHCHD10. A similar scenario is illustrated by the well-characterized forms of ALS caused by autosomal dominant SOD1 mutations, in which mitochondria become damaged by mutant protein aggregation (Igoudjil et al., 2011), irrespective of superoxide dismutase activity. We have generated cellular and mouse transgenic models of disease-associated mutant CHCHD10 in order to investigate this hypothesis.

In summary, this study provides novel insight into the function of CHCHD10 and its interactions with mitochondrial proteins CHCHD2 and P32. It also generated and characterized novel genetic models of CHCHD10 modulation in vitro and in vivo. Presently, these findings are being extended to the investigation of disease-associated CHCHD10 mutations, and to cellular mechanisms underlying ALS and other related diseases.

4. CONCLUDING REMARKS

Understanding and treating brain diseases has proven to be particularly challenging, which is not surprising giving the complexity and heterogeneity of the brain and the cell types within it. The evidence for mitochondrial dysfunction at the core of such diseases continues to accumulate, but targeting mitochondria for therapy is difficult. Targeting mitochondria is challenging because the mechanisms of mitochondrial involvement in disease are not fully understood. Furthermore, while much is known about the most studied proteins in mitochondria, many annotated mitochondrial proteins have yet unknown function (Pagliarini et al., 2008). At the start of this thesis work, it was estimated that up to 36% of mitochondrial proteins have no clearly established biochemical function and roughly 397 genes encoding mitochondrial proteins are associated with human diseases (Pagliarini and Rutter, 2013). In a more recent analysis (Floyd et al., 2016) using an updated inventory of mitochondrial proteins (Calvo et al., 2016), ~20% of the mammalian mitochondrial proteome was considered uncharacterized. The list of uncharacterized proteins includes CHCHD10, CHCHD2, and other twin CX_9C proteins. The uncharacterized 20% mitochondrial proteins could even be an underestimation, as proteins that are not necessarily “mitochondrial” have dual localizations in mitochondria and other cellular compartments are constantly being uncovered. Thus, a better characterization of the mitochondrial proteome can reveal aspects of both mitochondrial physiology and new diseases genes and pathways.

In this dissertation, we investigated the function of two proteins with unexpected, yet important disease implications. ERβ is not considered a

mitochondrial protein per se because of its known transcriptional roles in the nucleus. However, it also has a mitochondrial localization that cannot be overlooked. This work is the first to identify a role for mitochondrial ERβ in brain MPT regulation. The molecular composition of the MPT pore is not well understood, but the discovery of a novel regulator could lead to a better understanding of MPT. We find a CypD-dependent sex difference in calcium induced MPT in brain. While the observed sex difference in isolated mitochondria was not dependent on ERβ, the possibility that modulation of this ERβ-CypD axis could affect brain injury outcomes warrants further investigation. In the future, for example, we would like to manipulate ERβ in an *in vivo* stroke model.

We also examined the function of the mitochondrial protein CHCHD10 using cellular and animal models. Recently mutations in CHCHD10 have emerged as genetic causes of neurodegenerative diseases, but very little is known about the protein itself. We identified a functional and physical relationship between CHCHD10 and its homolog CHCHD2, and characterized the phenotype of CHCHD10 silencing in cell culture and animal models. Our findings partly challenge current theories on the localization and function of CHCHD10. Experiments to achieve a deeper understanding of the function of CHCHD10 in mitochondria as well as the effects of the mutations are ongoing. Studies of genetic causes of neurodegeneration have often contributed to revealing novel pathogenic pathways that could extend to the most common sporadic forms of the diseases. Such discoveries will be crucial for identifying therapeutic targets.

In addition to the main body of work that is described in this thesis, the appendix includes a recently published manuscript, of which I am a co-first

author, which describes a sex difference in the mitochondrial IMS unfolded protein response in a mouse model of ALS. In both this paper and the studies of brain MPT described above, we focused on sex differences in mitochondrial phenomena in stroke and neurodegenerative diseases. There has been a recent emphasis on the importance of including the effects of sex and gender in biological research, and the NIH has recently mandated the inclusion of females in experimental studies and the analysis of data by sex (Clayton and Collins, 2014). This is particularly important, as there are many human diseases, which have incidences and outcomes that differ between males and females. Sex differences in mitochondrial dysfunction and other mechanisms involved in disease pathogenesis need to be understood so that safe and effective therapies can be developed.

Overall, this work investigates novel functions of mitochondrial proteins and paves the way for future studies of these proteins in neurological diseases.

5. REFERENCES

Ajroud-Driss S, Fecto F, Ajroud K, Lalani I, Calvo SE, Mootha VK, Deng HX, Siddique N, Tahmoush AJ, Heiman-Patterson TD, Siddique T (2015) Mutation in the novel nuclear-encoded mitochondrial protein CHCHD10 in a family with autosomal dominant mitochondrial myopathy. Neurogenetics 16:1-9.

Akerman KE, Wikstrom MK (1976) Safranine as a probe of the mitochondrial membrane potential. FEBS Lett 68:191-197.

Alavian KN, Beutner G, Lazrove E, Sacchetti S, Park HA, Licznerski P, Li H, Nabili P, Hockensmith K, Graham M, Porter GA, Jr., Jonas EA (2014) An uncoupling channel within the c-subunit ring of the F1FO ATP synthase is the mitochondrial permeability transition pore. Proceedings of the National Academy of Sciences of the United States of America 111:10580-10585.

Alvarez-Delgado C, Mendoza-Rodriguez CA, Picazo O, Cerbon M (2010) Different expression of alpha and beta mitochondrial estrogen receptors in the aging rat brain: interaction with respiratory complex V. Exp Gerontol 45:580-585.

Aras S, Bai M, Lee I, Springett R, Huttemann M, Grossman LI (2015) MNRR1 (formerly CHCHD2) is a bi-organellar regulator of mitochondrial metabolism. Mitochondrion 20:43-51.

Argaud L, Gateau-Roesch O, Muntean D, Chalabreysse L, Loufouat J, Robert D, Ovize M (2005) Specific inhibition of the mitochondrial permeability transition prevents lethal reperfusion injury. J Mol Cell Cardiol 38:367-374.

Arieli Y, Gursahani H, Eaton MM, Hernandez LA, Schaefer S (2004) Gender modulation of Ca(2+) uptake in cardiac mitochondria. Journal of molecular and cellular cardiology 37:507-513.

Arnesano F, Balatri E, Banci L, Bertini I, Winge DR (2005) Folding studies of Cox17 reveal an important interplay of cysteine oxidation and copper binding. Structure 13:713-722.

Attwell D, Laughlin SB (2001) An energy budget for signaling in the grey matter of the brain. J Cereb Blood Flow Metab 21:1133-1145.

Auranen M, Ylikallio E, Shcherbii M, Paetau A, Kiuru-Enari S, Toppila JP, Tyynismaa H (2015) CHCHD10 variant p.(Gly66Val) causes axonal Charcot-Marie-Tooth disease. Neurol Genet 1:e1.

Baines CP, Kaiser RA, Purcell NH, Blair NS, Osinska H, Hambleton MA, Brunskill EW, Sayen MR, Gottlieb RA, Dorn GW, Robbins J, Molkentin JD (2005) Loss of cyclophilin D reveals a critical role for mitochondrial permeability transition in cell death. Nature 434:658-662.

Banci L, Bertini I, Ciofi-Baffoni S, Janicka A, Martinelli M, Kozlowski H, Palumaa P (2008) A structural-dynamical characterization of human Cox17. J Biol Chem 283:7912-7920.

Bannwarth S et al. (2014) A mitochondrial origin for frontotemporal dementia and amyotrophic lateral sclerosis through CHCHD10 involvement. Brain 137:2329-2345.
Basso E, Fante L, Fowlkes J, Petronilli V, Forte MA, Bernardi P (2005) Properties of the permeability transition pore in mitochondria devoid of Cyclophilin D. J Biol Chem 280:18558-18561.
Baughman JM, Perocchi F, Girgis HS, Plovanich M, Belcher-Timme CA, Sancak Y, Bao XR, Strittmatter L, Goldberger O, Bogorad RL, Koteliansky V, Mootha VK (2011) Integrative genomics identifies MCU as an essential component of the mitochondrial calcium uniporter. Nature 476:341-345.
Beck SJ, Guo L, Phensy A, Tian J, Wang L, Tandon N, Gauba E, Lu L, Pascual JM, Kroener S, Du H (2016) Deregulation of mitochondrial F1FO-ATP synthase via OSCP in Alzheimer's disease. Nat Commun 7:11483.
Bernardi P, von Stockum S (2012) The permeability transition pore as a Ca(2+) release channel: new answers to an old question. Cell Calcium 52:22-27.
Bernardi P, Di Lisa F (2015) The mitochondrial permeability transition pore: molecular nature and role as a target in cardioprotection. J Mol Cell Cardiol 78:100-106.
Bernardi P, Broekemeier KM, Pfeiffer DR (1994) Recent progress on regulation of the mitochondrial permeability transition pore; a cyclosporin-sensitive pore in the inner mitochondrial membrane. J Bioenerg Biomembr 26:509-517.
Birch-Machin MA, Turnbull DM (2001) Assaying mitochondrial respiratory complex activity in mitochondria isolated from human cells and tissues. Methods Cell Biol 65:97-117.
Brandt U (2006) Energy converting NADH:quinone oxidoreductase (complex I). Annu Rev Biochem 75:69-92.
Broekemeier KM, Dempsey ME, Pfeiffer DR (1989) Cyclosporin A is a potent inhibitor of the inner membrane permeability transition in liver mitochondria. J Biol Chem 264:7826-7830.
Brouillet E, Hantraye P, Ferrante RJ, Dolan R, Leroy-Willig A, Kowall NW, Beal MF (1995) Chronic mitochondrial energy impairment produces selective striatal degeneration and abnormal choreiform movements in primates. Proc Natl Acad Sci U S A 92:7105-7109.
Brown MR, Sullivan PG, Geddes JW (2006) Synaptic mitochondria are more susceptible to Ca2+overload than nonsynaptic mitochondria. J Biol Chem 281:11658-11668.
Brown MR, Sullivan PG, Dorenbos KA, Modafferi EA, Geddes JW, Steward O (2004) Nitrogen disruption of synaptoneurosomes: an alternative method to isolate brain mitochondria. J Neurosci Methods 137:299-303.

Brustovetsky N, Jemmerson R, Dubinsky JM (2002) Calcium-induced Cytochrome c release from rat brain mitochondria is altered by digitonin. Neurosci Lett 332:91-94.
Calvo SE, Clauser KR, Mootha VK (2016) MitoCarta2.0: an updated inventory of mammalian mitochondrial proteins. Nucleic Acids Res 44:D1251-1257.
Cavallaro G (2010) Genome-wide analysis of eukaryotic twin CX9C proteins. Mol Biosyst 6:2459-2470.
Chacinska A, Pfannschmidt S, Wiedemann N, Kozjak V, Sanjuan Szklarz LK, Schulze-Specking A, Truscott KN, Guiard B, Meisinger C, Pfanner N (2004) Essential role of Mia40 in import and assembly of mitochondrial intermembrane space proteins. EMBO J 23:3735-3746.
Chatzi A, Manganas P, Tokatlidis K (2016) Oxidative folding in the mitochondrial intermembrane space: A regulated process important for cell physiology and disease. Biochim Biophys Acta 1863:1298-1306.
Chauhan A, Moser H, McCullough LD (2017) Sex differences in ischaemic stroke: potential cellular mechanisms. Clin Sci (Lond) 131:533-552.
Chen C, Hu LX, Dong T, Wang GQ, Wang LH, Zhou XP, Jiang Y, Murao K, Lu SQ, Chen JW, Zhang GX (2013) Apoptosis and autophagy contribute to gender difference in cardiac ischemia-reperfusion induced injury in rats. Life Sci 93:265-270.
Chen JQ, Delannoy M, Cooke C, Yager JD (2004) Mitochondrial localization of ERalpha and ERbeta in human MCF7 cells. Am J Physiol Endocrinol Metab 286:E1011-1022.
Chinopoulos C, Konrad C, Kiss G, Metelkin E, Torocsik B, Zhang SF, Starkov AA (2011) Modulation of F0F1-ATP synthase activity by cyclophilin D regulates matrix adenine nucleotide levels. FEBS J 278:1112-1125.
Clayton JA, Collins FS (2014) Policy: NIH to balance sex in cell and animal studies. Nature 509:282-283.
Cohen-Gould L (2013) Handling Cell Culture Monolayers for Transmission Electron Microscopy. In: Microscopy Today, pp 10-12: Microscopy Society of America.
Compton DR, Sheng S, Carlson KE, Rebacz NA, Lee IY, Katzenellenbogen BS, Katzenellenbogen JA (2004) Pyrazolo[1,5-a]pyrimidines: estrogen receptor ligands possessing estrogen receptor beta antagonist activity. J Med Chem 47:5872-5893.
Connern CP, Halestrap AP (1994) Recruitment of mitochondrial cyclophilin to the mitochondrial inner membrane under conditions of oxidative stress that enhance the opening of a calcium-sensitive non-specific channel. Biochem J 302 (Pt 2):321-324.
Crompton M, Virji S, Doyle V, Johnson N, Ward JM (1999) The mitochondrial permeability transition pore. Biochem Soc Symp 66:167-179.
Curran SP, Leuenberger D, Schmidt E, Koehler CM (2002) The role of the Tim8p-Tim13p complex in a conserved import pathway for

mitochondrial polytopic inner membrane proteins. J Cell Biol 158:1017-1027.
Damiano M, Starkov AA, Petri S, Kipiani K, Kiaei M, Mattiazzi M, Flint Beal M, Manfredi G (2006) Neural mitochondrial Ca2+ capacity impairment precedes the onset of motor symptoms in G93A Cu/Zn-superoxide dismutase mutant mice. J Neurochem 96:1349-1361.
de Bruijn WC (1973) Glycogen, its chemistry and morphologic appearance in the electron microscope. I. A modified OsO 4 fixative which selectively contrasts glycogen. J Ultrastruct Res 42:29-50.
De Stefani D, Patron M, Rizzuto R (2015) Structure and function of the mitochondrial calcium uniporter complex. Biochim Biophys Acta 1853:2006-2011.
De Stefani D, Raffaello A, Teardo E, Szabo I, Rizzuto R (2011) A forty-kilodalton protein of the inner membrane is the mitochondrial calcium uniporter. Nature 476:336-340.
Ding C, Wu Z, Huang L, Wang Y, Xue J, Chen S, Deng Z, Wang L, Song Z, Chen S (2015) Mitofilin and CHCHD6 physically interact with Sam50 to sustain cristae structure. Sci Rep 5:16064.
Dols-Icardo O et al. (2015) Analysis of the CHCHD10 gene in patients with frontotemporal dementia and amyotrophic lateral sclerosis from Spain. Brain 138:e400.
Dotson AL, Offner H (2017) Sex differences in the immune response to experimental stroke: Implications for translational research. J Neurosci Res 95:437-446.
Floyd BJ et al. (2016) Mitochondrial Protein Interaction Mapping Identifies Regulators of Respiratory Chain Function. Mol Cell 63:621-632.
Folbergrova J, Memezawa H, Smith ML, Siesjo BK (1992) Focal and perifocal changes in tissue energy state during middle cerebral artery occlusion in normo- and hyperglycemic rats. J Cereb Blood Flow Metab 12:25-33.
Gahwiler BH, Thompson SM, Muller D (2001) Preparation and maintenance of organotypic slice cultures of CNS tissue. Curr Protoc Neurosci Chapter 6:Unit 6 11.
Gao Y, Signore AP, Yin W, Cao G, Yin XM, Sun F, Luo Y, Graham SH, Chen J (2005) Neuroprotection against focal ischemic brain injury by inhibition of c-Jun N-terminal kinase and attenuation of the mitochondrial apoptosis-signaling pathway. J Cereb Blood Flow Metab 25:694-712.
Genin EC et al. (2016) CHCHD10 mutations promote loss of mitochondrial cristae junctions with impaired mitochondrial genome maintenance and inhibition of apoptosis. EMBO Mol Med 8:58-72.
Giorgio V, Bisetto E, Soriano ME, Dabbeni-Sala F, Basso E, Petronilli V, Forte MA, Bernardi P, Lippe G (2009) Cyclophilin D modulates mitochondrial F0F1-ATP synthase by interacting with the lateral stalk of the complex. J Biol Chem 284:33982-33988.

Giorgio V, von Stockum S, Antoniel M, Fabbro A, Fogolari F, Forte M, Glick GD, Petronilli V, Zoratti M, Szabo I, Lippe G, Bernardi P (2013) Dimers of mitochondrial ATP synthase form the permeability transition pore. Proceedings of the National Academy of Sciences of the United States of America 110:5887-5892.
Girijala RL, Sohrabji F, Bush RL (2016) Sex differences in stroke: Review of current knowledge and evidence. Vasc Med:1-10.
Goldstein JC, Waterhouse NJ, Juin P, Evan GI, Green DR (2000) The coordinate release of cytochrome c during apoptosis is rapid, complete and kinetically invariant. Nat Cell Biol 2:156-162.
Gouriou Y, Demaurex N, Bijlenga P, De Marchi U (2011) Mitochondrial calcium handling during ischemia-induced cell death in neurons. Biochimie 93:2060-2067.
Greene GL, Gilna P, Waterfield M, Baker A, Hort Y, Shine J (1986) Sequence and expression of human estrogen receptor complementary DNA. Science 231:1150-1154.
Griffiths EJ, Halestrap AP (1991) Further evidence that cyclosporin A protects mitochondria from calcium overload by inhibiting a matrix peptidyl-prolyl cis-trans isomerase. Implications for the immunosuppressive and toxic effects of cyclosporin. Biochem J 274 (Pt 2):611-614.
Gu M, Gash MT, Mann VM, Javoy-Agid F, Cooper JM, Schapira AH (1996) Mitochondrial defect in Huntington's disease caudate nucleus. Ann Neurol 39:385-389.
Guegan C, Sola B (2000) Early and sequential recruitment of apoptotic effectors after focal permanent ischemia in mice. Brain Res 856:93-100.
Halestrap AP, Richardson AP (2015) The mitochondrial permeability transition: a current perspective on its identity and role in ischaemia/reperfusion injury. Journal of molecular and cellular cardiology 78:129-141.
Hansson CA, Frykman S, Farmery MR, Tjernberg LO, Nilsberth C, Pursglove SE, Ito A, Winblad B, Cowburn RF, Thyberg J, Ankarcrona M (2004) Nicastrin, presenilin, APH-1, and PEN-2 form active gamma-secretase complexes in mitochondria. J Biol Chem 279:51654-51660.
Hansson MJ, Morota S, Chen L, Matsuyama N, Suzuki Y, Nakajima S, Tanoue T, Omi A, Shibasaki F, Shimazu M, Ikeda Y, Uchino H, Elmer E (2011) Cyclophilin D-sensitive mitochondrial permeability transition in adult human brain and liver mitochondria. J Neurotrauma 28:143-153.
He L, Lemasters JJ (2003) Heat shock suppresses the permeability transition in rat liver mitochondria. The Journal of biological chemistry 278:16755-16760.
Hell K (2008) The Erv1-Mia40 disulfide relay system in the intermembrane space of mitochondria. Biochim Biophys Acta 1783:601-609.
Hofmann K, Stoffel W (1993) Tmbase-A database of membrane spanning proteins segments. Biol Chem 374:166.

Horn D, Al-Ali H, Barrientos A (2008) Cmc1p is a conserved mitochondrial twin CX9C protein involved in cytochrome c oxidase biogenesis. Mol Cell Biol 28:4354-4364.
Horn D, Zhou W, Trevisson E, Al-Ali H, Harris TK, Salviati L, Barrientos A (2010) The conserved mitochondrial twin Cx9C protein Cmc2 Is a Cmc1 homologue essential for cytochrome c oxidase biogenesis. J Biol Chem 285:15088-15099.
Igoudjil A, Magrane J, Fischer LR, Kim HJ, Hervias I, Dumont M, Cortez C, Glass JD, Starkov AA, Manfredi G (2011) In vivo pathogenic role of mutant SOD1 localized in the mitochondrial intermembrane space. J Neurosci 31:15826-15837.
Ito S, Karnovsky M (1968) Formaldehyde-Glutaraldehyde Fixatives Containing Trinitro Compounds. JCB 39.
Ivannikov MV, Sugimori M, Llinas RR (2010) Calcium clearance and its energy requirements in cerebellar neurons. Cell Calcium 47:507-513.
Janer A, Prudent J, Paupe V, Fahiminiya S, Majewski J, Sgarioto N, Des Rosiers C, Forest A, Lin ZY, Gingras AC, Mitchell G, McBride HM, Shoubridge EA (2016) SLC25A46 is required for mitochondrial lipid homeostasis and cristae maintenance and is responsible for Leigh syndrome. EMBO Mol Med 8:1019-1038.
Jiang D, Zhao L, Clapham DE (2009) Genome-wide RNAi screen identifies Letm1 as a mitochondrial Ca2+/H+ antiporter. Science 326:144-147.
Jiang J, Zhang Y, Krainer AR, Xu RM (1999) Crystal structure of human p32, a doughnut-shaped acidic mitochondrial matrix protein. Proc Natl Acad Sci U S A 96:3572-3577.
Jiao B, Xiao T, Hou L, Gu X, Zhou Y, Zhou L, Tang B, Xu J, Shen L (2016) High prevalence of CHCHD10 mutation in patients with frontotemporal dementia from China. Brain 139:e21.
Johnson JO, Glynn SM, Gibbs JR, Nalls MA, Sabatelli M, Restagno G, Drory VE, Chio A, Rogaeva E, Traynor BJ (2014) Mutations in the CHCHD10 gene are a common cause of familial amyotrophic lateral sclerosis. Brain 137:e311.
Kamer KJ, Mootha VK (2015) The molecular era of the mitochondrial calcium uniporter. Nat Rev Mol Cell Biol 16:545-553.
Kawamata H, Manfredi G (2010) Mitochondrial dysfunction and intracellular calcium dysregulation in ALS. Mech Ageing Dev 131:517-526.
Kim HJ, Magrane J, Starkov AA, Manfredi G (2012) The mitochondrial calcium regulator cyclophilin D is an essential component of oestrogen-mediated neuroprotection in amyotrophic lateral sclerosis. Brain : a journal of neurology 135:2865-2874.
Kluck RM, Bossy-Wetzel E, Green DR, Newmeyer DD (1997) The release of cytochrome c from mitochondria: a primary site for Bcl-2 regulation of apoptosis. Science 275:1132-1136.
Kluck RM, Esposti MD, Perkins G, Renken C, Kuwana T, Bossy-Wetzel E, Goldberg M, Allen T, Barber MJ, Green DR, Newmeyer DD (1999) The

pro-apoptotic proteins, Bid and Bax, cause a limited permeabilization of the mitochondrial outer membrane that is enhanced by cytosol. J Cell Biol 147:809-822.
Koc EC, Cimen H, Kumcuoglu B, Abu N, Akpinar G, Haque ME, Spremulli LL, Koc H (2013) Identification and characterization of CHCHD1, AURKAIP1, and CRIF1 as new members of the mammalian mitochondrial ribosome. Front Physiol 4:183.
Koehler CM, Tienson HL (2009) Redox regulation of protein folding in the mitochondrial intermembrane space. Biochim Biophys Acta 1793:139-145.
Kong J, Xu Z (1998) Massive mitochondrial degeneration in motor neurons triggers the onset of amyotrophic lateral sclerosis in mice expressing a mutant SOD1. J Neurosci 18:3241-3250.
Korde AS, Pettigrew LC, Craddock SD, Pocernich CB, Waldmeier PC, Maragos WF (2007) Protective effects of NIM811 in transient focal cerebral ischemia suggest involvement of the mitochondrial permeability transition. J Neurotrauma 24:895-908.
Krege JH, Hodgin JB, Couse JF, Enmark E, Warner M, Mahler JF, Sar M, Korach KS, Gustafsson JA, Smithies O (1998) Generation and reproductive phenotypes of mice lacking estrogen receptor beta. Proc Natl Acad Sci U S A 95:15677-15682.
Kristian T, Pivovarova NB, Fiskum G, Andrews SB (2007) Calcium-induced precipitate formation in brain mitochondria: composition, calcium capacity, and retention. J Neurochem 102:1346-1356.
Lai JC, Clark JB (1979) Preparation of synaptic and nonsynaptic mitochondria from mammalian brain. Methods Enzymol 55:51-60.
Langston JW, Ballard P, Tetrud JW, Irwin I (1983) Chronic Parkinsonism in humans due to a product of meperidine-analog synthesis. Science 219:979-980.
Lattante S, Ciura S, Rouleau GA, Kabashi E (2015) Defining the genetic connection linking amyotrophic lateral sclerosis (ALS) with frontotemporal dementia (FTD). Trends Genet 31:263-273.
Laupacis A, Keown PA, Ulan RA, McKenzie N, Stiller CR (1982) Cyclosporin A: a powerful immunosuppressant. Can Med Assoc J 126:1041-1046.
Le Lamer S, Paradis S, Rahmouni H, Chaimbault C, Michaud M, Culcasi M, Afxantidis J, Latreille M, Berna P, Berdeaux A, Pietri S, Morin D, Donazzolo Y, Abitbol JL, Pruss RM, Schaller S (2014) Translation of TRO40303 from myocardial infarction models to demonstration of safety and tolerance in a randomized Phase I trial. J Transl Med 12:38.
Li H, Pin S, Zeng Z, Wang MM, Andreasson KA, McCullough LD (2005) Sex differences in cell death. Ann Neurol 58:317-321.
Li H, Ruan Y, Zhang K, Jian F, Hu C, Miao L, Gong L, Sun L, Zhang X, Chen S, Chen H, Liu D, Song Z (2016) Mic60/Mitofilin determines MICOS assembly essential for mitochondrial dynamics and mtDNA nucleoid organization. Cell Death Differ 23:380-392.

Lin MT, Beal MF (2006) Mitochondrial dysfunction and oxidative stress in neurodegenerative diseases. Nature 443:787-795.
Liu F, Li Z, Li J, Siegel C, Yuan R, McCullough LD (2009) Sex differences in caspase activation after stroke. Stroke 40:1842-1848.
Liu J, Farmer JD, Jr., Lane WS, Friedman J, Weissman I, Schreiber SL (1991) Calcineurin is a common target of cyclophilin-cyclosporin A and FKBP-FK506 complexes. Cell 66:807-815.
Liu J, Lillo C, Jonsson PA, Vande Velde C, Ward CM, Miller TM, Subramaniam JR, Rothstein JD, Marklund S, Andersen PM, Brannstrom T, Gredal O, Wong PC, Williams DS, Cleveland DW (2004) Toxicity of familial ALS-linked SOD1 mutants from selective recruitment to spinal mitochondria. Neuron 43:5-17.
Liu Y, Clegg HV, Leslie PL, Di J, Tollini LA, He Y, Kim TH, Jin A, Graves LM, Zheng J, Zhang Y (2015) CHCHD2 inhibits apoptosis by interacting with Bcl-x L to regulate Bax activation. Cell Death Differ 22:1035-1046.
Longen S, Bien M, Bihlmaier K, Kloeppel C, Kauff F, Hammermeister M, Westermann B, Herrmann JM, Riemer J (2009) Systematic analysis of the twin cx(9)c protein family. J Mol Biol 393:356-368.
Lust WD, Taylor C, Pundik S, Selman WR, Ratcheson RA (2002) Ischemic cell death: dynamics of delayed secondary energy failure during reperfusion following focal ischemia. Metab Brain Dis 17:113-121.
Magrane J, Hervias I, Henning MS, Damiano M, Kawamata H, Manfredi G (2009) Mutant SOD1 in neuronal mitochondria causes toxicity and mitochondrial dynamics abnormalities. Hum Mol Genet 18:4552-4564.
Manczak M, Anekonda TS, Henson E, Park BS, Quinn J, Reddy PH (2006) Mitochondria are a direct site of A beta accumulation in Alzheimer's disease neurons: implications for free radical generation and oxidative damage in disease progression. Hum Mol Genet 15:1437-1449.
Manfredi G, Kawamata H (2016) Mitochondria and endoplasmic reticulum crosstalk in amyotrophic lateral sclerosis. Neurobiol Dis 90:35-42.
Mannella CA (2006) Structure and dynamics of the mitochondrial inner membrane cristae. Biochim Biophys Acta 1763:542-548.
Martin LJ, Semenkow S, Hanaford A, Wong M (2014a) Mitochondrial permeability transition pore regulates Parkinson's disease development in mutant alpha-synuclein transgenic mice. Neurobiol Aging 35:1132-1152.
Martin LJ, Fancelli D, Wong M, Niedzwiecki M, Ballarini M, Plyte S, Chang Q (2014b) GNX-4728, a novel small molecule drug inhibitor of mitochondrial permeability transition, is therapeutic in a mouse model of amyotrophic lateral sclerosis. Front Cell Neurosci 8:433.
Mattiazzi M, D'Aurelio M, Gajewski CD, Martushova K, Kiaei M, Beal MF, Manfredi G (2002) Mutated human SOD1 causes dysfunction of oxidative phosphorylation in mitochondria of transgenic mice. J Biol Chem 277:29626-29633.

McCormack JG, Halestrap AP, Denton RM (1990) Role of calcium ions in regulation of mammalian intramitochondrial metabolism. Physiol Rev 70:391-425.
Mesecke N, Terziyska N, Kozany C, Baumann F, Neupert W, Hell K, Herrmann JM (2005) A disulfide relay system in the intermembrane space of mitochondria that mediates protein import. Cell 121:1059-1069.
Milerova M, Drahota Z, Chytilova A, Tauchmannova K, Houstek J, Ostadal B (2016) Sex difference in the sensitivity of cardiac mitochondrial permeability transition pore to calcium load. Mol Cell Biochem 412:147-154.
Milner TA, Waters EM, Robinson DC, Pierce JP (2011) Degenerating processes identified by electron microscopic immunocytochemical methods. Methods Mol Biol 793:23-59.
Milner TA, Ayoola K, Drake CT, Herrick SP, Tabori NE, McEwen BS, Warrier S, Alves SE (2005) Ultrastructural localization of estrogen receptor beta immunoreactivity in the rat hippocampal formation. J Comp Neurol 491:81-95.
Milner TA, Thompson LI, Wang G, Kievits JA, Martin E, Zhou P, McEwen BS, Pfaff DW, Waters EM (2010) Distribution of estrogen receptor beta containing cells in the brains of bacterial artificial chromosome transgenic mice. Brain Res 1351:74-96.
Mosselman S, Polman J, Dijkema R (1996) ER beta: identification and characterization of a novel human estrogen receptor. FEBS Lett 392:49-53.
Muller K, Andersen PM, Hubers A, Marroquin N, Volk AE, Danzer KM, Meitinger T, Ludolph AC, Strom TM, Weishaupt JH (2014) Two novel mutations in conserved codons indicate that CHCHD10 is a gene associated with motor neuron disease. Brain 137:e309.
Muller M, Mironov SL, Ivannikov MV, Schmidt J, Richter DW (2005) Mitochondrial organization and motility probed by two-photon microscopy in cultured mouse brainstem neurons. Exp Cell Res 303:114-127.
Muta T, Kang D, Kitajima S, Fujiwara T, Hamasaki N (1997) p32 protein, a splicing factor 2-associated protein, is localized in mitochondrial matrix and is functionally important in maintaining oxidative phosphorylation. J Biol Chem 272:24363-24370.
Naga KK, Sullivan PG, Geddes JW (2007) High cyclophilin D content of synaptic mitochondria results in increased vulnerability to permeability transition. J Neurosci 27:7469-7475.
Nakagawa T, Shimizu S, Watanabe T, Yamaguchi O, Otsu K, Yamagata H, Inohara H, Kubo T, Tsujimoto Y (2005) Cyclophilin D-dependent mitochondrial permeability transition regulates some necrotic but not apoptotic cell death. Nature 434:652-658.

Nicholls DG, Crompton M (1980) Mitochondrial calcium transport. FEBS Lett 111:261-268.
Nilsen J, Chen S, Irwin RW, Iwamoto S, Brinton RD (2006) Estrogen protects neuronal cells from amyloid beta-induced apoptosis via regulation of mitochondrial proteins and function. BMC Neurosci 7:74.
Nunomura A, Perry G, Aliev G, Hirai K, Takeda A, Balraj EK, Jones PK, Ghanbari H, Wataya T, Shimohama S, Chiba S, Atwood CS, Petersen RB, Smith MA (2001) Oxidative damage is the earliest event in Alzheimer disease. J Neuropathol Exp Neurol 60:759-767.
Ogaki K et al. (2015) Mitochondrial targeting sequence variants of the CHCHD2 gene are a risk for Lewy body disorders. Neurology 85:2016-2025.
Ostadal B, Ostadal P (2014) Sex-based differences in cardiac ischaemic injury and protection: therapeutic implications. Br J Pharmacol 171:541-554.
Pagliarini DJ, Rutter J (2013) Hallmarks of a new era in mitochondrial biochemistry. Genes Dev 27:2615-2627.
Pagliarini DJ, Calvo SE, Chang B, Sheth SA, Vafai SB, Ong SE, Walford GA, Sugiana C, Boneh A, Chen WK, Hill DE, Vidal M, Evans JG, Thorburn DR, Carr SA, Mootha VK (2008) A mitochondrial protein compendium elucidates complex I disease biology. Cell 134:112-123.
Palomo GM, Manfredi G (2015) Exploring new pathways of neurodegeneration in ALS: the role of mitochondria quality control. Brain Res 1607:36-46.
Palty R, Silverman WF, Hershfinkel M, Caporale T, Sensi SL, Parnis J, Nolte C, Fishman D, Shoshan-Barmatz V, Herrmann S, Khananshvili D, Sekler I (2010) NCLX is an essential component of mitochondrial Na+/Ca2+ exchange. Proc Natl Acad Sci U S A 107:436-441.
Pasanen P, Myllykangas L, Poyhonen M, Kiuru-Enari S, Tienari PJ, Laaksovirta H, Toppila J, Ylikallio E, Tyynismaa H, Auranen M (2016) Intrafamilial clinical variability in individuals carrying the CHCHD10 mutation Gly66Val. Acta Neurol Scand 133:361-366.
Pasinelli P, Belford ME, Lennon N, Bacskai BJ, Hyman BT, Trotti D, Brown RH, Jr. (2004) Amyotrophic lateral sclerosis-associated SOD1 mutant proteins bind and aggregate with Bcl-2 in spinal cord mitochondria. Neuron 43:19-30.
Peng TI, Greenamyre JT (1998) Privileged access to mitochondria of calcium influx through N-methyl-D-aspartate receptors. Mol Pharmacol 53:974-980.
Penttila S, Jokela M, Bouquin H, Saukkonen AM, Toivanen J, Udd B (2015) Late onset spinal motor neuronopathy is caused by mutation in CHCHD10. Ann Neurol 77:163-172.
Perocchi F, Gohil VM, Girgis HS, Bao XR, McCombs JE, Palmer AE, Mootha VK (2010) MICU1 encodes a mitochondrial EF hand protein required for Ca(2+) uptake. Nature 467:291-296.
Perrone F, Nguyen HP, Van Mossevelde S, Moisse M, Sieben A, Santens P, De Bleecker J, Vandenbulcke M, Engelborghs S, Baets J, Cras P,

Vandenberghe R, De Jonghe P, De Deyn PP, Martin JJ, Van Damme P, Van Broeckhoven C, van der Zee J, Belgian Neurology c (2017) Investigating the role of ALS genes CHCHD10 and TUBA4A in Belgian FTD-ALS spectrum patients. Neurobiol Aging 51:177 e179-177 e116.
Peters OM, Ghasemi M, Brown RH, Jr. (2015) Emerging mechanisms of molecular pathology in ALS. J Clin Invest 125:1767-1779.
Pizzo P, Drago I, Filadi R, Pozzan T (2012) Mitochondrial Ca(2)(+) homeostasis: mechanism, role, and tissue specificities. Pflugers Arch 464:3-17.
Racay P, Tatarkova Z, Chomova M, Hatok J, Kaplan P, Dobrota D (2009) Mitochondrial calcium transport and mitochondrial dysfunction after global brain ischemia in rat hippocampus. Neurochemical research 34:1469-1478.
Rigby K, Zhang L, Cobine PA, George GN, Winge DR (2007) characterization of the cytochrome c oxidase assembly factor Cox19 of Saccharomyces cerevisiae. J Biol Chem 282:10233-10242.
Robberecht W, Philips T (2013) The changing scene of amyotrophic lateral sclerosis. Nat Rev Neurosci 14:248-264.
Ronchi D, Riboldi G, Del Bo R, Ticozzi N, Scarlato M, Galimberti D, Corti S, Silani V, Bresolin N, Comi GP (2015) CHCHD10 mutations in Italian patients with sporadic amyotrophic lateral sclerosis. Brain 138:e372.
Rosen DR, Siddique T, Patterson D, Figlewicz DA, Sapp P, Hentati A, Donaldson D, Goto J, O'Regan JP, Deng HX, et al. (1993) Mutations in Cu/Zn superoxide dismutase gene are associated with familial amyotrophic lateral sclerosis. Nature 362:59-62.
Rubino E, Brusa L, Zhang M, Boschi S, Govone F, Vacca A, Gai A, Pinessi L, Lopiano L, Rogaeva E, Rainero I (2017) Genetic analysis of CHCHD2 and CHCHD10 in Italian patients with Parkinson's disease. Neurobiol Aging.
Schapira AH, Cooper JM, Dexter D, Clark JB, Jenner P, Marsden CD (1990) Mitochondrial complex I deficiency in Parkinson's disease. J Neurochem 54:823-827.
Schinzel AC, Takeuchi O, Huang Z, Fisher JK, Zhou Z, Rubens J, Hetz C, Danial NN, Moskowitz MA, Korsmeyer SJ (2005) Cyclophilin D is a component of mitochondrial permeability transition and mediates neuronal cell death after focal cerebral ischemia. Proceedings of the National Academy of Sciences of the United States of America 102:12005-12010.
Scorrano L (2009) Opening the doors to cytochrome c: changes in mitochondrial shape and apoptosis. Int J Biochem Cell Biol 41:1875-1883.
Scorrano L, Ashiya M, Buttle K, Weiler S, Oakes SA, Mannella CA, Korsmeyer SJ (2002) A distinct pathway remodels mitochondrial cristae and mobilizes cytochrome c during apoptosis. Dev Cell 2:55-67.

Seo M, Lee WH, Suk K (2010) Identification of novel cell migration-promoting genes by a functional genetic screen. FASEB J 24:464-478.
Shi CH, Mao CY, Zhang SY, Yang J, Song B, Wu P, Zuo CT, Liu YT, Ji Y, Yang ZH, Wu J, Zhuang ZP, Xu YM (2016) CHCHD2 gene mutations in familial and sporadic Parkinson's disease. Neurobiol Aging 38:217 e219-213.
Siegel CS, McCullough LD (2013) NAD+ and nicotinamide: sex differences in cerebral ischemia. Neuroscience 237:223-231.
Sileikyte J, Forte M (2016) Shutting down the pore: The search for small molecule inhibitors of the mitochondrial permeability transition. Biochim Biophys Acta 1857:1197-1202.
Simpkins JW, Yi KD, Yang SH, Dykens JA (2010) Mitochondrial mechanisms of estrogen neuroprotection. Biochim Biophys Acta 1800:1113-1120.
Sims NR (1990) Rapid isolation of metabolically active mitochondria from rat brain and subregions using Percoll density gradient centrifugation. J Neurochem 55:698-707.
Sims NR, Anderson MF (2008) Isolation of mitochondria from rat brain using Percoll density gradient centrifugation. Nat Protoc 3:1228-1239.
Sims NR, Muyderman H (2010) Mitochondria, oxidative metabolism and cell death in stroke. Biochim Biophys Acta 1802:80-91.
Snyder MA, Smejkalova T, Forlano PM, Woolley CS (2010) Multiple ERbeta antisera label in ERbeta knockout and null mouse tissues. Journal of neuroscience methods 188:226-234.
Sohrabji F, Park MJ, Mahnke AH (2017) Sex differences in stroke therapies. J Neurosci Res 95:681-691.
Spychala MS, Honarpisheh P, McCullough LD (2017) Sex differences in neuroinflammation and neuroprotection in ischemic stroke. J Neurosci Res 95:462-471.
Starkov AA (2010) The molecular identity of the mitochondrial Ca2+ sequestration system. FEBS J 277:3652-3663.
Starkov AA, Chinopoulos C, Fiskum G (2004) Mitochondrial calcium and oxidative stress as mediators of ischemic brain injury. Cell calcium 36:257-264.
Stauch KL, Purnell PR, Fox HS (2014) Quantitative proteomics of synaptic and nonsynaptic mitochondria: insights for synaptic mitochondrial vulnerability. J Proteome Res 13:2620-2636.
Stojanovski D, Muller JM, Milenkovic D, Guiard B, Pfanner N, Chacinska A (2008) The MIA system for protein import into the mitochondrial intermembrane space. Biochim Biophys Acta 1783:610-617.
Sun J, Huang YR, Harrington WR, Sheng S, Katzenellenbogen JA, Katzenellenbogen BS (2002) Antagonists selective for estrogen receptor alpha. Endocrinology 143:941-947.
Sun N, Youle RJ, Finkel T (2016) The Mitochondrial Basis of Aging. Mol Cell 61:654-666.

Supnet C, Bezprozvanny I (2010) The dysregulation of intracellular calcium in Alzheimer disease. Cell Calcium 47:183-189.
Szabo I, Zoratti M (1991) The giant channel of the inner mitochondrial membrane is inhibited by cyclosporin A. J Biol Chem 266:3376-3379.
Taylor WA, Mejia EM, Mitchell RW, Choy PC, Sparagna GC, Hatch GM (2012) Human trifunctional protein alpha links cardiolipin remodeling to beta-oxidation. PloS one 7:e48628.
Therrien M, Dion PA, Rouleau GA (2016) ALS: Recent Developments from Genetics Studies. Curr Neurol Neurosci Rep 16:59.
Toledo FD, Perez LM, Basiglio CL, Ochoa JE, Sanchez Pozzi EJ, Roma MG (2014) The Ca(2+)-calmodulin-Ca(2+)/calmodulin-dependent protein kinase II signaling pathway is involved in oxidative stress-induced mitochondrial permeability transition and apoptosis in isolated rat hepatocytes. Arch Toxicol 88:1695-1709.
Tremblay GB, Tremblay A, Copeland NG, Gilbert DJ, Jenkins NA, Labrie F, Giguere V (1997) Cloning, chromosomal localization, and functional analysis of the murine estrogen receptor beta. Molecular endocrinology 11:353-365.
Tymianski M, Charlton MP, Carlen PL, Tator CH (1993) Source specificity of early calcium neurotoxicity in cultured embryonic spinal neurons. J Neurosci 13:2085-2104.
Venable JH, Coggeshall R (1965) A Simplified Lead Citrate Stain for Use in Electron Microscopy. J Cell Biol 25:407-408.
Vijayvergiya C, Beal MF, Buck J, Manfredi G (2005) Mutant superoxide dismutase 1 forms aggregates in the brain mitochondrial matrix of amyotrophic lateral sclerosis mice. J Neurosci 25:2463-2470.
Vives-Bauza C, Yang L, Manfredi G (2007) Assay of mitochondrial ATP synthesis in animal cells and tissues. Methods Cell Biol 80:155-171.
Warne J, Pryce G, Hill JM, Shi X, Lenneras F, Puentes F, Kip M, Hilditch L, Walker P, Simone MI, Chan AW, Towers GJ, Coker AR, Duchen MR, Szabadkai G, Baker D, Selwood DL (2016) Selective Inhibition of the Mitochondrial Permeability Transition Pore Protects against Neurodegeneration in Experimental Multiple Sclerosis. J Biol Chem 291:4356-4373.
Wei Y, Vellanki RN, Coyaud E, Ignatchenko V, Li L, Krieger JR, Taylor P, Tong J, Pham NA, Liu G, Raught B, Wouters BG, Kislinger T, Tsao MS, Moran MF (2015) CHCHD2 Is Coamplified with EGFR in NSCLC and Regulates Mitochondrial Function and Cell Migration. Mol Cancer Res 13:1119-1129.
Weis SN, Toniazzo AP, Ander BP, Zhan X, Careaga M, Ashwood P, Wyse AT, Netto CA, Sharp FR (2014) Autophagy in the brain of neonates following hypoxia-ischemia shows sex- and region-specific effects. Neuroscience 256:201-209.

Writing Group M et al. (2010) Heart disease and stroke statistics--2010 update: a report from the American Heart Association. Circulation 121:e46-e215.
Xiao T, Jiao B, Zhang W, Pan C, Wei J, Liu X, Zhou Y, Zhou L, Tang B, Shen L (2016) Identification of CHCHD10 Mutation in Chinese Patients with Alzheimer Disease. Mol Neurobiol.
Yang H, Wang H, Jaenisch R (2014) Generating genetically modified mice using CRISPR/Cas-mediated genome engineering. Nat Protoc 9:1956-1968.
Yang SH, Sarkar SN, Liu R, Perez EJ, Wang X, Wen Y, Yan LJ, Simpkins JW (2009) Estrogen receptor beta as a mitochondrial vulnerability factor. J Biol Chem 284:9540-9548.
Yang SH, Liu R, Perez EJ, Wen Y, Stevens SM, Jr., Valencia T, Brun-Zinkernagel AM, Prokai L, Will Y, Dykens J, Koulen P, Simpkins JW (2004) Mitochondrial localization of estrogen receptor beta. Proc Natl Acad Sci U S A 101:4130-4135.
Zamzami N, Marchetti P, Castedo M, Decaudin D, Macho A, Hirsch T, Susin SA, Petit PX, Mignotte B, Kroemer G (1995) Sequential reduction of mitochondrial transmembrane potential and generation of reactive oxygen species in early programmed cell death. J Exp Med 182:367-377.
Zhang L, Blackman BE, Schonemann MD, Zogovic-Kapsalis T, Pan X, Tagliaferri M, Harris HA, Cohen I, Pera RA, Mellon SH, Weiner RI, Leitman DC (2010) Estrogen receptor beta-selective agonists stimulate calcium oscillations in human and mouse embryonic stem cell-derived neurons. PLoS One 5:e11791.
Zhang M et al. (2015) Mutation analysis of CHCHD10 in different neurodegenerative diseases. Brain 138:e380.
Zhao L, Brinton RD (2007) Estrogen receptor alpha and beta differentially regulate intracellular Ca(2+) dynamics leading to ERK phosphorylation and estrogen neuroprotection in hippocampal neurons. Brain research 1172:48-59.
Zhou P, Qian L, D'Aurelio M, Cho S, Wang G, Manfredi G, Pickel V, Iadecola C (2012a) Prohibitin reduces mitochondrial free radical production and protects brain cells from different injury modalities. J Neurosci 32:583-592.
Zhou Z, Zhou J, Du Y (2012b) Estrogen receptor beta interacts and colocalizes with HADHB in mitochondria. Biochemical and biophysical research communications 427:305-308.
Zhu C, Xu F, Wang X, Shibata M, Uchiyama Y, Blomgren K, Hagberg H (2006) Different apoptotic mechanisms are activated in male and female brains after neonatal hypoxia-ischaemia. J Neurochem 96:1016-1027.
Zhu L, Gomez-Duran A, Saretzki G, Jin S, Tilgner K, Melguizo-Sanchis D, Anyfantis G, Al-Aama J, Vallier L, Chinnery P, Lako M, Armstrong L

(2016) The mitochondrial protein CHCHD2 primes the differentiation potential of human induced pluripotent stem cells to neuroectodermal lineages. J Cell Biol 215:187-202.
Zoratti M, Szabo I (1995) The mitochondrial permeability transition. Biochim Biophys Acta 1241:139-176.

APPENDIX

SEX SPECIFIC ACTIVATION OF THE ERα AXIS OF THE MITOCHONDRIAL UPR (UPR^{MT}) IN THE G93A-SOD1 MOUSE MODEL OF FAMILIAL ALS *

Abstract

The mitochondrial unfolded protein response (UPR^{mt}) is a transcriptional program aimed at restoring proteostasis in mitochondria. Upregulation of mitochondrial matrix proteases and heat shock proteins was initially described. Soon thereafter, a distinct UPR^{mt} induced by misfolded proteins in the mitochondrial intermembrane space (IMS) and mediated by the estrogen receptor alpha (ERα), was found to upregulate the proteasome and the IMS protease OMI. However, the IMS-UPR^{mt} was never studied in a neurodegenerative disease *in vivo*. Thus, we investigated the IMS-UPR^{mt} in the G93A-SOD1 mouse model of familial ALS, since mutant SOD1 is known to accumulate in the IMS of neural tissue and cause mitochondrial dysfunction. As the ERα is most active in females, we postulated that a differential involvement of the IMS-UPR^{mt} could be linked to the longer lifespan of females in the G93A-SOD1 mouse. We found a significant sex difference in the IMS-UPR^{mt}, because the spinal cords of female, but not male, G93A-SOD1 mice showed elevation of OMI and proteasome activity. Then, using a mouse in which G93A-SOD1 was selectively targeted to the IMS, we demonstrated that the IMS-UPR^{mt} could be specifically initiated by mutant SOD1 localized in the IMS. Furthermore, we showed that, in the absence of ERα, G93A-SOD1 failed to activate OMI and the proteasome, confirming the ERα dependence of the response. Taken together, these results demonstrate the IMS-UPR^{mt} activation in SOD1 familial ALS, and suggest that sex differences in the disease phenotype could be linked to differential activation of the ERα axis of the IMS-UPR^{mt}.

* Sex specific activation of the ERα axis of the mitochondrial UPR (UPR^{mt}) in the G93A-SOD1 mouse model of familial ALS. *Hum Mol Genet* 2017; 26 (7):1318-1327. doi: 10.1093/hmg/ddx049

Amanjot K. Riar[1*], Suzanne R. Burstein[2*], Gloria M. Palomo[2], Andrea Arreguin[2], Giovanni Manfredi[2#], Doris Germain[1#].

[1]Icahn School of Medicine at Mount Sinai, Tisch Cancer Institute, Department of Medicine, Division of Hematology/ Oncology, New York, 10029, NY, USA

[2]Brain and Mind Research Institute, Weill Cornell Medicine, New York, 10065 NY, USA

[*]These authors contributed equally to this work

[#]Co-corresponding authors

Introduction

Mutations in the Cu,Zn,superoxide dismutase (SOD1) are responsible for approximately 20% of fALS (Rosen, 1993).The pathophysiology of SOD1-ALS is not completely understood, and different mechanisms may participate in pathogenesis (Ilieva et al., 2009), including mitochondrial dysfunction (Hervias et al., 2006; Shi et al., 2010). The G93A amino acid substitution in SOD1 is one of the most extensively studied mutations, both in cultured cells and in mouse models of the disease. Transgenic mice express high levels of G93A-SOD1 ubiquitously, under the control of the SOD1 endogenous promoter. They develop rapid motor neuron degeneration, resulting in paralysis and death by 4 or 5 months of age, depending on the genetic background (Gurney et al., 1994).The prevalent theory for the pathogenesis of mutant SOD1 involves a gain of toxic function of G93A-SOD1. One critical observation is that misfolded SOD1 localizes to multiple cell compartments, including mitochondria. Mutant SOD1 accumulates on the mitochondrial outer membrane (Vande Velde et al., 2008) where it interacts with some crucial proteins, such as Bcl2 (Pedrini et al., 2010) and VDAC (Israelson et al., 2010). However, mutant SOD1 also localizes inside the mitochondrial IMS, where it accumulates and misfolds, potentially interfering with the assembly and maturation of mitochondrial proteins (Vijayvergiya et al., 2005; Ferri et al., 2006; Kawamata and Manfredi, 2008). The pathogenic role of the IMS pool of mutant SOD1 is also supported by evidence from cultured motor neurons, where it causes mitochondrial functional, morphological, and axonal transport abnormalities (Cozzolino et al., 2009; Magrane et al., 2009). Furthermore, we recently developed transgenic mice containing G93A-SOD1 in the IMS but not the cytoplasm (G93A IMS-SOD1), and showed that these mice develop some of the symptoms of ALS, including motor defects and mitochondrial abnormalities (Igoudjil et al., 2011). However, one important difference between this mouse and the G93A-SOD1 mouse (where G93A-SOD1 is present in both the cytosol and the IMS) is that the IMS-only mice develop disease symptoms almost one year later. Taken together, these findings indicate that eventually the accumulation of misfolded G93A-SOD1 in the IMS is toxic for mitochondria and neurons, but they also suggest that IMS proteotoxic stress may initially activate cytoprotective responses.

A mitochondrial unfolded protein response (UPR^{mt}) was first described as a consequence of the accumulation of misfolded proteins in the matrix (Martinus et al., 1996; Zhao et al., 2002). These studies revealed that CHOP promotes the expression of matrix protein quality control systems, such as proteases and chaperones, namely hsp10 and hsp60 (Martinus et al., 1996; Zhao et al., 2002). Unlike in the matrix, there are no chaperones in the IMS, and while AAA proteases face the IMS, none of their substrates are IMS proteins (Augustin et al., 2005; Koppen and Langer, 2007).

We previously reported that the proteasome plays an active role in limiting the accumulation of misfolded proteins in the IMS (Radke et al., 2008), and that the IMS protease OMI plays a role in IMS protein quality control

(Radke et al., 2008). Then, we reported that accumulation of misfolded proteins in the IMS did not activate the CHOP-hsp60 axis of the UPR^{mt}, but rather a distinct response driven by the estrogen receptor alpha (ERα) (Papa and Germain, 2011). The ERα axis of the UPR^{mt} implicates a cross talk between phosphorylated Akt and the ERα, expression of the mitochondrial transcription factor NRF-1, and most importantly for the current study, the up-regulation of the proteasome and OMI (Papa and Germain, 2011).

The ERα dependency of the IMS-UPR^{mt} raises intriguing questions. First, since not all cell types express ERα, how do ERα negative cells cope with accumulation of misfolded proteins in the IMS? Our studies in breast cancer cells suggested that in absence of the ERα, the CHOP-hsp60 could partially compensate (Papa and Germain, 2014). Second, since the ERα is most active in females, do the mechanisms to cope with proteotoxic stress in the IMS caused by misfolding of disease related mutant proteins, such as SOD1, differ between sexes, and if so, do they correlate with sex differences in the disease phenotype? To address this question we studied a G93A-SOD1 mouse model of familial ALS, in which females have a longer lifespan than males (Heiman-Patterson et al., 2005), in order to evaluate whether differences in the activation of the IMS-UPR^{mt} could be detected *in vivo* and correlated with the sexual dimorphism. These questions could be directly relevant to human ALS, since the frequency of the disease is significantly higher in males than in females (McCombe and Henderson, 2010), suggesting that sex hormones and receptors may be involved in sexual dimorphism in ALS.

Materials and Methods

Animals

We used the B6SJL-Tg(SOD1*G93A)1Gur/J, the Tg(SOD1)2Gur, the B6SJL-Tg(Prnp-Immt/SOD1*G93A)7Gmnf/J, and the B6SJL-Tg(Prnp-Immt/SOD1)1Gmnf/J from The Jackson Laboratory. Estrogen Receptor α knockout animals with the G93A-SOD1 mutation (ERαKO-G93A) in the C57BL/6J congenic background were generated by crossing the G93A-SOD1 line (B6.Cg-Tg (SOD1-G93A)1Gur/J) with ERαKO heterozygote mice (B6.129P2-Esr1tm1Ksk/J), both available from The Jackson Laboratory. Females heterozygous for ERαKO were bred with males heterozygous for ERαKO, which also had the G93A-SOD1 mutation. At the indicated ages, animals were sacrificed and tissues harvested in storage solution (10mM Tris pH 7.4, 320 mM sucrose, 20% DMSO), and immediately frozen in liquid nitrogen.

All experiments were approved by the Weill Cornell Medical College Institutional Animal Care and Use Committee. Principles of laboratory animal care" (NIH publication No. 86-23, revised 1985) were followed, as well as specific national laws (e.g. the current version of the German Law on the Protection of Animals), where applicable.

Western blotting

Spinal cords were lysed in NP-40 lysis buffer, sonicated for 1 sec at an amplitude of 20% and centrifuged at 14,000 rpm at 4°C for 20 min. Proteins were separated on 10% or 4-20% Mini-PROTEAN TGX gels (Bio-Rad,CA) and transferred to nitrocellulose blotting membrane (GE Healthcare Life Sciences). Membranes were probed with primary antibodies against phosphorylated-Akt (Cell Signaling), Akt (Cell Signaling), Omi/HtrA2 (Biovison), NRF-1 (Abcam), hsp60 (BD Bioscience), CHOP (Cell Signaling), BiP (BD Bioscience), Ub-48 (EMD Millipore) and Actin (EMD Millipore) overnight at 4˚C. Blots were then probed with horseradish peroxidase-conjugated anti-mouse (Jackson ImmunoResearch) or anti-rabbit (Thermo Scientific) secondary antibodies and detected using enhanced chemiluminescence (GE Healthcare or Millipore).

Proteasome assay

Spinal cord lysates (10 µg) were incubated in proteasome activity assay buffer (50mM Tris-HCl, pH 7.5) with 10 µM trypsin fluorogenic substrate Ac-Ala-Leu-Ala-AMC (Ac-ALA-AMC) or chymotrypsin fluorogenic substrate succinly-Leu-Leu-Val-Tyr-7-amino-4-methylcoumarin (Suc-LLVY-AMC), or caspase fluorogenic substrates N-acetyl-Gly-Pro-Leu-Ala-AMC (Ac-GPLA-AMC) for 3 hours at 37˚ C. Release of free hydrolysed 7-amino-4-methylcoumarin (AMC) groups was measured at 380 nm excitation and 460nm emission using SpectraMax M5e microplate reader (Molecular Devices).

Statistical analysis

Data is presented as mean ± SEM. Two-tailed Students's *t*-test was used to determine the significance between two datasets. **p*<0.05 was considered as statistically significant. All statistical analysis was performed using GraphPad Instat software.

Results

The CHOP/hsp60 axis of the UPR^{mt} is transiently activated in females during the symptomatic phase of the G93A-SOD1 model of fALS.

The first described axis of the UPR^{mt} is regulated by the transcription factor CHOP, which promotes the expression of proteases as well as the chaperone hsp60 (Martinus et al., 1996; Zhao et al., 2002). As a consequence, the promoter of hsp60 has been widely used in subsequent studies of the UPRmt, notably in C. elegans (Benedetti et al., 2006) (Haynes et al., 2007; Fiorese et al., 2016; Lin et al., 2016) (Durieux et al., 2011; Nargund et al., 2012; Mohrin et al., 2015; Nargund et al., 2015) (Tian et al., 2016).

We therefore initiated our analysis of the UPRmt in the spinal cord of G93A-SOD1 mouse model of familial ALS by monitoring the levels of CHOP and hsp60. G93A-SOD1 transgenic mice develop an aggressive form of motor neuron disease, with paralysis onset at 90 days of age and death at 130 days

of age (Gurney et al., 1994). Therefore, studies were performed in male and female G93A-SOD1 mice and non-transgenic control littermates at different

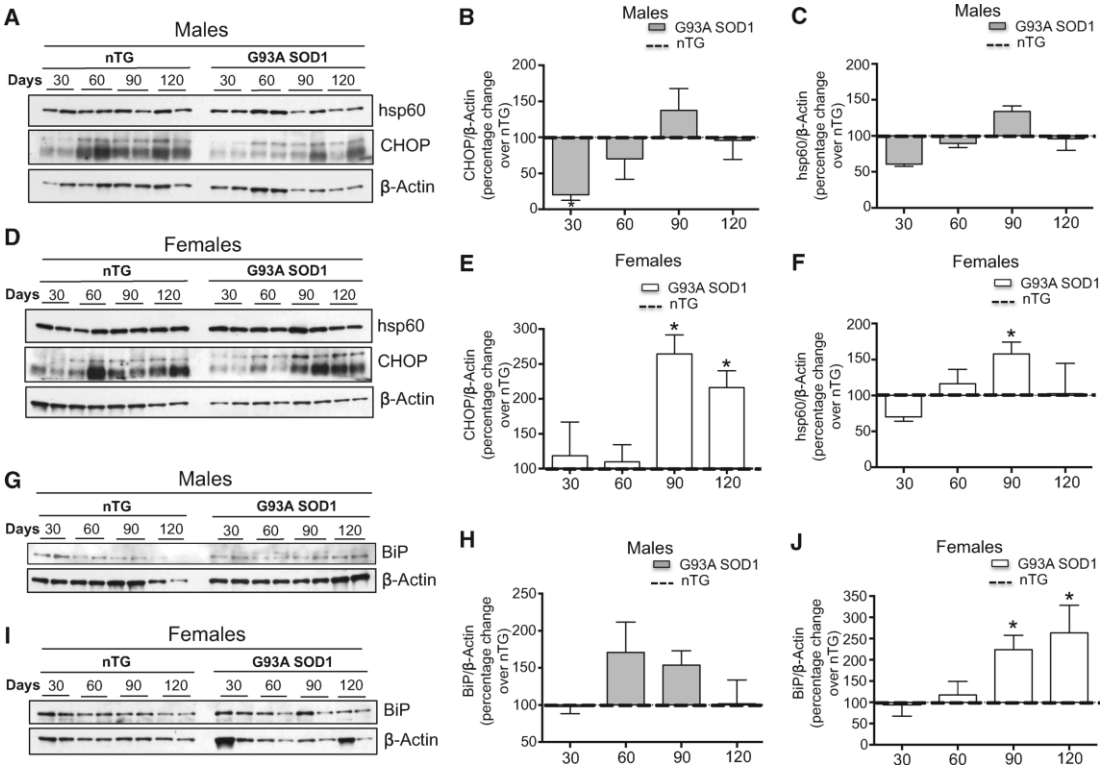

Appendix Figure 1. The CHOP/hsp60 axis is activated during the symptomatic phase in the G93A-SOD1 model of fALS. (A) Representative western blot of hsp60 and CHOP in 2 non-transgenic males and 2 G93A-SOD1 males at day 30, 60, 90 and 120. β-actin was used as a loading control. (B) Quantification of the level of CHOP at each time point in males. n = 4. The level of CHOP relative to β-actin was determined for 4 non-transgenic males and the average of the 4 values set to 100 percent for each time point. The average level of CHOP relative to β-actin was also determined in 4 G93A-SOD1 transgenic males at each time point and expressed as a percentage change relative to the non-transgenic males (dotted line). (C) Quantification of the level of hsp60 in males, as in B. n = 4. (D) Representative western blot of hsp60 and CHOP in 2 non-transgenic females and 2 G93A-SOD1 females at day 30, 60, 90 and 120. β-actin was used as a loading control. (E) Quantification of the level of CHOP in females, as in B. n = 4. (F) Quantification of the level of hsp60 in females, as in B. n = 4. (G) Representative western blot of BiP in 2 non-transgenic males and 2 G93A-SOD1 males at day 30, 60, 90 and 120. β-actin was used as a loading control. (H) Quantification of the level of BiP in males, as in B. n = 4. (I) Representative western blot of BiP in 2 non-transgenic females and 2 G93A-SOD1 females at day 30, 60, 90 and 120. β-actin was used as a loading control. (J) Quantification of the level of BiP in females, as in B. n = 4. *P < 0.05 when compared to the respective non-transgenic.

ages, starting at 30 and 60 days, representing pre-symptomatic disease stages, and at 90 and 120 days, representing early and late symptomatic stages, respectively.

To study the effect of the mutant transgene on UPRmt markers in spinal cord, protein levels were normalized to non-transgenic control values at each age. We found that in males, CHOP levels were significantly lower as compared to age-matched transgenic males at 30 days (Fig. 1A,B). However, at day 60 and thereafter CHOP levels in mutant mice were no longer lower. In females, there was no CHOP decrease at 30 days, and remarkably a robust CHOP increase was observed during the symptomatic phase, at 90 and 120 days (Fig. 1D,E). In female G93A-SOD1 mice, but not in males (Fig. 1A,C), hsp60 was significantly higher at 90 days of age, but it reverted to control levels at 120 days (Fig. 1D,F).

Since CHOP also regulates the expression of the chaperone BiP during the UPRER independently of its role in the UPRmt, we tested whether BiP is elevated in transgenic females. We found that the levels of BiP closely matched CHOP levels at every time point tested (Fig. 1G,H). This finding is in agreement with the extensively characterized ER-stress activation in ALS mice (Matus et al., 2013). To test whether this response was specific to regions of the CNS affected by the disease, such as the spinal cord. CHOP and hsp60 were measured in the cerebellum, which is unaffected in G93A-SOD1 mice, of females at 60 and 120 days of age, when a significant increase was observed in the spinal cord. We found no significant differences in CHOP or hsp60 in the cerebellum of G93A-SOD1 transgenic mice compared to non-transgenic mice (Suppl. Fig 1, A, B, C), suggesting that the response did not take place in unaffected regions of the CNS.

Taken together these results indicate that in ALS spinal cord there is activation of CHOP-mediated stress responses. However, there was a clear sex difference in CHOP axis activation, since increases of all markers at symptomatic stages were only observed in G93A-SOD1 females, whereas in males the responses were absent, and even below control levels at early stages.

Sex-specific activation of the ERα axis of the UPR^{mt} in G93A-SOD1 mice.

We had previously reported that accumulation of misfolded proteins in the mitochondrial IMS in breast cancer cells activates a UPR^{mt} response pathway initiated by the phosphorylation of Akt and leading to activation of ERα, expression of the transcription factor NRF-1, increase of the IMS protease OMI, and upregulation of proteasome activity (Papa and Germain, 2011). The upregulation of OMI and proteasome activities was instrumental in promoting the degradation of misfolded IMS proteins (Papa and Germain, 2011) (Radke et al., 2008). Since misfolded SOD1 is known to accumulate and aggregate in the IMS (Ferri et al., 2006; Kawamata and Manfredi, 2010) we investigated whether the ERα axis of the UPR^{mt} was activated in the G93A-SOD1 mouse spinal cord.

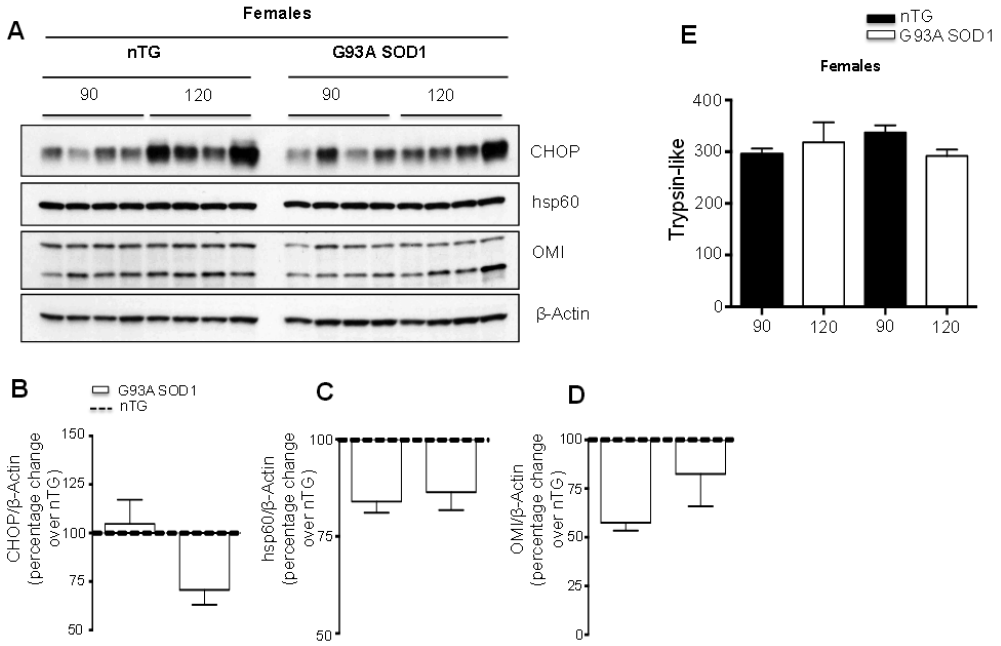

Appendix Supplementary Figure 1. *The CHOP/hsp60 and the ERα axes of the UPR^{mt} are not activated in the cerebellum during the symptomatic phase in the G93A-SOD1 model of fALS.* A) Representative western blot of CHOP, hsp60 and OMI in 4 non-transgenic females and 4 G93A-SOD1 females at day 90 and 120. β-actin was used as a loading control. B) Quantification of the level of CHOP at each time point in females. n=4. The level of CHOP relative to β-actin was determined for 4 non-transgenic females and the average of the 4 values set to 100 percent for each time point. The average level of CHOP relative to β-actin was also determined in 4 G93A-SOD1 transgenic females at each time point and expressed as a percentage change relative to the non-transgenic females value (dotted line). C) Quantification of the level of hsp60 in females, as in B. n=4. D) Quantification of the level of OMI in females, as in B. E) The trypsin-like activity of the 26S proteasome in 4 non-transgenic females (black bar) and 4 G93A-SOD1 transgenic females (gray bar) at day 90 and 120. n=4.

In males, we found an early elevation in Akt phosphorylation, NRF-1 and OMI at day 30 relative to non-transgenic mice (Fig. 2A, B, C, D). However the levels of phospho-Akt, NRF-1, and OMI decreased in G93A-SOD1 mice at later time points, suggesting that in these mice the IMS-UPR^{mt} started to decline as early as 60 days of age. In females, neither phospho-Akt nor NRF-1 were elevated relative to non-transgenic mice at any of the time points tested (Fig. 2E, F, G). However, OMI was markedly elevated in female G93A-SOD1 mice at the symptomatic stage (Fig. 2H). We then tested whether the

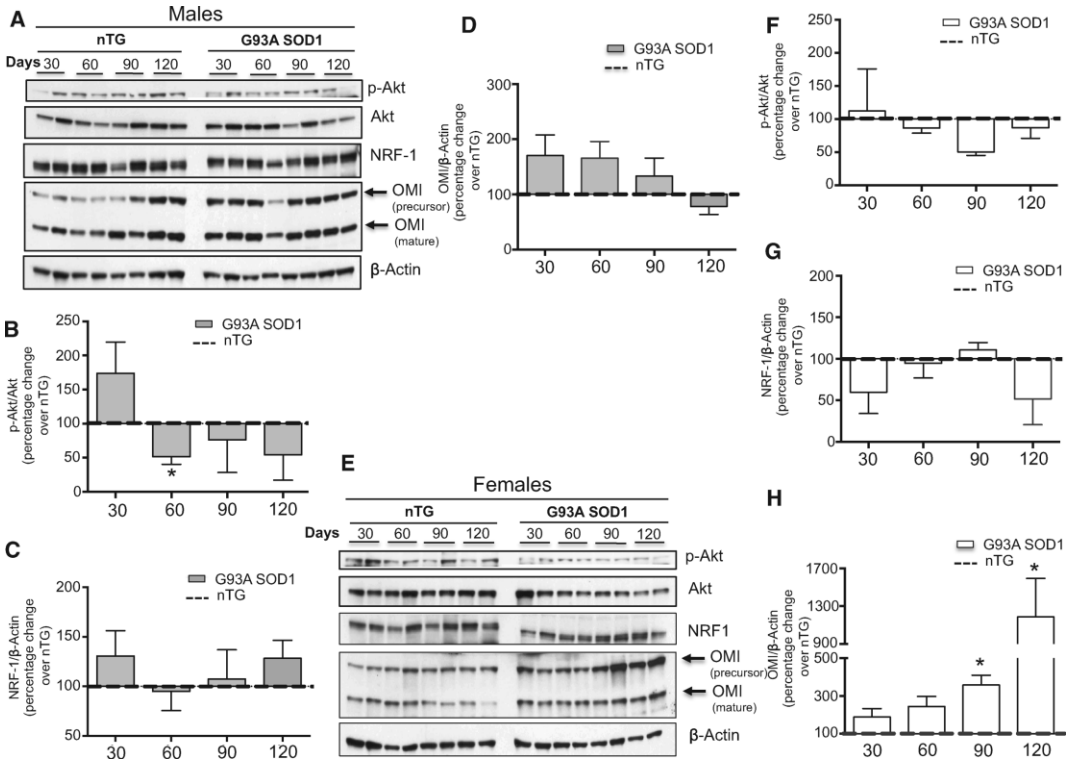

Appendix Figure 2. The UPR^{mt} is activated during the symptomatic phase the G93A-SOD1 model of fALS. (A) Representative western blot of phospho-Akt, Akt, NRF-1 and OMI in 2 non-transgenic males and 2 G93A-SOD1 males at day 30, 60, 90 and 120. β-actin was used as a loading control. (B) Quantification of the ratio of phospho-Akt to total Akt at each time point in males. n = 4. The ratio of phospho-Akt to total Akt was determined for 4 non-transgenic males and the average of the 4 values set to 100 percent for each time point. The ratio of phospho-Akt to total Akt was also determined in 4 G93A-SOD1 transgenic males at each time point and expressed as a percentage change relative to the non-transgenic males value (dotted line). (C) Quantification of the level of NRF-1 in males, as in in B. n = 4. (D) Quantification of the level of OMI in males, as in B. n = 4. (E) Representative western blot of phospho-Akt, Akt, NRF-1 and OMI in 2 non-transgenic females and 2 G93A-SOD1 females at day 30, 60, 90 and 120. β-actin was used as a loading control. (F) Quantification of the ratio of phospho-Akt to total Akt in females, as in B. n = 4. (G) Quantification of the level of NRF-1 in females, as in B. n = 4. (H) Quantification of the level of OMI in females, as in B. n = 4. *P < 0.05 when compared to the respective non-transgenic.

activation of OMI is specific to the spinal cord. We found no significant difference in OMI in the cerebellum of G93A-SOD1 transgenic mice compared to non-transgenic mice (Suppl. Fig 1D), indicating that the effect was tissue specific. We then monitored the activity of the proteasome in spinal cord homogenates of males and females over the course of disease progression. First, proteasome activity was measured fluorimetrically, using small peptide substrates of the trypsin-like, chymotrypsin-like, and caspase-like activities. As previously reported (Papa and Germain, 2011), we found that the trypsin-like activity of the proteasome was decreased in male G93A-SOD1 mice

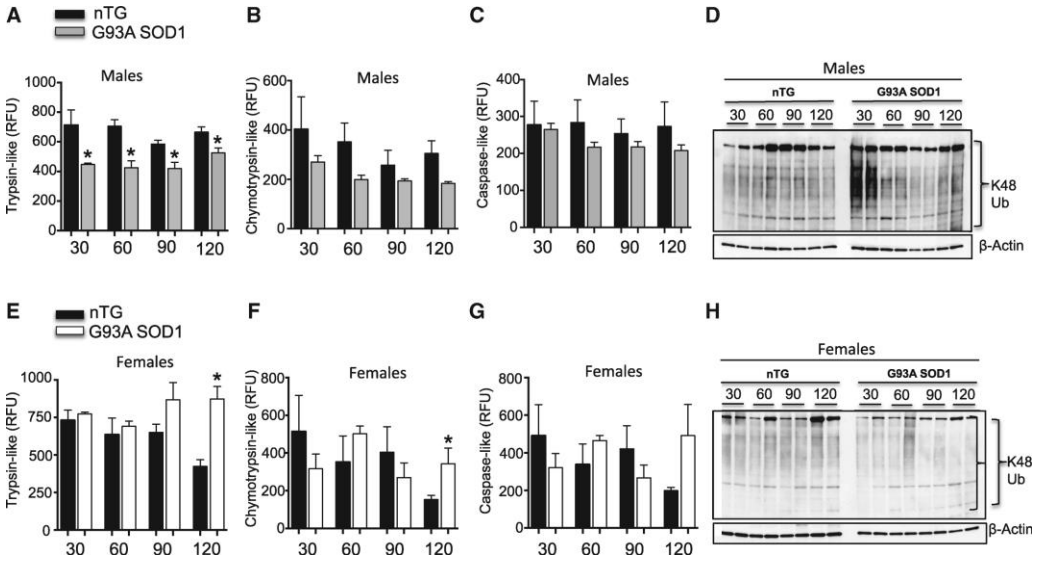

Appendix Figure 3. Proteasome activity is decreased in G93A-SOD1 males. (A) The trypsin-like activity of the 26S proteasome in 4 non-transgenic males (black bar) and 4 G93A-SOD1 males (gray bar). n = 4. (B) The chymotrypsin-like activity of the 26S proteasome in 4 non-transgenic males (black bar) and 4 G93A-SOD1 transgenic males (gray bar). n = 4. (C) The caspase-like activity of the 26S proteasome in 4 non-transgenic males (black bar) and 4 G93A-SOD1 transgenic males (gray bar). n = 4. (D) Representative Western blot of total lysine 48 ubiquitin chains in 2 non-transgenic and 2 G93A-SOD1 transgenic males. β-actin was used as a loading control. (E) The trypsin-like activity of the 26S proteasome in 4 non-transgenic females (black bar) and 4 G93A-SOD1 transgenic females (gray bar). n = 4. (F) The chymotrypsin-like activity of the 26S proteasome in 4 non-transgenic females (black bar) and 4 G93A-SOD1 transgenic females (gray bar). n = 4. (G) The caspase-like activity of the 26S proteasome in 4 non-transgenic females (black bar) and 4 G93A-SOD1 transgenic females (gray bar). n = 4. (H) Representative Western blot of total lysine-48 ubiquitin chains in 2 non-transgenic and 2 G93A-SOD1 transgenic females. β−actin was used as a loading control. *P < 0.05 when compared to the respective non-transgenic.

compared to age matched controls (Fig. 3A). In females, there was no decline of the activity at any time point; meanwhile, the trypsin-like and chymotrypsin-like activities were significantly increased at 120 days of age (Fig. 3E,F).

Again, we found no significant difference in the activity of the proteasome in the cerebellum of G93A-SOD1 transgenic females at these time points (Suppl. Fig 1E). Since the proteasome degrades ubiquitinated proteins, we studied levels of ubiquitinated proteins by western blot, using an antibody against lysine-48 ubiquitin chains, which target proteins to the proteasome. We found

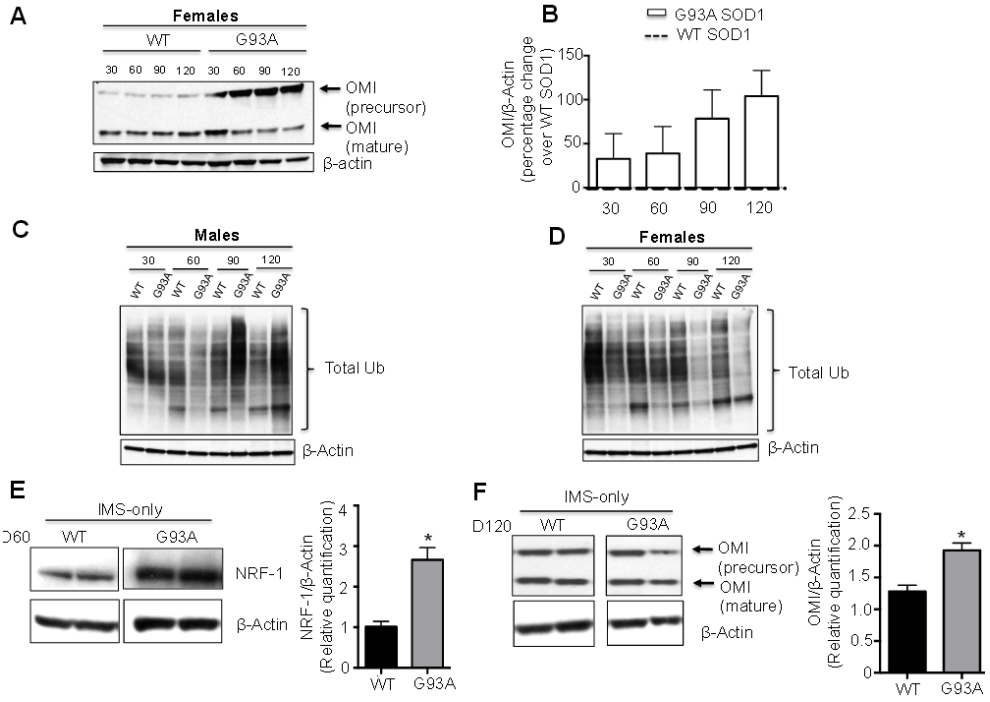

Appendix Supplementary Figure 2. The ERα axis of the UPR^{mt} is not activated in mice expressing wild-type SOD1. A) Representative western blot of OMI in 4 wild type (WT) SOD1 transgenic females and 4 G93A-SOD1 females at day 30, 60, 90 and 120. β-actin was used as a loading control. B) Quantification of the level of OMI at each time point in females in A. n=4. C) Western blot of total ubiquitin in WT-SOD1 and G93A-SOD1 transgenic males at day 30, 60, 90 and 120. β-actin was used as a loading control. D) Western blot of total ubiquitin in WT-SOD1 and G93A-SOD1 transgenic females at day 30, 60, 90 and 120. β-actin was used as a loading control. E) Western blot of NRF-1 at day 60 in two WT IMS-SOD1 transgenic females and two G93A IMS-SOD1 transgenic females. Quantification is shown on the right. F) Western blot of OMI at day 120 in two WT IMS-SOD1 transgenic females and two G93A IMS-SOD1 transgenic females. Quantification is shown on the right.

each time point in females in A. n=4.

a general increase in the levels of proteins reactive to Ub48 antibodies in G93A-SOD1 males, which was most evident at 30 and 120 days (Fig. 3D). This finding was consistent with a decrease in the activity of the proteasome in males. In female G93A-SOD1 mice, there was no increase in the levels of proteins reactive to Ub48 antibodies (Fig. 3H), in agreement with the preserved proteasome activity.

Since the G93A-SOD1 mouse overexpresses the protein, to exclude that observed effects were due to overexpression of SOD1, we examined the levels of OMI and ubiquitin in the spinal cord of mice overexpressing wild type SOD1. We found that G93A-SOD1 females showed increased OMI relative to wild type SOD1 females (Suppl. Fig 2A, B). The level of spinal cord protein ubiquitination was also increased in G93A-SOD1 males compared to wild type SOD1 males (Suppl. Fig. 2C), but was decreased in G93A-SOD1 females compared to wild type SOD1 females (Suppl. Fig. 2D). These results indicated that the effects on OMI and the proteasome are caused by mutant, and not by wild type, SOD1 expression.

Overall, these findings suggest significant sex differences in the activation of the IMS-UPR^{mt} pathway in the G93A-SOD1 mouse spinal cord. In females, we observed an increase in OMI levels and proteasome activity in symptomatic disease stages, whereas the absence of this response in males was associated with increased levels of ubiquitinated proteins.

Activation of the UPR^{mt} is observed in G93A IMS-SOD1 mice.

SOD1 is localized both in the cytosolic and mitochondrial IMS cellular compartment (Okado-Matsumoto and Fridovich, 2001). Therefore, to determine whether SOD1 localized in the IMS was specifically involved in activating the UPR^{mt} we took advantage of a transgenic mouse in which G93A-SOD1 is targeted selectively to the IMS by the addition of an N-terminus targeting sequence (G93A IMS-SOD1). As a result, G93A-SOD1 is absent from the cytosol and only concentrated in the IMS (Igoudjil et al., 2011). Since the pre-symptomatic phase is much longer in G93A IMS-SOD1mice than in the untargeted model (Igoudjil et al., 2011), we only analyzed the UPR^{mt} markers and proteasome activity at 60, 90 and 120 days.

In G93A IMS-SOD1 males, NRF-1 was significantly increased relative to the non-transgenic controls only at day 60, while no other markers of the IMS-UPR^{mt} were significantly different (Fig. 4A, B, C, D). In females, while phospho-Akt did not differ from controls, NRF-1 was significantly increased G93A IMS-SOD1 at 60 days (Fig. 4E, F, G). This observation indicates that, unlike in the untargeted model, mutant SOD1 targeted to the IMS leads to an early activation of NRF-1 in both males and females. Importantly, in female G93A IMS-SOD1 mice, OMI was significantly elevated compared to controls at 120 days of age, similarly to the untargeted females (Fig. 4H). This suggested that localization of mutant SOD1 in the IMS was sufficient to cause OMI elevation in female mice.

The activity of the proteasome in G93A IMS-SOD1 males was unaffected until 120 days of age, when a decrease in trypsin-like activity was

observed (Fig. 5A), while the other activities were unchanged at all time points (Fig. 5B, C). This suggested that IMS-restricted protein was less effective in causing proteasomal dysfunction than untargeted, mostly cytosolic, G93A-SOD1. The accumulation of lysine-48 ubiquitin was less in G93A IMS-SOD1

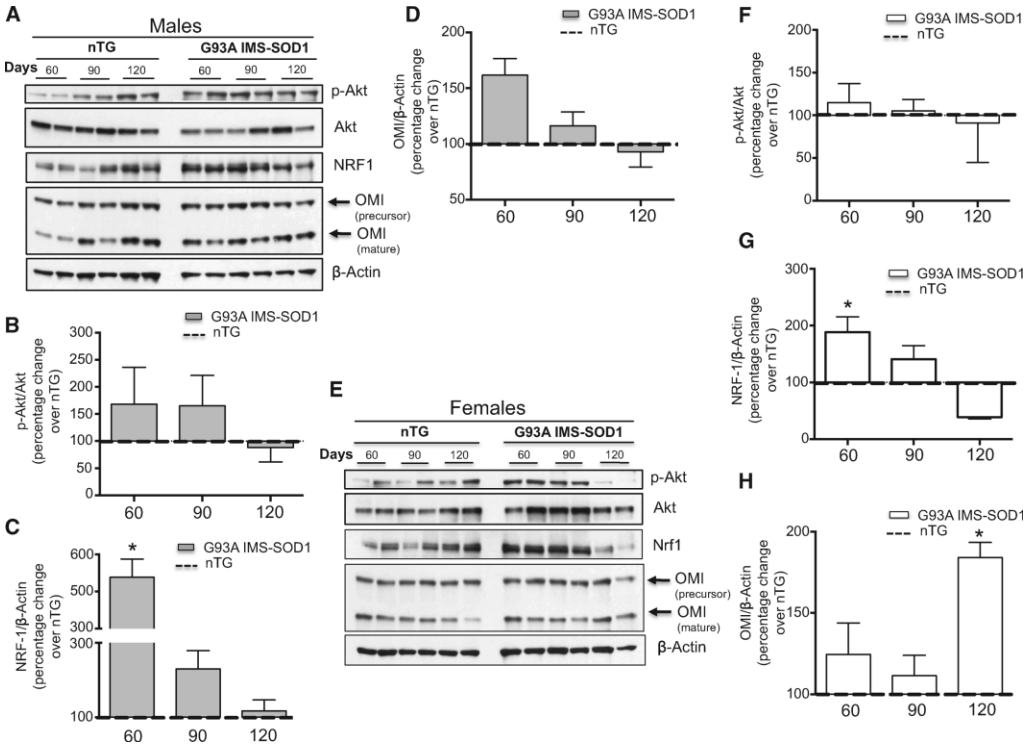

Appendix Figure 4. The UPR^{mt} is activated in G93A IMS-SOD1 mice. (A) Representative western blot of phospho-Akt, Akt, NRF-1 and OMI in 2 non-transgenic males and 2 G93A IMS-SOD1 males at day 60, 90 and 120. β-actin was used as a loading control. (B) Quantification of the ratio of phospho-Akt to total Akt at each time point in males. n = 4. The ratio of phospho-Akt to total Akt was determined for 4 non-transgenic males and the average of the 4 values set to 100 percent for each time point. The ratio of phospho-Akt to total Akt was also determined in 4 G93A IMS-SOD1 transgenic males and the average of these 4 values was expressed as a percentage change relative to the non-transgenic males (dotted line). (C) Quantification of the level of NRF-1 in males, as in B. n = 4. (D) Quantification of the level of OMI in males, as in B. n = 4. (E) Representative western blot of phospho-Akt, Akt, NRF-1 and OMI in 2 non-transgenic females and 2 G93A IMS-SOD1 females at day 60, 90 and 120. β-actin was used as a loading control. (F) Quantification of the ratio of phospho-Akt to total Akt in females, as in B. n = 4. (G) Quantification of the level of NRF-1 in females, as in B. n = 4. (H) Quantification of the level of OMI in females, as in B. n = 4. *P < 0.05 when compared to the respective non-transgenic.

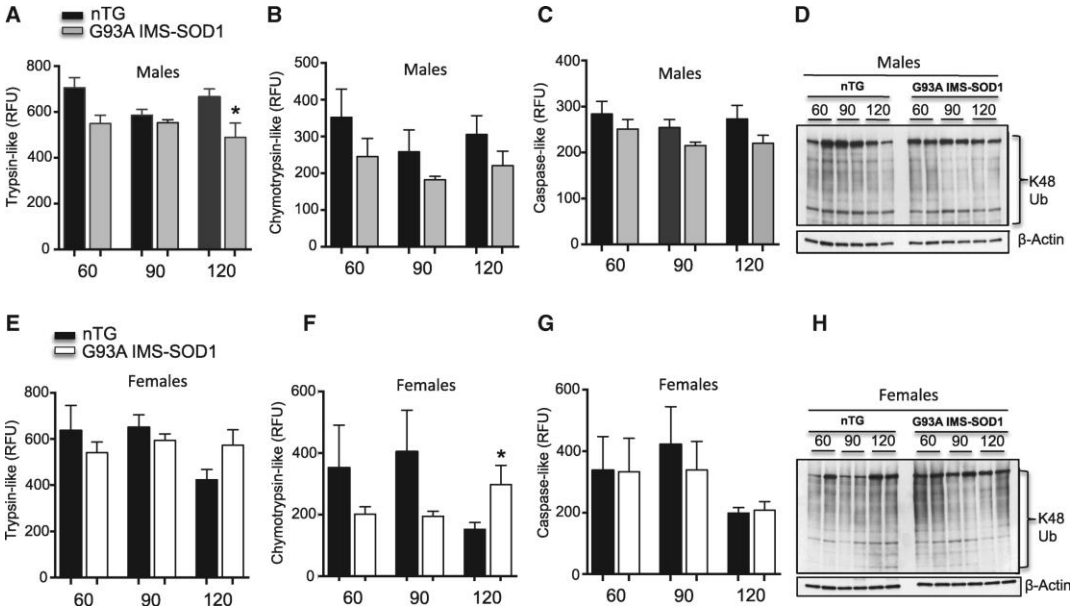

Appendix Figure 5. Monitoring the proteasome activity in the G93A IMS-SOD1 mouse model over disease progression. (A) The trypsin-like activity of the 26S proteasome in 4 non-transgenic males (black bar) and 4 G93A IMS-SOD1 transgenic males (gray bar). n = 4. (B) The chymotrypsin-like activity of the 26S proteasome in 4 non-transgenic males (black bar) and 4 G93A IMS-SOD1 transgenic males (gray bar). n = 4. (C) The caspase-like activity of the 26S proteasome in 4 non-transgenic males (black bar) and 4 G93A IMS-SOD1 transgenic males (gray bar). n = 4. (D) Representative Western blot of total lysine 48 ubiquitin chains in 2 non-transgenic and 2 G93A IMS-SOD1 transgenic males. β-actin was used as a loading control. (E) The trypsin-like activity of the 26S proteasome in 4 non-transgenic females (black bar) and 4 G93A IMS-SOD1 transgenic females (gray bar). n = 4. (F) The chymotrypsin-like activity of the 26S proteasome in 4 non-transgenic females (black bar) and 4 G93A IMS-SOD1 transgenic females (gray bar). n = 4. (G) The caspase-like activity of the 26S proteasome in 4 non-transgenic females (black bar) and 4 G93A IMS-SOD1 transgenic females (gray bar). n = 4. (H) Representative Western blot of total lysine-48 ubiquitin chains in 2 non-transgenic and 2 IMS-only G93A-SOD1 transgenic females. β-actin was used as a loading control. *P < 0.05 when compared to respective non-transgenic.

SOD1 transgenic females. β-actin was used as a loading control. *P < 0.05 when compared to respective non-transgenic.

males than age matched controls (Fig. 5D), further suggesting that the cytosolic, and not the IMS, G93A-SOD1 was responsible for proteasome impairment.

In female G93A IMS-SOD1 mice, the proteasome activity was not decreased at any time point, and, similar to the untargeted G93A-SOD1 females, the chymotrypsin activity was increased at 120 days of age (Fig. 5E, F, G). Like males, female G93A IMS-SOD1 mice did not exhibit an increase of lysine-48 ubiquitin (Fig. 5H).

Having established that NRF-1 is increased at day 60 in male G93A IMS-SOD1 mice and that OMI is elevated at day 120 in female G93A IMS-SOD1 mice, we examined NRF-1 and OMI wild type IMS-SOD1 mice at 60 and 120 days, respectively. We found that in both cases, the effect was specific to G93A IMS-SOD1 mice (Suppl. Fig. 2E, F). These results indicated that the effects on NRF-1 and OMI are caused by mutant, and not by wild type, SOD1 in the mitochondrial IMS.

Collectively, these results suggest that the IMS localization of G93A-SOD1 is responsible for the activation of the IMS-UPR^{mt} as demonstrated by the elevation of NRF-1 and OMI. They also suggest that the cytosolic localization of G93A-SOD1 is necessary to cause proteasomal dysfunction, which was absent in the G93A IMS-SOD1 mice.

Genetic ablation of ERα in G93A-SOD1 mice abolishes the activation of OMI but stimulates the CHOP/hsp60 axis of the UPR^{mt}.

In cancer cells, we reported that inhibition of the ERα by shRNA prevented the activation of OMI in response to accumulation of misfolded proteins in the IMS (Papa and Germain, 2011). Since OMI was the most affected marker of the activation of the UPR^{mt} in female G93A-SOD1 mice, we tested whether genetic ablation of the ERα in this model would affect the expression of OMI. We therefore crossed the G93A-SOD1 mouse with an ERα knockout mouse. We obtained wild type non transgenic mice, ERα knockout mice (ERαKO), and ERαKO-G93A-SOD1 mice. We tested the UPR^{mt} markers in the three genotypes and found that in males and females ER□KO-G93A-SOD1 mice OMI was not upregulated relative to both ERα knockout and wild type non-transgenic controls (Fig. 6A, B).

We then analyzed levels of CHOP and hsp60 in these mice. We found that in both male and female ERαKO-G93A-SOD1 mice there was an elevation in CHOP, which was more pronounced in females than in males (Fig. 6 C, D) and was not observed in G93A-SOD1 mice (Fig. 1). This result suggested that in the absence of the ERα-dependent axis of the UPR^{mt}, an ERα-independent axis, involving CHOP, but not OMI, could be activated as a compensatory mechanism. This result is in agreement with our finding in breast cancer cell lines, where in the absence of ERα the accumulation of misfolded proteins in the IMS activates CHOP (Papa and Germain, 2014).

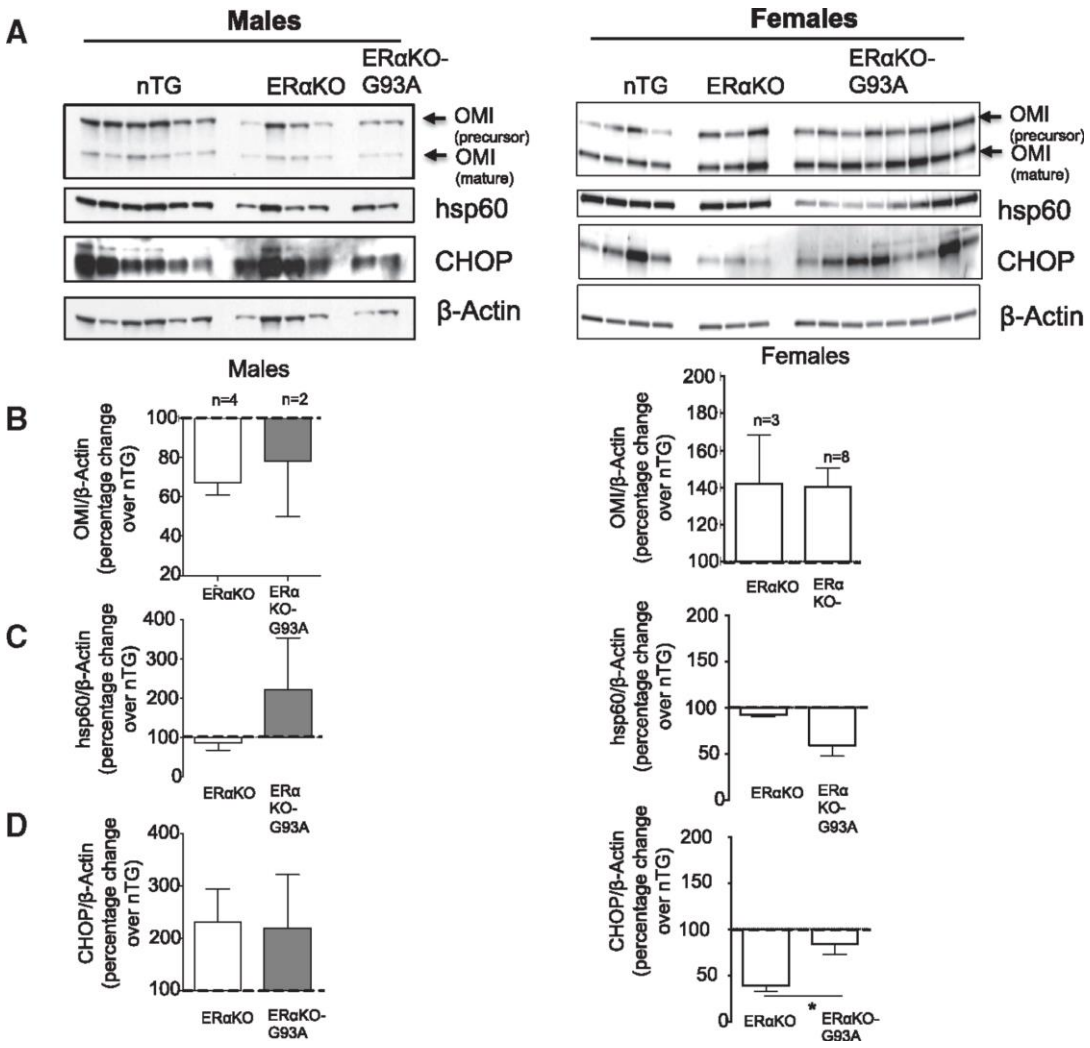

Appendix Figure 6. Genetic ablation of the ERα abolishes the activation of OMI but stimulates the CHOP/hsp60 axis of the UPR^{mt}. (A) Western blot of non-transgenic, ERαKO or ERαKO-G93A males (left) and females (right) of OMI, hsp60 and CHOP. β-actin is used as a loading control. All mice were harvested at day 60. (B) Quantification of the ratio of OMI to β−actin. For this experiment the number of mice per group varied: non-transgenic males, n = 6, ERαKO males, n= 4, ERαKO-G93A knockout males, n = 2, non-transgenic females, n = 4, ERαKO females, n = 3, ERαKO-G93A females, n = 8. Because n = 2 in some groups, the males and the females were combined to perform statistical analyses. (C) Quantification of the level of hsp60 in non-transgenic, ERαKO or ERαKO-G93A males and females. The quantification was performed as described in B. (D) Quantification of the level of CHOP in non-transgenic, ERαKO or ERαKO-G93A males and females. The quantification was performed as described in B. *P < 0.05 when compared to respective non-transgenic.

Discussion

The ERα axis of the UPR^{mt} was first identified in breast cancer cells using accumulation of misfolded protein specifically in the IMS as a tool to dissect the relative contribution of the matrix and IMS in the activation of the UPR^{mt} (Papa and Germain, 2011). However, *in vivo* validation of this pathway in a disease relevant mouse model of neurodegeneration was lacking. Since G93A-SOD1 misfolds and accumulates in the IMS, this mouse model was ideal to investigate the IMS-UPR^{mt} *in vivo* in a mammalian model of familial ALS.

The findings from this study confirmed previous observations and revealed a novel role of the IMS-specific axis of UPR^{mt}. Our results concur with previous observations that the CHOP-hsp60 axis is activated (Mohrin et al., 2015) and the proteasome inhibited during disease progression (Kabashi and Durham, 2006). While these results validate the hypothesis that the UPR^{mt} is active in G93A-SOD1 mice, they also bring additional information regarding these effects according to sex. Notably, while the proteasome was inhibited in males, it was activated in females. Differential proteasomal responses could have a disease-modifying function, but also directly participate in accumulation of misfolded SOD1 in mitochondria, since it was shown that degradation of IMS misfolded proteins involves the proteasome (Bragoszewski et al., 2013).

In addition to proteasome activation, our data revealed that the IMS protease OMI is upregulated in females. Therefore, both components of IMS protein quality control are upregulated in females. This result is consistent with the more potent role of the ERα in females.

The G93A IMS-SOD1 mouse model made it possible to dissect the specific contribution of the IMS fraction of G93A-SOD1 to the activation of the UPR^{mt}, and revealed that this fraction is sufficient to promote the activation of OMI and the proteasome in females. In addition, the comparison between the G93A-SOD1 and G93A IMS-SOD1 models showed that the inhibition of the proteasome observed in males is mainly dependent on the cytosolic mutant SOD1. Further, since OMI and NRF-1 were higher in G93A IMS-SOD1 males than in the G93A-SOD1 mice, collectively these results support the notion that the IMS fraction of mutant SOD1 plays a direct role in the activation of the UPR^{mt}.

One of the most striking effects observed was the activation of OMI in G93A-SOD1 female mice. Interestingly, in sporadic ALS patient post-mortem studies, OMI was found to accumulate in spinal motor neurons (Kawamoto et al., 2010). On the other hand, a decrease in OMI was reported to contribute to neurodegeneration (Jones et al., 2003; Strauss et al., 2005; Moisoi et al., 2009). In light of these findings, we propose that increased OMI levels induced by the UPR^{mt} may enhance protein quality control in the IMS and delay the onset of mitochondrial damage. However, as mitochondrial damage progresses, despite its increase, OMI becomes insufficient to maintain the integrity of mitochondria. In fact, since release of OMI in the cytosol upon

mitochondrial outer membrane permeabilization plays a role in apoptosis, an initial protective effect of elevated OMI in the IMS could eventually contribute to the acceleration of cell death, if mitochondrial damage promotes its release into the cytosol. This could contribute possibly to the delay in disease progression in ALS female mice relative to males.

Finally, our results in the ERαKO mice suggested that, as we previously reported in breast cancer cells (Papa and Germain, 2011), upon inhibition of the ERα the CHOP axis of the UPR^{mt} could play a compensatory role in an attempt to maintain the integrity of the mitochondria. The UPR^{mt} pathway is rapidly gaining attention, and this study is the first to identify activation of this pathway in a disease relevant model *in vivo*. Considering that the UPR^{mt} regulates the communication between stressed mitochondria and the nucleus, it is likely to be implicated in the pathology of several diseases with mitochondrial involvement. Importantly, as some tissues and cell types do not express ERα and the function of the ERα is tissue specific (Bhat-Nakshatri et al., 2008) (Carroll et al., 2006) one interesting possible implication of our findings is that the UPR^{mt} could help explain some aspects of the sex differences and cell type specificity observed in ALS. Clearly, more work needs to be done to determine if our findings in the SOD1 mouse model apply to humans affected by the much more common sporadic forms of ALS, but the higher incidence of sporadic ALS in males (McCombe and Henderson, 2010) suggests that estrogen hormones and their receptors could indeed be involved in sex differences through the ERα axis of the UPR^{mt}. Moreover, considering that estrogen has been reported to affect the severity of primary mitochondrial diseases with strong male bias, such as Leber's hereditary optic neuropathy (Giordano et al., 2011), whether this pathway also plays a role in gender differences in these diseases remains to be explored.

References

Augustin S, Nolden M, Muller S, Hardt O, Arnold I, Langer T (2005) Characterization of peptides released from mitochondria: evidence for constant proteolysis and peptide efflux. J Biol Chem 280:2691-2699.

Benedetti C, Haynes CM, Yang Y, Harding HP, Ron D (2006) Ubiquitin-like protein 5 positively regulates chaperone gene expression in the mitochondrial unfolded protein response. Genetics 174:229-239.

Bhat-Nakshatri P, Wang G, Appaiah H, Luktuke N, Carroll JS, Geistlinger TR, Brown M, Badve S, Liu Y, Nakshatri H (2008) AKT alters genome-wide estrogen receptor alpha binding and impacts estrogen signaling in breast cancer. Mol Cell Biol 28:7487-7503.

Bragoszewski P, Gornicka A, Sztolsztener ME, Chacinska A (2013) The ubiquitin-proteasome system regulates mitochondrial intermembrane space proteins. Mol Cell Biol 33:2136-2148.

Carroll JS, Meyer CA, Song J, Li W, Geistlinger TR, Eeckhoute J, Brodsky AS, Keeton EK, Fertuck KC, Hall GF, Wang Q, Bekiranov S, Sementchenko V, Fox EA, Silver PA, Gingeras TR, Liu XS, Brown M (2006) Genome-wide analysis of estrogen receptor binding sites. Nat Genet 38:1289-1297.

Cozzolino M, Pesaresi MG, Amori I, Crosio C, Ferri A, Nencini M, Carri MT (2009) Oligomerization of mutant SOD1 in mitochondria of motoneuronal cells drives mitochondrial damage and cell toxicity. Antioxid Redox Signal 11:1547-1558.

Durieux J, Wolff S, Dillin A (2011) The cell-non-autonomous nature of electron transport chain-mediated longevity. Cell 144:79-91.

Ferri A, Cozzolino M, Crosio C, Nencini M, Casciati A, Gralla EB, Rotilio G, Valentine JS, Carri MT (2006) Familial ALS-superoxide dismutases associate with mitochondria and shift their redox potentials. Proc Natl Acad Sci U S A 103:13860-13865.

Fiorese CJ, Schulz AM, Lin YF, Rosin N, Pellegrino MW, Haynes CM (2016) The Transcription Factor ATF5 Mediates a Mammalian Mitochondrial UPR. Curr Biol 26:2037-2043.

Giordano C, Montopoli M, Perli E, Orlandi M, Fantin M, Ross-Cisneros FN, Caparrotta L, Martinuzzi A, Ragazzi E, Ghelli A, Sadun AA, d'Amati G, Carelli V (2011) Oestrogens ameliorate mitochondrial dysfunction in Leber's hereditary optic neuropathy. Brain 134:220-234.

Gurney ME, Pu H, Chiu AY, Dal Canto MC, Polchow CY, Alexander DD, Caliendo J, Hentati A, Kwon YW, Deng HX, et al. (1994) Motor neuron degeneration in mice that express a human Cu,Zn superoxide dismutase mutation. Science 264:1772-1775.

Haynes CM, Petrova K, Benedetti C, Yang Y, Ron D (2007) ClpP mediates activation of a mitochondrial unfolded protein response in C. elegans. Dev Cell 13:467-480.

Heiman-Patterson TD, Deitch JS, Blankenhorn EP, Erwin KL, Perreault MJ, Alexander BK, Byers N, Toman I, Alexander GM (2005) Background and gender effects on survival in the TgN(SOD1-G93A)1Gur mouse model of ALS. J Neurol Sci 236:1-7.
Hervias I, Beal MF, Manfredi G (2006) Mitochondrial dysfunction and amyotrophic lateral sclerosis. Muscle Nerve 33:598-608.
Igoudjil A, Magrane J, Fischer LR, Kim HJ, Hervias I, Dumont M, Cortez C, Glass JD, Starkov AA, Manfredi G (2011) In vivo pathogenic role of mutant SOD1 localized in the mitochondrial intermembrane space. J Neurosci 31:15826-15837.
Ilieva H, Polymenidou M, Cleveland DW (2009) Non-cell autonomous toxicity in neurodegenerative disorders: ALS and beyond. J Cell Biol 187:761-772.
Israelson A, Arbel N, Da Cruz S, Ilieva H, Yamanaka K, Shoshan-Barmatz V, Cleveland DW (2010) Misfolded mutant SOD1 directly inhibits VDAC1 conductance in a mouse model of inherited ALS. Neuron 67:575-587.
Jones JM, Datta P, Srinivasula SM, Ji W, Gupta S, Zhang Z, Davies E, Hajnoczky G, Saunders TL, Van Keuren ML, Fernandes-Alnemri T, Meisler MH, Alnemri ES (2003) Loss of Omi mitochondrial protease activity causes the neuromuscular disorder of mnd2 mutant mice. Nature 425:721-727.
Kabashi E, Durham HD (2006) Failure of protein quality control in amyotrophic lateral sclerosis. Biochim Biophys Acta 1762:1038-1050.
Kawamata H, Manfredi G (2008) Different regulation of wild-type and mutant Cu,Zn superoxide dismutase localization in mammalian mitochondria. Hum Mol Genet 17:3303-3317.
Kawamata H, Manfredi G (2010) Import, maturation, and function of SOD1 and its copper chaperone CCS in the mitochondrial intermembrane space. Antioxid Redox Signal 13:1375-1384.
Kawamoto Y, Ito H, Kobayashi Y, Suzuki Y, Akiguchi I, Fujimura H, Sakoda S, Kusaka H, Hirano A, Takahashi R (2010) HtrA2/Omi-immunoreactive intraneuronal inclusions in the anterior horn of patients with sporadic and Cu/Zn superoxide dismutase (SOD1) mutant amyotrophic lateral sclerosis. Neuropathol Appl Neurobiol 36:331-344.
Koppen M, Langer T (2007) Protein degradation within mitochondria: versatile activities of AAA proteases and other peptidases. Crit Rev Biochem Mol Biol 42:221-242.
Lin YF, Schulz AM, Pellegrino MW, Lu Y, Shaham S, Haynes CM (2016) Maintenance and propagation of a deleterious mitochondrial genome by the mitochondrial unfolded protein response. Nature 533:416-419.
Magrane J, Hervias I, Henning MS, Damiano M, Kawamata H, Manfredi G (2009) Mutant SOD1 in neuronal mitochondria causes toxicity and mitochondrial dynamics abnormalities. Hum Mol Genet 18:4552-4564.
Martinus RD, Garth GP, Webster TL, Cartwright P, Naylor DJ, Hoj PB, Hoogenraad NJ (1996) Selective induction of mitochondrial chaperones

in response to loss of the mitochondrial genome. Eur J Biochem 240:98-103.
Matus S, Valenzuela V, Medinas DB, Hetz C (2013) ER Dysfunction and Protein Folding Stress in ALS. Int J Cell Biol 2013:674751.
McCombe PA, Henderson RD (2010) Effects of gender in amyotrophic lateral sclerosis. Gend Med 7:557-570.
Mohrin M, Shin J, Liu Y, Brown K, Luo H, Xi Y, Haynes CM, Chen D (2015) Stem cell aging. A mitochondrial UPR-mediated metabolic checkpoint regulates hematopoietic stem cell aging. Science 347:1374-1377.
Moisoi N, Klupsch K, Fedele V, East P, Sharma S, Renton A, Plun-Favreau H, Edwards RE, Teismann P, Esposti MD, Morrison AD, Wood NW, Downward J, Martins LM (2009) Mitochondrial dysfunction triggered by loss of HtrA2 results in the activation of a brain-specific transcriptional stress response. Cell Death Differ 16:449-464.
Nargund AM, Pellegrino MW, Fiorese CJ, Baker BM, Haynes CM (2012) Mitochondrial import efficiency of ATFS-1 regulates mitochondrial UPR activation. Science 337:587-590.
Nargund AM, Fiorese CJ, Pellegrino MW, Deng P, Haynes CM (2015) Mitochondrial and nuclear accumulation of the transcription factor ATFS-1 promotes OXPHOS recovery during the UPR(mt). Mol Cell 58:123-133.
Okado-Matsumoto A, Fridovich I (2001) Subcellular distribution of superoxide dismutases (SOD) in rat liver: Cu,Zn-SOD in mitochondria. J Biol Chem 276:38388-38393.
Papa L, Germain D (2011) Estrogen receptor mediates a distinct mitochondrial unfolded protein response. J Cell Sci 124:1396-1402.
Papa L, Germain D (2014) SirT3 regulates the mitochondrial unfolded protein response. Mol Cell Biol 34:699-710.
Pedrini S, Sau D, Guareschi S, Bogush M, Brown RH, Jr., Naniche N, Kia A, Trotti D, Pasinelli P (2010) ALS-linked mutant SOD1 damages mitochondria by promoting conformational changes in Bcl-2. Hum Mol Genet 19:2974-2986.
Radke S, Chander H, Schafer P, Meiss G, Kruger R, Schulz JB, Germain D (2008) Mitochondrial protein quality control by the proteasome involves ubiquitination and the protease Omi. J Biol Chem 283:12681-12685.
Rosen DR (1993) Mutations in Cu/Zn superoxide dismutase gene are associated with familial amyotrophic lateral sclerosis. Nature 364:362.
Shi P, Gal J, Kwinter DM, Liu X, Zhu H (2010) Mitochondrial dysfunction in amyotrophic lateral sclerosis. Biochim Biophys Acta 1802:45-51.
Strauss KM, Martins LM, Plun-Favreau H, Marx FP, Kautzmann S, Berg D, Gasser T, Wszolek Z, Muller T, Bornemann A, Wolburg H, Downward J, Riess O, Schulz JB, Kruger R (2005) Loss of function mutations in the gene encoding Omi/HtrA2 in Parkinson's disease. Hum Mol Genet 14:2099-2111.

Tian Y, Merkwirth C, Dillin A (2016) Mitochondrial UPR: A Double-Edged Sword. Trends Cell Biol 26:563-565.
Vande Velde C, Miller TM, Cashman NR, Cleveland DW (2008) Selective association of misfolded ALS-linked mutant SOD1 with the cytoplasmic face of mitochondria. Proc Natl Acad Sci U S A 105:4022-4027.
Vijayvergiya C, Beal MF, Buck J, Manfredi G (2005) Mutant superoxide dismutase 1 forms aggregates in the brain mitochondrial matrix of amyotrophic lateral sclerosis mice. J Neurosci 25:2463-2470.
Zhao Q, Wang J, Levichkin IV, Stasinopoulos S, Ryan MT, Hoogenraad NJ (2002) A mitochondrial specific stress response in mammalian cells. Embo J 21:4411-4419.